ESSENTIAL ROLE OF B-CELL LYMPHOMA-9 IN HUMAN BREAST DUCTAL CARCINOMA IN SITU PROGRESSION TO INVASIVE BREAST CANCER

BY

Hanan Sataa Elsarraj

M.D., University of Tripoli, 2007

M.A., University of Kansas Medical Center, 2012

Submitted to the graduate degree program in Pathology and Laboratory Medicine, and the Graduate Faculty of the University of Kansas in partial fulfillment of the requirements for the degree of Doctor of Philosophy.

_____
Chairperson, Fariba Behbod, Pharm.D, Ph.D

_____
Timothy Fields, M.D, Ph.D

_____
Andrew Godwin, Ph.D

_____
Roy Jensen, M.D

_____
Nikki Cheng, Ph.D

_____
Lane Christenson, Ph.D

_____
Fang Fan, M.D, Ph.D

Date Defended: December 3rd, 2015

The Dissertation Committee for HANAN SATAA ELSARRAJ
certifies that this is the approved version of the following dissertation:

ESSENTIAL ROLE OF B-CELL LYMPHOMA-9 IN HUMAN BREAST DUCTAL CARCINOMA IN SITU PROGRESSION TO INVASIVE BREAST CANCER

_____

Chairperson, Fariba Behbod, Pharm.D, Ph.D

Date approved: December 14th, 2015

Abstract

B-cell lymphoma-9 (BCL9) is a recently identified co-activator of β-catenin mediated transcription. BCL9 has been shown to promote tumor metastasis in multiple myeloma and colon carcinoma. However, BCL9's role in a switch from non-invasive to invasive cancers has not been recognized. By utilizing two unique *in vivo* models of human non-invasive to invasive breast cancers, tandem ductal carcinoma in situ (DCIS) to invasive ductal carcinoma (IDC) and mouse-intraductal models, we have shown for the first time that BCL9 may be an important molecular switch in the malignant transition of at least a subset of non-invasive cancers by enhancing canonical WNT signaling and promotion of epithelial-mesenchymal transition (EMT). Analysis of RNA and protein at distinct stages of DCIS to IDC using both models showed BCL9 up-regulation to be associated with DCIS transition to IDC. *In vivo* silencing of BCL9 led to inhibition of DCIS invasion and reversal of EMT. Reverse phase protein analysis (RPPA)on DCIS cell lines Knockdown (KD) BCL9 vs. control indicated that BCL9 KD showed decreased expression of a number of genes in the EGFR signaling pathway, including p-EGFR, p-HER2, p-STAT3, and p-Src. In addition, BCL9 was evaluated as a biomarker of DCIS risk of recurrence. Analysis of 28 DCIS patients revealed high nuclear BCL9 expression to be associated with pathologic characteristics known to be correlated with an increased risk for recurrence: ER and PR negative, high nuclear grade, and HER2 positive ($p < 0.05$). Analysis of the TCGA database showed BCL9 to be highly amplified in many cancers including breast, bladder and liver. Furthermore, BCL9 was amplified in a significantly higher proportion of invasive basal breast cancers compared to other subtypes.

We conclude that BCL9 plays a key role in the malignant transition of a subset of non-invasive breast cancers and may promote invasion through enhancement of canonical WNT, EGFR and STAT3 signaling. The data also support that BCL9 is a potential biomarker to identify the risk of recurrence in DCIS patients.

Acknowledgements

I would like to express my deep appreciation and gratitude to my mentor Dr. Fariba Behbod for her unwavering support and encouragement throughout the past five years. I am also indebted to my graduate and comprehensive exam committee members, Drs. Timothy Fields, Andrew Godwin, Fang Fan, Nikki Cheng, Lane Christenson, Roy Jensen, and Patrick Fields for all the constructive criticism and for the important suggestions during the production of this research and dissertation.

I would also like to thank my fellow lab members, past and present: Dr. Kelli Valdez, Mrs. Darlene Limback, Ellie Heddens, Dr. Stephanie Bishop, Caroline Hodge, Aria Alsabbagh, Saloumeh Arjmand, and Jenna Berger, for their support and assistance, and for the laughs and lunches, and for all the fun that we had over the past years. Special thanks for Yan Hong, for her friendship and support, and for teaching me different techniques in the lab, and for her technical assistance.

I also like to thank the director of the graduate program in the Department of Pathology and Laboratory Medicine, Dr. Soumen Paul, for all that he is doing to make the department a productive environment for the graduate students. I also thank Mrs. Zoe Baldwin for her guidance and help in resolving any issues that I encountered with my coursework or paperwork during my graduate career.

I would also like to acknowledge the CBIE- Libyan North American Scholarship Program for funding my PhD training.

I would like to thank my wonderful parents, Sataa and Salha, and my three lovely sisters, Afaf, Ebtehaj, and Esra for always believing in me, and for their support and encouragement throughout the years.

Finally, I would like to thank my loving husband, Ziad, for sticking with me through all the good times and bad, and for never failing to lift my spirit. I thank my amazing son, Ayhem, and my beautiful daughter, Elaf, for giving me joy during the sad times, and for giving me strength during the hard times.

Table of contents

List of Tables and Figures

Chapter one: Introduction

Chapter two: Expression Profiling of *In Vivo* Ductal Carcinoma In Situ Progression Models Identified B Cell Lymphoma-9 as a Molecular Driver of Breast Cancer Invasion

Chapter Three: Novel Role of BCL9 in the Activation of Other Oncogenic Signaling Pathways

Chapter Four: BCL9 as a Potential Biomarker of High Risk DCIS

List of Abbreviations

aCGH	Array comparative genomic hybridization
APC	Adenomatous polyposis coli
APCDD1	Adenomatosis Polyposis Coli Down-Regulated 1
BCL9	B cell lymphoma-9
BCL9L	B cell lymphoma-9 Like
BLBC	Basal-like breast cancer
β-TrCP	Beta-transducin repeat containing protein
CAF	Carcinoma-associated fibroblasts
CD24	cluster of differentiation 24
CD44	cluster of differentiation 44
CK1α	Casein kinase 1 alpha
CM	Conditional medium
COX2	Cyclooxygenase-2
DAPI	4′,6-diamidino-2-phenylindole
DCIS	Ductal carcinoma in situ
DKK	Dickkopf
DVL	Dishevelled
EGFR	Epidermal growth factor receptor
EMT	Epitelial mesenchymal transition
EpCAM	Epithelial cell adhesion molecule
EPS8	Epidermal growth factor receptor kinase substrate 8
Esr1, ER	Estrogen receptor (gene and protein)
Erbb2, HER2	Human epidermal growth factor receptor 2 (gene and protein)
FGF	Fibroblast growth factor
FGFR	Fibroblast growth factor receptor
FZD	Frizzled
Gli2	GLI Family Zinc Finger 2
GPCR	G-protein-coupled receptors
GSK-3β	Glycogen synthase kinase 3 beta
GSTM1	Glutathione S-Transferase Mu 1
HAN	Hyperplastic alveolar nodules
HCC	Hepatocellular carcinoma
H2AFJ	H2A Histone Family, Member J
IBTR	Ipsilateral breast tumor recurrence
IDC	Invasive ductal carcinoma
IF	Immunofluorescence
IGFBP-4	Insulin-like growth factor binding protein 4
IL6	Interleukin-6
IPA	Ingenuity Pathway Analysis
JAK	Janus kinase
K5	Keratin 5
K19	Keratin 19
KD	Knockdown

LEF1	Lymphoid enhancer-binding factor 1
LIF	Leukemia inhibitory factor
LRP	LDL-receptor related protein
MIND	Mouse intraductal xenograft model
MMP	Matrix metalloproteinase
MMTV	Mouse mammary tumor virus
MUC1	Mucin 1
MYBL2	Myb-Like Protein 2
NSABP	National Surgical Adjuvant Breast and Bowel Project
NSG	NOD-SCID IL2Rgamma null
PR	Progesterone receptor
PYGO	Pygopus
qPCR	quantitative Polymerase Chain Reaction
ROR1 and 2	Receptor Tyrosine Kinase-Like Orphan Receptor 1 and 2
RPPA	Reverse phase protein array
Rspo	Rspondin
RT	Reverse transcription
RYK	Receptor-Like Tyrosine Kinase
SAGE	Serial analysis of gene expression
SAM	Significance analysis of microarrays
Sca-1	Stem cell antigen-1
SDF-1	Stromal cell-derived factor 1
SMA	Smooth muscle actin
SOX6	SRY (Sex Determining Region Y)-Box 6
SP1	Specificity protein 1
sRFP	Secreted frizzled-related protein
STAT3	Signal transducer and activator of transcription 3
STK15	Aurora A kinase
TCF	T-cell specific, HMG-box
TCGA	The cancer genome atlas
TGFβ	Transforming growth factor beta
TGFBR2	Transforming Growth Factor, Beta Receptor 2
TLR	Toll-like receptors
TMA	Tissue microarray
UTR	Untranslated region
VNPI	Van Nuys Prognostic index
WAP	Whey Acidic Protein
WIF	WNT inhibitory factor

CHAPTER ONE

Introduction

1.1. Ductal Carcinoma in Situ (DCIS):

Ductal carcinoma in situ (DCIS) is a non-invasive precursor lesion of breast carcinoma in which the malignant cells proliferate inside the duct without invading the surrounding stromal tissue. The American Cancer Society estimated that 60,290 new cases of breast carcinoma in situ will be diagnosed in 2015. Carcinoma in situ accounts for 20% of all breast cancers, and 83% of these lesions are DCIS.

The natural history of DCIS is not well understood. Studies from DCIS cases that were initially misdiagnosed as benign suggest that 14-53% of the cases will become invasive in 10-15 years [1], while autopsy studies reveal a higher incidence of undetected DCIS in the population [1], which means that not all lesions progress to invasive disease. Thus, a large percentage of DCIS patients are over-treated. Therefore, molecular characterization of DCIS is extremely important to identify biologically and clinically meaningful molecules that can serve as therapeutic targets and/or as biomarkers for risk stratification.

DCIS classification:

Multiple classification systems have been proposed to standardize diagnosis of DCIS. The traditional classification system is based on the predominant microscopic growth pattern, which includes: cribriform, comedo, solid, papillary and micropapillary [2]. Other classifications are based on the degree of differentiation (resemblance to normal cells), mitotic activity, and the presence or absence of central necrosis, most of which classify DCIS into three grades: well (grade 1), moderately (grade 2), and poorly (grade 3) differentiated DCIS [2].

On the molecular level, Allred *et al.* evaluated 25 pure DCIS cases for 392 genes that define intrinsic subtypes of invasive breast cancer (IDC). Their gene expression profiling subclassified DCIS into luminal, human epidermal growth factor receptor 2 (HER2) overexpressing and basal. These subtypes existed at the same frequencies as previously shown for IDC (44%, 8%, and 28%, respectively) [3]. These findings reflect the complexity of DCIS, and demonstrate that the heterogeneity of breast cancers arises at the early non-invasive stages in DCIS.

Current therapies of DCIS:

DCIS treatment is controversial, and the ultimate goal is breast conservation and reduction of future risk of invasion. The National Adjuvant Breast and Bowel Project (NSABP) initiated a prospective randomized trial (NSABP-B17) that compared the risk of ipsilateral breast tumor recurrence (IBTR) after lumpectomy alone to IBTR after lumpectomy followed by radiation. Women treated with lumpectomy plus radiotherapy had a 60% lower risk of IBTR compared with patients treated with lumpectomy only [4, 5]. Mastectomy showed no difference in survival from lumpectomy and is reserved for patients with multicentric disease, large lesions, other contraindications to breast conservation, or a personal preference for mastectomy [6]. The third treatment option is adjuvant therapy with tamoxifen or with aromatase inhibitors after surgery in Estrogen Receptor (ER)-positive DCIS patients. Another prospective randomized trial (NSABP-B24) evaluated the value of tamoxifen in conjunction with lumpectomy and radiotherapy in the treatment of DCIS. This trial showed that adding tamoxifen reduced the risk of IBTR up to 31% compared to lumpectomy plus radiotherapy [2, 5]. However, tamoxifen carries potentially fatal toxicities, such as deep vein thrombosis, pulmonary embolism and stroke [7, 8]. As previously mentioned, due to lack of risk stratification methods in DCIS patients, there are no reliable

means to identify cases that would benefit from observation alone and cases that require more aggressive treatment.

Current biomarkers of high risk DCIS:

The decision for DCIS treatment depends on the morphological classification of the lesion. The Van Nuys prognostic index (VNPI) is one scoring method based on grade, size, presence or absence of comedo necrosis and margin width [9]. This scoring system is used to determine whether or not the patient will benefit from radiotherapy after surgery.

Molecular biomarkers can provide insight into the association of DCIS and risk of invasive progression. There are many parallels between DCIS and invasive breast cancer in regards to these markers and their prognostic implications. The most common biomarkers used are ER and progesterone receptor (PR), the expression of which are associated with less aggressive DCIS. ER status also drives decision making with regard to adding tamoxifen or aromatase inhibitors to the treatment. In addition, HER2, cyclooxygenase-2 (COX-2), Ki-67 and p53 are well-known DCIS markers that show higher percentage in patients with high grade/ comedo type of DCIS [10]. However, they are not routinely performed for DCIS patients in the clinical setting.

Recently a recurrence scoring system (Oncotype DX®) has been developed [11]. Oncotype DX® is a multigene expression test, that predicts response to chemotherapy as well as recurrence in early-stage breast cancer patients that are node negative and ER-positive. The Oncotype DX® assay is performed on RNA extracted from formalin-fixed, paraffin-embedded tumor tissue and is analyzed using RT-PCR. For early stage breast cancer, the expression of 21 genes is measured. Sixteen are cancer related genes, which are then normalized to five housekeeping genes. This 21-gene panel is a result of three independent clinical trials that analyzed 250 candidate genes in a

total of 447 patients and demonstrated a statistical link between these genes and distant breast cancer recurrence. For DCIS patients, Oncotype DX DCIS Score™ is a genomically validated diagnostic test that provides prediction of 10-year risk of local recurrence [12]. DCIS score is calculated using a DCIS-specific algorithm and coefficients from only 7 of the 16 cancer-related genes, (Ki-67, STK15, Survivin, Cyclin B1, MYBL2, PR, GSTM1). This can guide treatment decisions after surgical tumor removal [13]. The DCIS score was validated by the Eastern Cooperative Oncology Group (ECOG) E5194 prospective cohort study [13]; the study showed that the DCIS score can predict risk of IBTR. However, participants in ECOG E5194 were highly selected for patients having DCIS treated by lumpectomy and with an expected low risk of local recurrence [13]. Therefore, the predictive value of this assay is small. Furthermore, physicians claim that seven genes are not enough to predict DCIS outcome and that the existing biomarkers are better predictors of high-risk DCIS than DCIS Score™ [14].

Currently known molecular mechanisms of DCIS progression to IDC:

The mechanism underlying DCIS progression to invasion is complex, and depends on many factors including epithelial cell properties and tumor microenvironment. Many studies have performed gene expression profiling in an attempt to elucidate molecular changes in DCIS epithelia that drive invasion [15-18]. Ma *et al*. showed extensive similarities at the transcriptome level among the distinct stages of progression from DCIS to IDC, and proposed that the gene expression profile in DCIS may reflect the invasive potential of the disease [16]. Furthermore, several studies performed comparative genomic hybridization (CGH) on a panel of breast tumors, including DCIS and IDC, and showed that the frequency of copy number alterations was higher in invasive tumors than that in DCIS. These studies support the hypothesis that the

invasive potential is already programmed in the genome of DCIS lesions [19, 20]. Yao *et al.* combined CGH with serial analysis of gene expression (SAGE) in DCIS and IDC patient samples. They showed that high-fold amplifications and deletions (>0.5 or less than −0.35, calculated based on array CGH log 2 ratio) correspond to previously identified regions (1q21, 8q24, 11q13, 12q13, 15q26, 17q21, 20q13 and 1p32, 11q11-12, 13q, 16q24, and 17p13, respectively). By correlating gene expression levels and copy number within these commonly amplified regions of DCIS and IDC theyidentified new oncogenes, such as H2A Histone Family, Member J (H2AFJ) and Epidermal Growth Factor Receptor Pathway Substrate 8 (EPS8), as drivers of DCIS to IDC invasive progression [19].

The role of microenvironment in DCIS progression to IDC has been studied. The microenvironment consists of fibroblasts, adipocytes, endothelial cells, immune cells and extracellular matrix. The role of fibroblast-induced invasion is widely accepted [21]. Orimo *et al.* demonstrated that primary breast carcinoma-associated fibroblasts (CAFs) enhanced tumor growth in MCF7-ras xenografts when compared to normal tissue-derived fibroblasts [22]. Hu *et al.* showed that co-transplantation of CAFs with DCIS.COM cells promoted tumor growth, while co-transplantation with normal fibroblasts showed no change in tumor weight [23, 24]. Furthermore, the tumor promoting effect of fibroblasts was reversed by co-injection with normal myoepithelial cells [24]. Paracrine signaling can play a major role in fibroblast-epithelial interaction. Allinen *et al.* used SAGE to describe gene expression profiles of normal breast tissue, DCIS, and IDC [25]. This study showed extensive gene expression changes in all cell types during DCIS-IDC progression, specifically increased expression level of secreted proteins in activated fibroblasts. One of the overexpressed secreted factors was Stromal cell-derived factor-1 (SDF-1) that was shown to bind to tumor epithelial cells [25]. Furthermore, fibroblasts,

by promoting angiogenesis, enhanced tumor growth. SDF-1 secreted from CAFs were shown to recruit endothelial progenitor cells that promote angiogenesis and increased tumor growth [22]. In addition, Dang *et al.* performed *in vitro* organotypic co-culture of mammary fibroblasts with basal and luminal-type breast cancer cell lines. They demonstrated that fibroblasts were recruited selectively to basal-type DCIS-spheroids and reorganized collagen fibers to induce invasion [21]. This was mediated by Rho-family small GTP-binding protein (Cdc42) in fibroblasts [21]. However, invasive progression in luminal-type DCIS-spheroids was not induced by fibroblasts co-culture [21].

The presence or absence of an intact myoepithelial cell layer is a major diagnostic feature to differentiate DCIS from IDC. Myoepithelial cells have a suppressor effect on tumor cell growth, invasion, and angiogenesis [26]. The mechanism of myoepithelial cell disappearance during DCIS progression is unknown. Polyak's group highlighted the importance of myoepithelial cells in DCIS progression by demonstrating that normal myoepithelial cells inhibited DCIS invasion [24]. Molecular profiling of myoepithelial cells purified from DCIS.COM xenografts identified preferential activation of Transforming growth factor-β (TGFβ), hedgehog, and p63 pathway. They showed that collaboration of these pathways might regulate myoepithelial phenotype. Inhibiting TGFβ and hedgehog pathway activity via downregulation of TGFBR2/SMAD4 and Gli2 expression, respectively, led to myoepithelial loss and progression to invasion [3].

A study by Ma and colleagues on DCIS stromal cells showed upregulation of Matrix Metalloproteinases (MMPs) such as MMP11, MMP2, and MMP14 in the stroma associated with DCIS compared with normal breast epithelium suggesting that they may play a role in DCIS progression. This group also showed that WNT inhibitors such as secreted Frizzled-related

protein (sFRPs) and WNT-inhibitory factor (WIF) were downregulated in stroma associated with DCIS suggesting that aberrant activation of WNT signaling in the tumor epithelia can be a consequence of down-regulation of its inhibitors in the surrounding microenvironment [15]. Another key step in DCIS to IDC transition is extracellular matrix (ECM) degradation. Proteolytic enzymes MMP2 and MMP9 were shown to be expressed at higher levels in DCIS compared to normal and hyperplastic epithelia, while MMPs 1, 2, 3, 9, and 11 were found to be upregulated in adjacent stromal tissue [23]. The interplay of these proteolytic enzymes on ECM degradation may play a role in DCIS progression.

In vivo models of premalignant breast cancer:

Multiple transgenic mouse models of premalignant breast lesions have been identified. Transgenes have been developed with a variety of promotors, combinations of different genes and knockouts including genes functioning as growth factors, receptors, signal transducers, and cell cycle proteins [27]. An example of these transgenic mice are the whey acidic protein (WAP)-TAg transgenic mice/BALB/c. In WAP-TAg transgenic mice, the SV40 large tumor antigen expression is driven by the WAP promoter, and causes pregnancy-induced DCIS lesions. SV40 TAg is an inducer of cell transformation and tumor formation through its ability to inactivate the tumor suppressor proteins pRb and p53 [28, 29]. The MMTV-rtTA, tet-op-ERα mouse is a conditional tetracycline-responsive transgenic mouse model with deregulated ERα expression in mammary epithelial cells driven by addition of exogenous doxocycline. In the presence of ovarian hormones these mice develop ERα-positive ductal and lobular hyperplasias as well as DCIS lesions by 4 months of age. However, no palpable tumors were observed in these mice [28].

Cleared fat pad transplantation is a strategy to study premalignant lesions. The mouse mammary fat pad is surgically removed at three weeks of age followed by transplantation of hyperplastic lesions and tumors into mammary gland-free fat pads of syngeneic mice. Growing hyperplastic lesions can replicate their original phenotypes. Medina *et al.* is the first who developed hyperplastic alveolar nodule (HAN) models in which hyperplastic cells are developed in mice by different strategies such as MMTVs, chemical carcinogens [30], irradiation and prolonged hormonal stimulation [31]. HAN lesions are maintained by serial transplantation into cleared mammary fat pads, and show distinct growth properties compared to invasive lesions. HAN models are the basis of much information about premalignant mammary lesions and cancer. Mouse DCIS models improved our understanding of the molecular mechanisms underlying progression to invasive disease. However, these models do not recapitulate the architecture and complexity of human DCIS.

Human in mouse xenografts is another DCIS model that has been developed. In previous models, human DCIS cells were inoculated in Matrigel and injected subcutaneously or into fatpads of immunodeficient mice. This is not ideal, since the cells are introduced outside their natural environment. Recently, Behbod and colleagues established a novel human xenograft model: the mouse intraductal (MIND) model. This model involves the injection of primary human DCIS or DCIS cell lines intraductally through the cleaved nipple of immunodeficient mice. This model mimics the natural progression of the disease and the DCIS microenvironment inside the ducts [32]. Furthermore, Valdez *et al.* demonstrated that primary DCIS cells grow and proliferate in MIND xenografts, and that DCIS biomarkers in xenografts are similar to the original patient samples' biomarkers [33]. However, one limitation of this model is that DCIS cells are transplanted into immunodeficient mice, which may mask effects of immune cells in

tumorigenesis. To date, only two DCIS cell lines are utilized as xenograft models, DCIS.COM and SUM225, both of which are described in detail in chapter two.

In this dissertation, DCIS.COM and SUM225-MIND models were utilized to screen for gene expression changes in DCIS cells during progression to IDC. Analysis of gene expression profiles from our *in vivo* model showed WNT signaling pathway was one of the top upregulated pathways during DCIS progression to IDC.

1.2. WNT signaling pathway:

WNTs consist of 19 secreted glycoproteins that play key roles in various processes, including cell proliferation, survival, migration, cell fate, and self-renewal. WNTs regulate downstream pathways through both: β-catenin-dependent (canonical) and β-catenin-independent (non-canonical) mechanisms. There are ten reported Frizzled (FZD) receptors, along with receptor tyrosine kinases, Receptor Tyrosine Kinase-Like Orphan Receptor 1 and 2 (ROR1 and 2), and RTK-like protein (RYK) that stimulate WNT signaling.

Canonical WNT signaling is activated when FZD and LDL- receptor-related protein (LRP) on the target cells bind WNT proteins. These receptors transduce a signal to several intracellular proteins including Dishevelled (DVL), Glycogen Synthase Kinase-3β (GSK-3β), casein kinase Iα (CKIα), Axin, Adenomatous Polyposis Coli (APC), and the transcriptional regulator, β-catenin. In the absence of WNT signaling, a destruction complex containing GSK-3/APC/Axin controls cytoplasmic β-catenin levels. APC and Axin are scaffold proteins that facilitate kinase binding. CKIα and GSK-3 are serine/threonine kinases that phosphorylate β-catenin to be recognized by β-TrCP and directs it towards proteosomal degradation. When WNT signaling is active, phosphorylation of β-catenin is inhibited and hence its degradation. β-catenin will accumulate in the cell and translocate to the nucleus. Nuclear β-catenin will interact with other co-factors to stimulate transcription of WNT target genes such as lymphoid enhancer-binding factor 1/T cell-specific transcription factor (LEF/TCF), and B-Cell Lymphoma 9 (BCL9)/ B-Cell Lymphoma 9-Like (BCL9L) (Figure 1.1) [34].

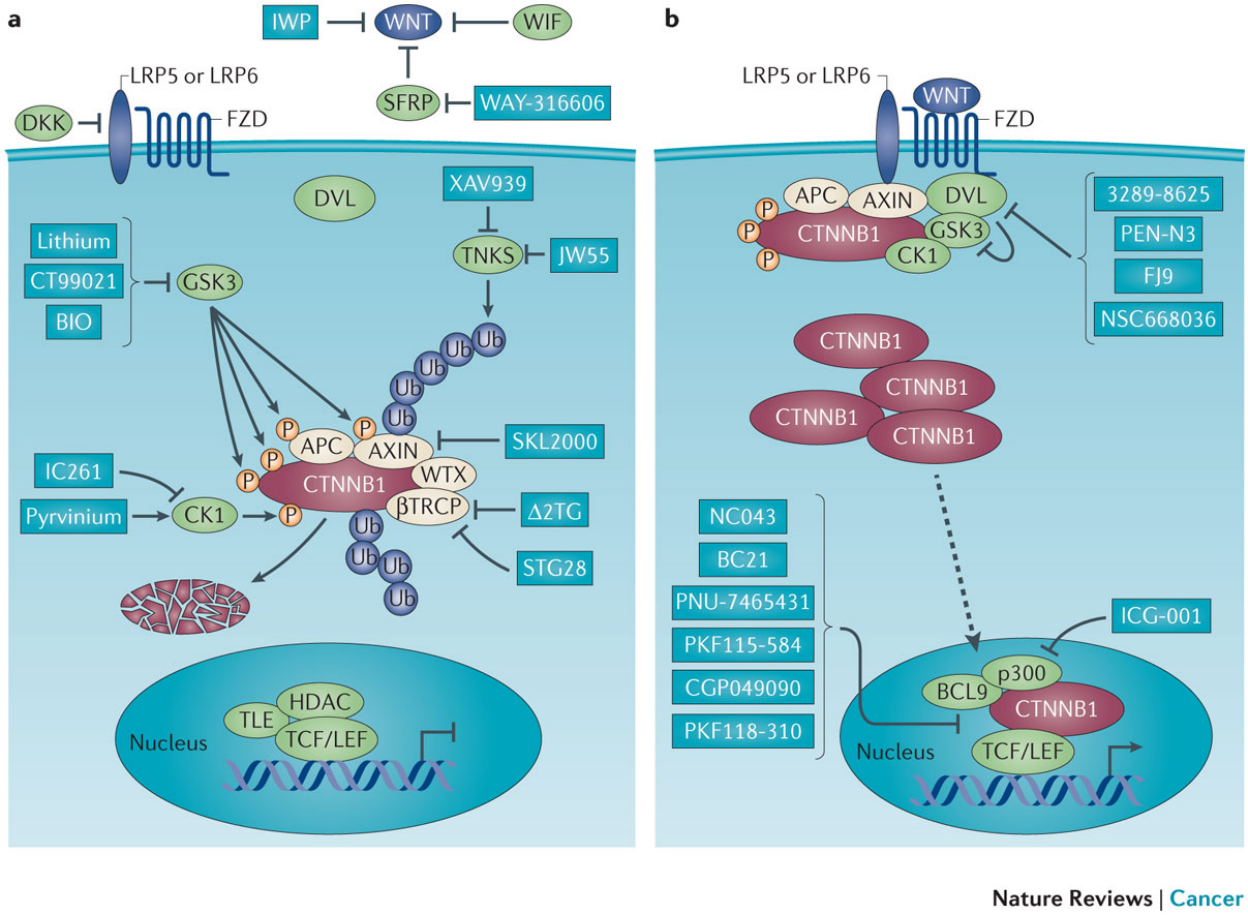

Figure 1.1. The canonical Wnt signaling pathway and its identified small molecular inhibitors and activators. (Obtained from Anastas, et al 2013) Illustrates canonical Wnt signaling pathway in the presence **(**A), and absence (B) of Wnt stimulation.

Activators and inhibitors of WNT signaling:

WNT signaling can be regulated at various levels by different inhibitors and activators. These effectors can act extracellularly or intracellularly. WNT inhibitors can naturally exist and are divided into six families of secreted and four families of transmembrane inhibitors.

Secreted WNT inhibitors known to date are: Dickkopf proteins (DKKs), sFRPs, WIF-1, Wise/SOST, Cerberus, and Insulin-like growth-factor binding protein 4 (IGFBP-4). Among these, the DKK family is the best characterized. They are secreted glycoproteins that composed of four members 1-4. DKK3 is different from other members in that it regulates TGF-β signaling and has no effect on WNT signaling. DKK1 and 2 inhibit WNT signaling by high affinity binding to LRP5/6. DKK1 prevents WNT-LRP6 interaction and disrupts FZD8-LRP6 formation [35]. sFRP family of inhibitors act by sequestering WNTs away from active receptor complexes, thus inhibiting WNT signaling. The mechanisms of action of WIF-1, Wise/SOST, Cerberus, and IGFBP-4 are not fully understood. However, silencing of *WIF-1* by promoter hypermethylation in primary human osteosarcomas is associated with loss of differentiation and increased tumor cell proliferation [36]. In addition, manipulation of WIF-1 and IGFBP-4 expression impedes biological cancer processes such as tumor cell proliferation and degree of differentiation [37]. In addition to secreted WNT inhibitors, transmembrane WNT inhibitors include: Shisa, Waif/5T4, and Adenomatosis polyposis coli down-regulated 1 (APCDD1). Shisa proteins reside in the endoplasmic reticulum, and inhibit WNT and fibroblast growth factor (FGF) signaling by suppressing FZD and fibroblast growth factor receptor (FGFR) maturation [38]. Waif1a is a plasma membrane protein and a WNT/β-catenin signaling target shown to activate non-canonical WNT signaling and to antagonize canonical WNT signaling by binding to LRP6 and regulating

LRP6 subcellular localization [37, 39]. APCDD1 is a membrane bound glycoprotein and a direct target of WNT signaling [40] that inhibits WNT/β-catenin signaling by binding to WNT3A and possibly preventing FZD from binding WNT [37].

Well known activators of WNT signaling are: R-spondins and Norrin. The R-spondin family (Rspo1-4) are secreted growth factors that synergize with WNTs and require WNTs to activate WNT/β-catenin signaling through LGR4 and LGR5 [41]. Rspo binds LGR4 and 5 causing subsequent phosphorylation and internalization of LRP5/6, followed by inhibition of GSKβ and stabilization of β-catenin [41]. Previous studies revealed a possible role of Rspo2 and 3 to promote tumorigenesis *in vivo* [42]. Norrin is a small secreted factor structurally unrelated to WNT but functionally equivalent. It cooperates with FZD4 and activates WNT signaling through LRP5/6 [43].

Deregulation of WNT signaling in cancer:

Aberrations in WNT signaling and alterations in tumor suppressor and oncogenic pathways can collaborate to drive cancer initiation and progression. Most of the observed WNT pathway mutations in cancer lead to hyperactivation of WNT/β-catenin signaling.

On the receptor level, over expression of several WNT receptors was found in different cancers compared to normal tissues; for example, FZD6 in B-cell leukemias and lymphomas [44], and FZD7 in gastric carcinomas [45] and in colon cancers [46]. Inhibition of FZD7 decreased proliferation and progression of colon cancer [47] and hepatocellular carcinomas [47]. In addition, ROR1 and ROR2 knock-down decreases growth of gastric, lung, breast, and renal carcinoma in xenograft models. Stimulation of various types cancer cells with different WNT

ligands have multiple effects on the growth and survival. WNT3A and WNT7A promote stabilization of β-catenin and activate growth of myeloma cells and prostate cancers [48]. WNT5A and WNT11 act as growth suppressor of ovarian cancer and hepatocellular carcinoma, respectively [49, 50].

In addition, APC deletions in colon crypt progenitors induce growth of adenomas [51]. Missense mutations of β-catenin that disrupt phosphorylation and degradation were observed in hepatocellular carcinomas, medulloblastomas and ovarian cancers [52-54]. Furthermore, high levels of nuclear β-catenin correlate with poor prognosis in breast and colon cancers [55, 56].

In this dissertation, the discovery of a new role of BCL9 in promoting breast cancer progression through the enhancement of WNT signaling is described.

WNT signaling in breast cancer:

Historic studies of MMTV-Wnt1 transgenic mice, which overexpress Wnt1 in mammary the mammary epithelium, showed that these mice will develop extensive ductal hyperplasia early in life which will further progress into mammary carcinomas [57]. Previous studies sought evidence of mutations that stabilize β-catenin in breast cancer, such as mutations in the N-terminal region of β-catenin, and loss of function mutations in APC and Axin. Interestingly, no β-catenin mutations have been reported in breast cancer [58]. Furthermore, APC and Axin mutations were found to be very rare, as only a single case out of 227 breast carcinomas was found to have APC truncation [59, 60]. Other mutations in surface proteins such as Frizzled receptors and LRP5/6 have not yet been investigated [60]. On the WNT protein level, some reports showed that several tumors overexpress WNTs 2,3,4, and 7B [61].

WNT signaling was also shown to support self-renewal in both normal and cancer stem cells. Tumors in transgenic mice expressing Wnt1, β-catenin and c-Myc were more enriched in progenitor populations that express keratin-6 (K-6) and stem cell antigen-1 (Sca-1) compared to transgenic mice expressing HER2 and H-ras [62]. Furthermore, a study by Zeng, *et al.* showed that WNT reporter positive cells were enriched for mammary stem cells based on Lin^{-}, $CD24^{+}$, $CD29^{hi}$ markers [63]. In the same study, Wnt3A was shown to promote self-renewal of mammary stem cells *in vitro* and to enhance their ability to reconstitute mammary glands in mice [63].

A more recent study by Jang, *et al.* showed a correlation between negative (GSK3β) and positive (TCF4) regulators of WNT/β-catenin signaling and breast cancer stage. In addition, inhibition of WNT/β-catenin signaling pathway by knocking down WNT1 expression preferentially reduced metastatic potential by altering cancer stem cell activity in 4T1 mouse xenograft model of breast cancer [64].

In addition, previous studies indicated that activation of WNT signaling pathway may promote epithelial to mesenchymal transition (EMT), for example, WNT1, stabilized β-catenin, and Axin2 induced EMT in MCF7 cells [65]. An interesting study by Dr. Weinberg's group [66], demonstrated that sequential exposure of the luminal EpCAM-positive subpopulation of primary human mammary epithelial cells to TGF-β, canonical and non-canonical WNT signaling resulted in collaborative induction of mesenchymal and basal traits [66].

Therapeutic targeting of WNT pathway:

There are several strategies to target WNT signaling, which comprise small molecules, blocking antibodies and peptide agonists and antagonists. Small molecular inhibitors are promising therapies that modulate WNT signaling at many levels. The Porcupine inhibitor-IWP (Inhibitor of WNT Production) inhibits palmitoylation of WNTs, preventing their secretion and signaling activity. Tankyrase inhibitors enhance Axin stability and degradation of β-catenin. Pyrvinium promotes β-catenin phosphorylation and degradation through casein kinase activation. However, the above inhibitors are not suitable when hyperactivation in WNT/β-catenin pathway is due to mutations in APC and Axin1. To overcome this challenge, inhibitors that target downstream signaling components are required, and some studies have identified molecules that inhibit interactions between TCF7L2 and β-catenin [67].

Blocking antibodies that target WNT and WNT receptors such as anti-FZD7, FZD10 and LRP can inhibit cell growth and induce apoptosis of cancer cells [68, 69]. They are now in development and can be used as potential future therapies for cancer patients.

1.3. B-cell CLL/lymphoma 9 protein (BCL9):

BCL9 resides on chromosome 1q21. Willis *et al.* discovered human BCL9 in a leukemia cell line and showed that the break point translocation of chromosome 1 t(1;14)(q21;q32) in this line falls in the 3'UTR of BCL9 gene. This translocation results in 50x increase in BCL9 expression [70]. BCL9 function was first described by Kramps and coworkers [71]. They reported that Lgs, a homolog of human BCL9 in Drosophila, functions as an adaptor protein that physically links Pygopus (PYGO) to the β-catenin-TCF complex, and that recruitment of PYGO is required for β-catenin to function as a transcriptional coactivator in Drosophila [71].

BCL9 is composed of 1426 amino acids, and shares with B-cell CLL/lymphoma 9 Like (BCL9L) three conserved (in Drosophila, Zebrafish, and mammals) regions called homology domains (HD1, HD2, and HD3). In addition, Sustmann *et al*. identified two more homology domains that are conserved between BCL9 and BCL9L in vertebrates (not in Drosophila), and discovered a transactivation domain in the C terminal region about 170 amino acids in length. This study revealed that BCL9 is not just an adaptor protein for PYGO but can function independently of PYGO binding and synergizes with the C terminal domain of β-catenin in a cell-type-specific manner [72].

BCL9 binding partners:

BCL9 binds β-catenin and activates transcription and translocation into the nucleus [71]. Residues 352-374 of human BCL9-HD2 form an alpha helix that pack against the groove in first armadillo repeat of β-catenin [73]. Thus, the BCL9/β-catenin binding site serves as a novel drug target for cancers with oncogenic WNT signaling and altered BCL9 expression [73]. BCL9 is an essential adaptor protein to recruit other cofactors including PYGO1 and PYGO2. The HD1-

BCL9 domain binds to Homeodomain (PHD) of PYGO1 and the complex increases PYGO1 affinity to histone H3 Lys 4 methylation. In chapter three discovery of a novel interaction between BCL9 and STAT3 has been described and STAT3 signaling activity was evaluated in BCL9 knockdown DCIS cell lines.

BCL9 in disease:

BCL9 variants are linked to mental disorders such as schizophrenia [74]. Microduplications and microdeletions of 1q21, the chromosomal location of BCL9, are associated with mental retardation, autism and congenital abnormalities [75]. In addition, BCL9 has a critical role in myogenic progenitor cell fate. Brack *et al.* generated conditional BCL9 deletion in the myogenic lineage in mice. This group observed that BCL9 deletion resulted in muscle degeneration and abrogation of myogenic differentiation [76]. BCL9 and other WNT pathway genes such as FZD5, DVL2, LRP5 and TCF7L1 were shown to be upregulated in tissue samples from osteoarthritic patients [77]. This observation suggests that BCL9 plays a role in pathogenesis of osteoarthritis.

BCL9 as an oncogene:

Mani *et al.* provided the first evidence that BCL9 can act as an oncogene [78]. BCL9 is overexpressed in colon cancers and multiple myelomas, and its aberrant expression increases proliferative, metastatic and angiogenic properties of cancer cells [78]. Deka *et al.* utilized conditional BCL9 knockout in the intestinal epithelium to examine the role of BCL9 in epithelial homeostasis and stem cell maintenance. The study demonstrated that ablation of BCL9 expression decreased LGR5-positive intestinal stem cell population and impaired mucosal regeneration in mutant mice. Furthermore, BCL9 knockout adenocarcinomas showed reduced

expression of EMT and stem cell–associated genes [79]. Several studies evaluated BCL9 in hepatocellular carcinoma (HCC). For example, Wang *et al.* identified BCL9 as a molecular driver in HCC and reported that BCL9 location at 1q21 was amplified in 8.7% of HCCs. The same study showed a correlation between copy number and BCL9 expression levels, as well as a correlation between BCL9 protein expression by immunohistochemistry and mRNA expression levels in primary HCCs. SiRNA mediated knockdown of BCL9 decreased cell growth and survival in both proliferation and colony formation assays in HCC cell lines that showed BCL9 gene amplification [80]. Another study by Hyeon *et al*. evaluated BCL9 protein expression in 288 primary HCC patients. In normal hepatocytes, 3-10% of cells expressed weak to moderate cytoplasmic staining while in HCC BCL9 was observed in the nuclei. The study demonstrated that BCL9 might be a marker of shorter disease free survival after curative hepatectomy [81]. Furthermore, DNA copy number analysis in esophageal cancers revealed that more than 50% of the tumors showed gains in 1q21 centered on BCL9 and MUC1 [82]. This indicated that aberrant BCL9 expression might be found in these tumors and might play a role in tumorigenesis. However, there are no reports about BCL9's role in breast cancer pathogenesis.

Regulation of BCL9:

To date there are limited studies on transcriptional regulation of BCL9. At the post transcriptional level, Jia *et al*. demonstrated that BCL9 is regulated by miR-30c-2* in ovarian cancer cell lines. A potent growth factor-like molecule called lysophophatidic acid (LPA) can induce the expression of miR-30c-2* thus reducing cellular proliferation in SKOV-3 and OVCAR-3 cells [83]. Zhao *et al.* demonstrated that BCL9 is regulated by the miR-30 family in multiple myeloma (miR-30a/b/c/d/e) [84]. In addition, Large Tumor Suppressor 2 (LATS 2), a

member of the canonical Hippo signaling pathway, was shown to be a negative regulator of WNT/β-catenin signaling through inhibiting BCL9 recruitment by β-catenin to WNT target gene promoters [85]. These studies suggest that BCL9 may be therapeutically inhibited by targeting upstream modulators of BCL9.

Targeting BCL9:

Targeting β-catenin/BCL9 transcriptional complex is a potential new strategy to inhibit oncogenic WNT signaling. Variable approaches have been explored including stabilized alpha-helix peptides of BCL9, which were shown to inhibit tumorigenicity of colon cancer and multiple myeloma cell lines *in vitro* and *in vivo* [86, 87]. Small molecule compounds such as carnosic acid have been identified to disrupt β-catenin/BCL9 binding [88]. Furthermore, inhibition of BCL9 translation with miRNAs can be used as another approach, since miR-30-5p inhibits BCL9 expression in multiple myelomas [84, 89].

Efforts to block binding of PYGO-BCL9 complex to methylated histone H3 tail have been documented to prevent activation of β-catenin oncogenic signaling. Miller *et al.* utilized nuclear magnetic resonance (NMR) to screen for small molecular inhibitors of PHD-HD1 interaction in the PYGO-BCL9 complex. They identified two benzothiazole compounds that bound to the complex with high ligand affinity, and complementary to Pygo-BCL9 cognate pockets [90].

CHAPTER TWO

Expression Profiling of *In Vivo* Ductal Carcinoma In Situ Progression Models Identified B Cell Lymphoma-9 as a Molecular Driver of Breast Cancer Invasion

2.1. Introduction

Ductal carcinoma in situ (DCIS) is a complex pathologic condition in which malignant breast epithelial cells proliferate inside mammary ducts but do not invade the surrounding stroma. Modern screening technologies have made DCIS a more common diagnosis than in the past, but insufficient understanding of DCIS biology has limited advances in therapy. For example, can a subset of DCIS patients be safely monitored with a "watchful waiting" as has been adopted for certain prostate cancers in men? As it now stands, a large proportion of DCIS cases are over-treated, since it is estimated that, if left untreated, only 25-50% of cases progress to invasive cancer [8, 91, 92]. Given the current understanding of DCIS, it remains challenging to reliably stratify DCIS lesions with appropriate sensitivity and specificity to predict progression to invasion [8]. My first aim for this dissertation *is to identify key molecular mechanisms underlying DCIS progression to IDC,* which is addressed in this and next chapters.

It is generally agreed that the molecular profiles of DCIS and IDC are similar and that the genetic program necessary for invasive progression already exists in the pre-invasive stages of breast cancer [16, 93]. However, there are conflicting reports making this area of research worth further exploration. For example, one study suggested there might be gene dosage changes during the transition from DCIS to IDC [19]. Liao and colleagues found differential genomic copy number aberrations in DCIS with an invasive potential compared to pure DCIS by array comparative genomic hybridization (aCGH) [20]. Another study found amplification of distinct loci restricted to a specific population of cancer cells in 3 of 13 matched DCIS to IDC pairs [94]. Collectively, these latter studies suggest that unique genomic aberrations in some cancer cells or distinct population of cancer cells may drive DCIS to IDC.

Herein, sequential and temporal changes in gene expression during DCIS invasive progression are characterized by utilizing two systems: DCIS cell line-derived mouse intraductal (MIND) xenograft models (SUM225 and DCIS.COM) and a tandem DCIS/IDC model which uses samples from patients afflicted with DCIS that are synchronous with IDC within the same breast. Both models involve DCIS non-invasive to invasive transition and provide valuable tools for studying the temporal molecular changes associated with DCIS invasive transition.

The MIND is a novel DCIS *in vivo* model that has been developed by Dr. Behbod's group [32]. MIND involves injection of DCIS cell lines or cells derived from primary patient DCIS within mammary ducts of immunocompromised mice. MIND xenotransplantation is a realistic human DCIS model because it mimics the entire process of DCIS progression, including ductal growth as *in situ* lesions followed by their invasion as they escape the natural barriers of normal myoepithelial cells and the basement membrane. As previously reported by our group [32], DCIS.COM MIND xenografts generate basal-like lesions and become invasive by 10 weeks post-injection, whereas those generated by SUM225 cells generate HER2 over-expressing luminal lesions that invade the myoepithelial layer by 14 weeks. The second model includes tandem DCIS/IDC lesions. The lesions are identified radiologically by an area of clustered microcalcifications adjacent to (contiguous with) an invasive mass and sampled by core biopsy. For these studies, six pairs were collected and analyzed by RNA sequencing for differential gene expression comparing DCIS to the corresponding IDC.

Molecular profiling of both *in vivo* DCIS progression models revealed a significant increase in BCL9 mRNA and protein expression when comparing non-invasive to invasive lesions in our DCIS cell line MIND xenografts and in five of six DCIS/IDC tandem lesions. BCL9 is a recently

identified WNT pathway activator, which plays an important role in transcriptional activity of β-catenin in association with LEF/TCF family members [95]. BCL9 plays a critical role in progression of colorectal cancers and multiple myeloma by activating WNT oncogenic signaling [78]. However, the role of BCL9 in mammary gland biology and breast cancer has not been explored previously. In this chapter, we propose that there is evidence that BCL9 serves as a molecular driver of EMT and DCIS invasion by enhancing canonical WNT signaling. Therefore, BCL9 may serve as a potential therapeutic target for prevention of IDC.

2.2. Materials and Methods

Animals and animal surgeries: Mouse surgeries were performed on 8- to 10-week-old virgin female NOD-SCID IL2Rgamma^{null} (NSG) mice that were either bred or purchased from Jackson Laboratories (Bar Harbor, ME, USA) as previously described [32]. Animal experiments were conducted following protocols approved by the University of Kansas School of Medicine Animal Care.

Cell culture: DCIS.COM and SUM225 were purchased from Asterand, Inc. (Detroit, MI) in 2007 and were maintained according to the supplier's guidelines. Both cell lines have been authenticated by genomic profiling validating the ER$^-$/PR$^-$/HER2$^+$ status of the SUM225 cells and the ER$^-$/PR$^-$/HER2$^-$ expression pattern in the DCIS.COM [96].

Tandem lesions biopsies: All human experiments were approved by the University of Kansas Medical Center Institutional Review Board (IRB). All patients gave written informed consent for participation in this research. Recruits included patients undergoing image-guided core needle biopsy due to suspicion of DCIS or IDC. In all cases, research specimens were obtained only after acquisition of diagnostic specimens. Our radiologists applied minimally

invasive ultrasound guided selective tissue harvest of contiguous lesions with a “tandem” appearance and provided us with biopsy cores from each region. Biopsy tissue was placed in preservation media (LiforCell, *Life*blood Medical, Inc., Freehold, NJ) and stored at 4°C on ice until RNA isolation.

RNA Isolation, Quantitative PCR (qPCR): Total RNA was isolated with miRNeasy Mini Kit (Qiagen #217004) using the manufacturer's protocol, and cDNA was synthesized from 250 ng of total RNA with miScript Reverse Transcription Kit (Qiagen #218061). TaqMan® Gene Expression Master Mix (Applied Biosystems #4369016) and TaqMan® Gene Expression assays were used. Primers specific for human BCL9 (Applied Biosystems #Hs00979216_m1) were utilized and target gene expression was normalized to human β-actin (Applied Biosystems #Hs99999903_m1). The standard curve method was used for quantification. Reactions were performed in the StepOnePlus™ Real-Time PCR System [97].

Statistical analysis: Data are presented as mean normalized expression ± s.e.m. Unless otherwise noted, one-way analysis of variance (ANOVA) was used for statistical comparisons. A value of $P \leq 0.05$ was considered significant.

Microarray gene expression profiling and analysis: We utilized DCIS MIND models, a novel model developed in our laboratory which most closely mimics the human DCIS environment, with both SUM225 and DCIS.COM cell lines to characterize sequential and temporal changes in mRNA expression over a time course of 2, 6, and 10 weeks during *in vivo* progression in the epithelial cells. Microarray technology was utilized to analyze gene expression profiles from RNA isolated from magnetically sorted epithelial cells from MIND xenografts at 2, 6 and 10 weeks post-injection. For these studies, five mice per replicate (3 replicates) per time

point (3 time points; 2, 6, and 10 weeks) for each cell line (two cell lines; DCIS.COM and SUM225) were used. The mammary epithelial cells were magnetically sorted from five mice at each time point per replicate. After sorting, Qiazol extraction of total RNA was performed according to the manufacturer's instructions. Labeling was performed using the GeneChip 3' IVT Express Kit (Affymetrix) which utilizes an oligo dT based reverse transcription reaction followed by a T7 promoted in-vitro transcription biotin labeling reaction. Hybridization was performed using the GeneChip Hybridization, Wash and Stain Kit (900720). Platform used was [HG-U133_Plus_2] Affymetrix Human Genome U133 Plus 2.0 Array. GeneChips were scanned using the Affymetrix GeneChip Scanner 3000 7G. Raw mRNA expression values from the 2, 6 and 10 week samples were normalized and converted to the log2 scale. Data was median-centered and analyzed by unsupervised average-linkage hierarchical clustering using Cluster 3.0 software (http://bonsai.hgc.jp/~mdehoon/software/cluster/cluster3.pdf). The computed data matrix was then uploaded into Java TreeView software and visualized as heatmaps (http://bonsai.hgc.jp/~mdehoon/software/cluster/software.htm#ctv). Clustering of expression data from DCIS.COM and SUM225 cell lines revealed that the majority of expression changes had already occurred at the 6-week time point with few changes occurring from 6 to 10 weeks. This suggests that mechanisms of invasion are already in place by 6 weeks. Further analysis focused on the 2 to 6 week time-frame.

Significance analysis for microarrays (SAM) software was utilized to determine differentially expressed genes between the 2 to 6 week time-point in both DCIS.COM and SUM225 cell lines (http://statweb.stanford.edu/~tibs/SAM). The cut-off for significance was determined by <5% false-discovery rate. Two-class unpaired SAM analysis generated a list of significant genes and fold-change values between 2 and 6 weeks in DCIS.COM (18,590 down regulated; 10,227 up-

regulated) and SUM225 (19,953 down regulated and 14,691 up-regulated). These genes were further analyzed using QIAGEN's Ingenuity® Pathway Analysis (IPA®, QIAGEN Redwood City,www.qiagen.com/ingenuity). IPA software integrates expression changes with known molecular interactions and disease processes (http://www.ingenuity.com). The WNT/β-catenin canonical pathway was identified as a significantly upregulated pathway in both cell line-MIND xenografts during transition from 2 to 6 weeks. The raw and analyzed microarray data have been deposited in NCBI's Gene Expression Omnibus [21] and are accessible through GEO Series accession number: GSE65890 (http://www.ncbi.nlm.nih.gov/geo/query/acc.cgi?acc=GSE65890) [21, 22].

RNA Sequencing & Analysis: Total RNA was prepared using (All prep Qiagen Kit) according to the manufacturer's protocol. Libraries were prepared by illumina TruSeq RNA Sample Preparation Kit (A cat#FC-122-1001, B cat#FC122-1002) according to the manufacturer's protocol. The DCIS and IDC samples were sequenced using a HiSeq2500 2x100bp version 3 sequencing run. Eight sample libraries were multiplexed 4 per lane resulting in 46.9X – 58.2X coverage per sample. Four sample libraries were multiplexed 2 per lane resulting in 107.4X – 124X coverage per sample. Paired Fastq sequence files were imported to CLC Genomics Workbench (version 7.5) and mapped to the human reference genome (hg19) using approach previously described [98]. Ensembl database (GRCh37.74.gtf) was used for gene annotation. Total number of reads mapped to the gene was used as the total counts for the gene, and the values were transformed by adding 1 followed by log2 transformation. Transformed data was quantile normalized before analyzing differential gene expression between two groups (DCIS vs IDC). Empirical analysis of differential gene expression was performed between two groups (DCIS vs IDC) using 'Exact Test' as previously described [99].

Raw and analyzed RNA sequencing data were deposited in NCBI's Gene Expression Omnibus [21] and are accessible through GEO Series accession number: GSE66301 (http://www.ncbi.nlm.nih.gov/geo/query/acc.cgi?acc=GSE66301) [21, 22].

Immunofluorescence staining (IF): IF was performed as previously described [33]. Antibodies are listed in Table 2.1. Nuclei were counterstained with 4′,6-diamidino-2-phenylindole (DAPI; Vector Laboratories, # H-1200). Negative controls were carried out using secondary antibodies without primary antibodies. Imaging was performed on a laser-scanning confocal microscope (Model 510; Carl Zeiss MicroImaging, Inc, Thornwood, NY, USA). The acquisition software used was Pascal (Carl Zeiss MicroImaging, Inc). Fluorescence quantitation and analysis was done using imageJ (http://imagej.nih.gov/ij/). Images were analyzed for area of selection, mean gray value, and integrated density. Both the areas of interest and their background were measured, then the corrected total cell fluorescence (CTCF) was calculated by the following formula: CTCF = Integrated Density – Area of selected cells X Mean fluorescence of background readings.

Plasmids, Transfection, and Luciferase Reporter Assay: Plasmid constructs: pSuper8X–TOPFlash reporter (Addgene plasmid 12456) and Super 8x FOPFlash (TOPFlash mutant) (Addgene plasmid 12457) were provided by Randall Moon via Addgene [100]. Renilla luciferase plasmid phRG was from Promega. The β-catenin∆N (Addgene plasmid 19288) construct was acquired from Eric Fearon via Addgene [101]. PCDH-BCL9 (BCL9-OE), PLKO.1-BCL9-shRNA (BCL9-KD) (CCTCTGTTGAATATCCCTGGAA) and PLKO.1-non-silencing control (Control) were acquired from Dr. Carrasco [78]. pGIPZ Human BCL9 shRNA (BCL9 KD 2) (TGCAAACTTGGACATTCGA), and pGIPZ-non-silencing control (Control 2) obtained from Dharmacon (#RHS4430-200265260). Transfection: DCIS.COM and SUM225 were transfected

with electroporation using Amaxa ™ Cell line Nucleofector kit V (Lonza #VCA-1003), while HEK293T cells were transfected using Lipofectamine 2000 reagent (Invitrogen #11668-027) according to manufacturer's protocols. Luciferase assay was performed using Dual-Luciferase® Reporter Assay System (Promega #E1910).

Lentivirus production: Glycerol stocks of pLKO.1 shRNA-based BCL9 and PLKO.1 non-silencing control were cultured with 100 μg/ml of ampicillin (Amresco # 0339) and plasmids were purified using HiSpeed Plasmid midi kit (Qiagen #12643). Preparation of viral particles was performed by co-transfecting individual pLKO.1 vectors (10 μg), packaging plasmid pCMV-dR8.2 (contains Gag, Pol, Rev, and Tat) (Addgene plasmid 8455; 5 μg), and the envelope plasmid pCMV-VSVG (Addgene plasmid 8454; 5 μg) in HEK293T cells. Both plasmids were acquired from Robert Weinberg via Addgene [102]. Transfection was performed in a 10 cm plate, nearly 75% confluent using Lipofectamine 2000 transfection reagent (Invitrogen #11668-027) in antibiotic free Opti-MEM media (Invitrogen #51985-034) following manufacturer's protocol. Media was collected after 48, 72, and 96 h of transduction, pooled and subjected to ultracentrifugation at 80,000 x g for 2 hours (Beckman Coulter, Optima L-100 XP, 70Ti rotor) at room temperature. Pellets of the concentrated viral particles were re-suspended in 250 μl of DMEM (GIBCO #21063029), and stored in aliquots at -80^{o}C until further use. Lentiviral titers were measured using Lenti-X^{TM} p24 Rapid Titer kit (Clontech #632200). Transduction was performed at an MOI of 3 and 20 for DCIS.COM and SUM225, respectively, and cells continued to grow in the presence of puromycin (Thermo Scientific #100552). For various experiments, transduced cells from up to 5 passages were used.

MTS, invasion and migration assays: For MTS assays, Cell Titer 96® Aqueous Non-Radioactive Cell Proliferation Assay (Promega #G5421) was used according to the manufacturer's protocol. Transwell assays were used to measure invasion and migration. The upper and underside of the transwells (Corning #3422) were coated with Corning™ Matrigel™ Membrane Matrix (Fisher Scientific #CB-40230) (1mg/ml in serum free media) for the invasion assay, and with Corning ™ Human Fibronectin (Fisher scientific #CB-40008) (50 μg/ml PBS/0.1% gelatin) for migration assay. DCIS.COM and SUM225 cells were starved of serum for 24 h prior to use. Cells were irradiated at 10 gray and 2.5×10^4 cells were plated in serum free media in the upper well. Percent area of migration and invasion were analyzed in DCIS.COM and SUM225 cells after 24 and 96 hours, respectively. Invasion and migration were determined by ImageJ (http://imagej.nih.gov/ij/) analysis of microscopic images.

For *in vivo* invasion studies, BCL9-KD, non-transduced (NT), and scrambled shRNA control (control) SUM225 and DCIS.COM cells were injected at 10,000 cells per gland. A total of 3 glands and 3 animals in control groups, 5 glands and 4 animals in KD groups and 4 glands in 4 animals in NT groups were examined. Glands were collected at 10 and 14 weeks post-intraductal injection in DCIS.COM and SUM225 xenografts, respectively. Mammary glands containing DCIS-like lesions were then fixed, embedded and sectioned at 5 μm. Every 10^{th} section was stained with H&E to identify sections with the greatest xenograft growth for each gland. Then 4 sections adjacent (2 sections on each side) to the one with the greatest growth were prepared for IF as described above, stained for human-specific K5/K19, SMA and counterstained with DAPI. Imaging was performed as described above. Invasive lesions were identified by the lack of a SMA-expressing myoepithelial layer. LSM image browser was used to measure the maximum distance of an invasive lesion to the closest DCIS lesion in each section. To determine the

number of invasive lesions per section, confocal images (20x magnification) were taken of all invasive lesions and counted. Measurements (i.e.distance of invasion and number of invasive lesions) for the 4 sections were averaged to represent each gland. Data were presented as the maximum distance of invasion (μm) and number of invasive areas in each section.

Western blot analysis and co-immunoprecipitation: For co-immunoprecipitation, 1000 μg of protein was incubated with antibodies at 4^{o}C overnight followed by centrifugation at 3000 rpm for 1 min in 4^{o}C. Supernatants were incubated with Protein A/G PLUS-Agrose beads (Santa Cruz #sc-2003) at 4°C for 1 hour, followed by a wash in PBS. Proteins bound to the beads were eluted with SDS-loading buffer at 99°C for 5 min and then loaded for western blot, and 2μg of whole cell lysates were loaded as input. Western blots analysis was carried out as previously described [103]. For western blots, 25 μg of DCIS.COM and 50 μg of SUM225 cell lysates were loaded into each lane. Antibodies used are listed in **Table 2.1**.

FACS analysis and magnetic sorting: Cells were stained at a final concentration of 1:20 for 30 min on ice followed by washes in Hanks' Balanced Salt Solution (Invitrogen #24020-117) containing 2% fetal bovine serum. Antibodies used are listed in **Table 2.1**. FACS and data analysis were performed using the BD LSR II flow cytometer and FlowJo software (Tree Star). Magnetic sorting was performed using Easy Sep® human Epcam positive selection kit (Stem Cell Technology #18356) according to the manufacturer's protocol.

	Company	Catalog #	Isotype
IF staining			
Primary antibodies			
BCL9	Abcam	37305	Rabbit
BCL9L	Abcam	113110	Rabbit
Cytokeratin 5	Vector	VPC400	Mouse
Cytokeratin 19	Thermoscientific	MS198	Mouse
SMA	Thermoscientific	PA5-18292	Goat
Phospho-histone3	Abcam	ab47297	Rabbit
Cleaved caspase 3	Cell signaling	9664S	Rabbit
Secondary antibodies			
Alexa Fluor 488 anti-rabbit	Invitrogen	A11008	Goat
Alexa Fluor 594 anti-mouse	Invitrogen	A21203	Donkey
Alexa Fluor 488 anti-mouse	Invitrogen	A11012	Goat
Co-immunoprecipitation			
IgG	Cell signaling	2729S	Rabbit
BCL9	Santa Cruz	sc-68915	Rabbit
Western blot analysis			
BCL9	Abcam	37305	Rabbit
β-catenin	BD	610153	Mouse
β-actin	Chemicon	MAB1501	Mouse
BCL9L	Abcam	113110	Rabbit
FACS analysis			
Human CD44 (PE)-conjugated	BD Pharmingen	555479	
Human CD24 (FITC)-conjugated	BD Pharmingen	555427	

Table 2.1. List of antibodies and sources for use in immunofluorescence staining, co-immunoprecipitation, Western analysis, and FACS analysis.

2.3. Results:

BCL9 up-regulation is associated with DCIS epithelia that progress to invasion. To explore the temporal molecular changes associated with DCIS non-invasive to invasive transition, DCIS cell line MIND models as well as DCIS/IDC tandem lesions were utilized. Mammary glands containing DCIS-like lesions were excised followed by digestion to isolate epithelial cell components at three time points: 2, 6 and 10 weeks post injection. These time points were selected in order to accurately reflect the molecular changes, as the DCIS lesions are formed between 2-6 weeks and progress past the myoepithelial layer and the basement membrane by 10 weeks, **Figure 2.1**. To separate human DCIS epithelial cells from mouse mammary cells, EpCAM-positive cells were magnetically sorted followed by RNA isolation and microarray analysis. The majority (>90%) of DCIS.COM and SUM225 cells express EpCAM, **Figure 2.2**. Additionally, we performed RNA sequencing of patient DCIS/IDC tandem lesion pairs. A heatmap of analyzed MIND xenograft microarray data is shown in **Figure 2.3**.

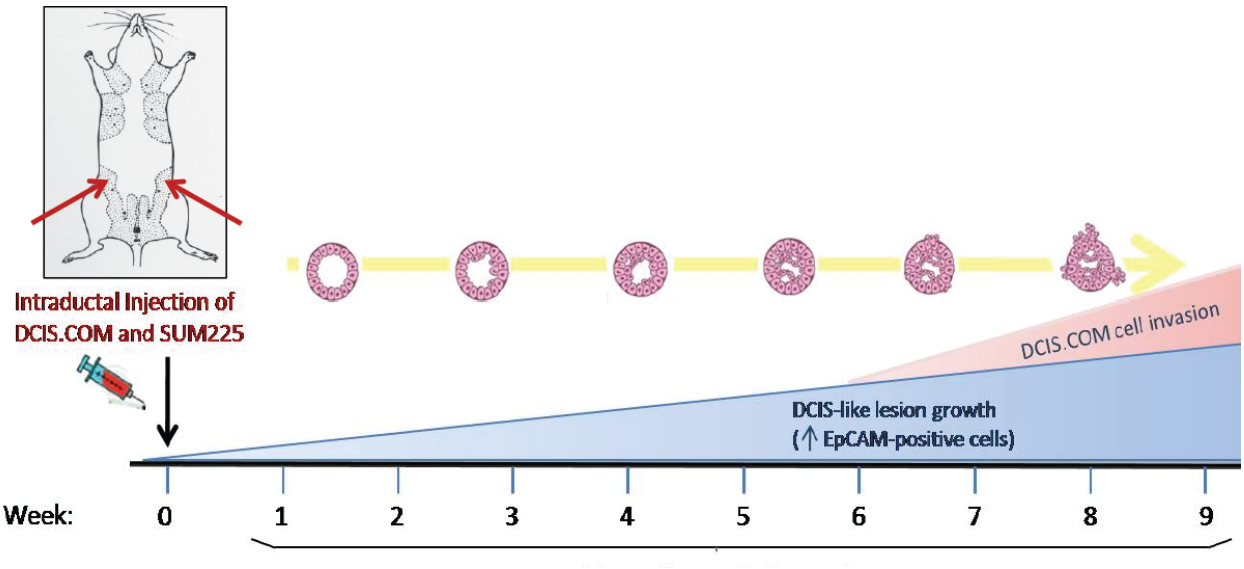

Figure 2.1. A figure depicting the MIND model. MIND xenografts were generated by intraductal injection of DCIS.COM and SUM225 cells into the mammary ducts of immunocompromised mice. Mammary glands containing DCIS-like lesions were collected at the distinct stages of in situ to invasion (2, 6 and 10 weeks) followed by digestion, magnetic sorting of epithelial cells and RNA isolation. RNA was subjected to microarray analysis.

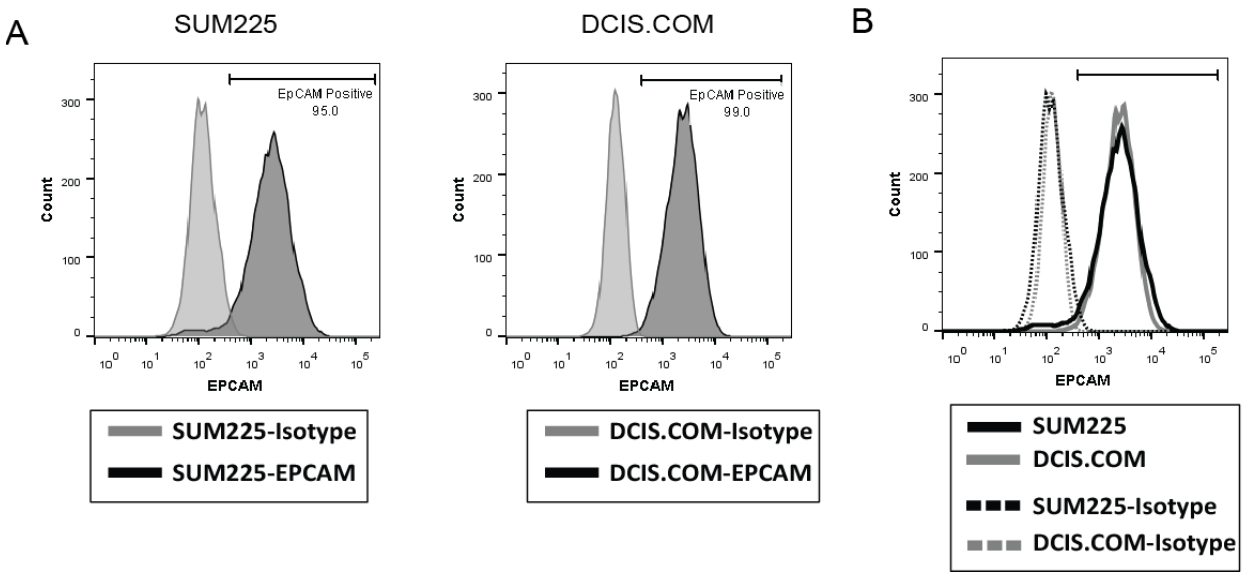

Figure 2.2. The majority of SUM225 and DCIS.COM cells are EPCAM-positive by flow analysis. Representative flow analysis of (A) SUM225 (left) and DCIS.COM cells (right) for EpCAM (black line) compared to isotype control (grey line) show that 95% of SUM225 cells and 99% of DCIS.COM cells are EPCAM positive. (B) Histogram overlaying SUM225 and DCIS.COM EPCAM positive cells.

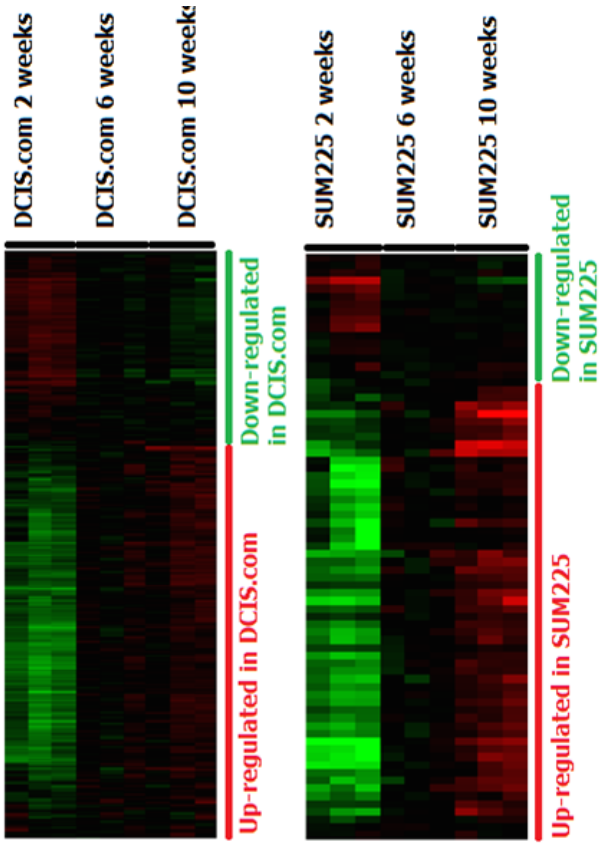

Figure 2.3. Differentially expressed genes in DCIS.COM and SUM225 MIND xenografts. (A) (B) Heatmap of differentially expressed genes in DCIS.COM and SUM225 MIND xenografts at 2, 6 and 10 weeks. Unsupervised average-linkage hierarchical clustering of expression data from DCIS.COM and SUM225 MIND xenografts revealed that the majority of expression changes occurred at the 2 to 6-week time point with few changes occurring from 6 to 10 weeks.

The analysis was focused on canonical WNT signaling since a recent report by Scheel and colleagues demonstrated that the collaboration of three signaling pathways, TGF-β, canonical and non-canonical WNT signaling induced and maintained an EMT state in mammary epithelial cells [66]. Acquisition of an EMT-like phenotype is believed to be the initiating event prior to cell invasion. An EMT-like phenotype can result from aberrant basal differentiation program in differentiated luminal/epithelial cells or in stem/progenitor cells [104]. Furthermore, this study showed that pre-treatment of epithelial cells with WNT activators followed by TGF-β and down regulation of E-cadherin resulted in a synergistic enhancement in EMT and cellular migration. These data suggest that WNT signaling is the earliest event in the process of EMT and cellular invasiveness. A candidate gene in the canonical WNT signaling pathway, B cell lymphoma-9 (BCL9), was selected since it was found to serve as a co-factor of β-catenin in early 2000 [71][71]; however, there were no previous studies on the role of BCL9 in breast cancer. BCL9 is located on chromosome 1q21, a common amplified region in breast cancer [105]. Analysis of microarray data from MIND samples showed canonical WNT signaling to be among the significantly upregulated pathways in our dataset (**Figure 2.4**, **Table 2.3 and 2.4**), BCL9 was significantly upregulated in the transition from DCIS to IDC (q value <5%) (**Figure 2.4**). BCL9 expression was assessed in six pairs of DCIS/IDC tandem lesions by RNA sequencing. Tandem DCIS/IDC are defined as DCIS lesions that have concurrent IDC within the same breast (**Figure. 2.5**). The analysis of tandem lesions' RNA sequencing data for BCL9 expression comparing DCIS to IDC is shown in (**Figure. 2.6**). This analysis showed a significant upregulation in BCL9 expression in the IDC component compared to DCIS (**Figure. 2.6**).

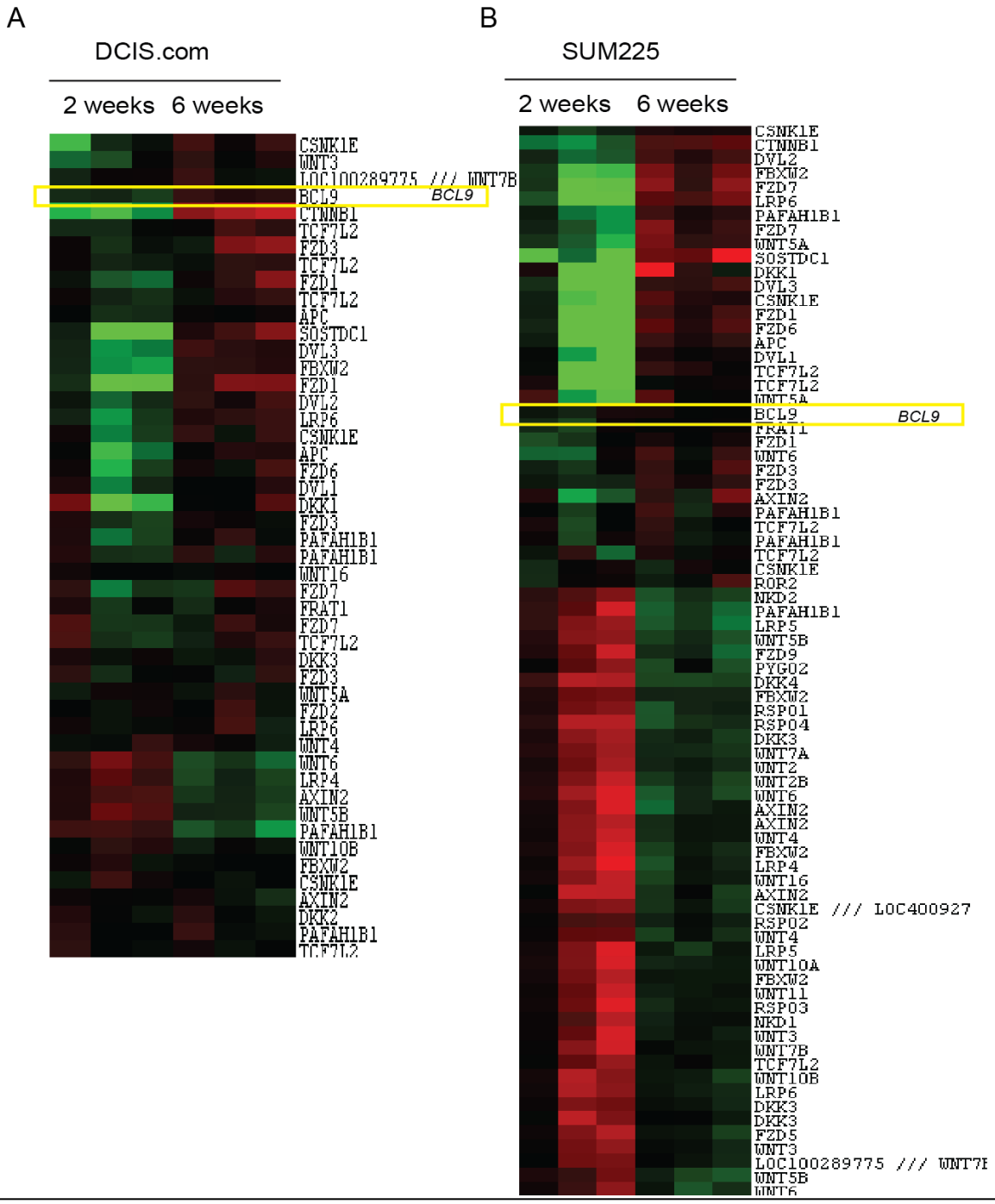

Figure 2.4. Differentially expressed Wnt genes in DCIS.COM and SUM225 MIND xenografts. (A) (B) Heatmap of differentially expressed genes in the canonical Wnt pathway from 2 to 6 weeks in DCIS.COM (A) and SUM225 (B) MIND xenografts. Unsupervised average-linkage hierarchical clustering was used to visualize significantly up or down-regulated genes in the WNT pathway, using a cut off of <5% false-discovery rate.

Table 2.2 Significant differentially expressed WNT genes in DCIS.COM			
Gene Symbol	Probeset ID	Fold Change	q-value(%)
APC	203525_s_at	**2.181328**	**0**
APC	216933_x_at	**1.486683**	**0**
BCL9	204129_at	**1.868612**	**0**
CSNK1E	225756_at	**2.220647**	**0**
CTNNB1	223679_at	**5.370228**	**0**
DVL2	57532_at	**1.9175**	**0**
DVL3	201908_at	**2.35002**	**0**
FBXW2	235195_at	**2.415927**	**0**
FZD1	204451_at	**4.327389**	**0**
FZD1	204452_s_at	**2.212632**	**0**
FZD3	227499_at	**1.919654**	**0**
LRP6	225745_at	**2.14176**	**0**
SOSTDC1	213456_at	**5.450216**	**0**
TCF7L2	216035_x_at	**1.533357**	**0**
TCF7L2	212761_at	**1.706515**	**0**
TCF7L2	216037_x_at	**1.583251**	**0**
WNT3	229103_at	**1.804226**	**0**
WNT5A	231227_at	**1.307759**	**0**
WNT6	71933_at	**0.672037**	**0**
CSNK1E	226858_at	**1.871161**	**1.493429**
FBXW2	241736_at	**1.219233**	**1.493429**
FZD2	210220_at	**1.374081**	**1.493429**
FZD3	227524_at	**1.470612**	**1.493429**
FZD6	203987_at	**1.953449**	**1.493429**
LOC100289775 / WNT7B	217681_at	**1.385542**	**1.493429**
LRP6	34697_at	**1.381827**	**1.493429**
PAFAH1B1	200816_s_at	**1.695291**	**1.493429**
WNT16	224022_x_at	**1.257333**	**1.493429**
AXIN2	222695_s_at	**0.812279**	**1.929012**
LRP4	212850_s_at	**0.793273**	**1.929012**
PAFAH1B1	200815_s_at	**0.662306**	**1.929012**
WNT5B	223537_s_at	**0.78629**	**2.805836**
DVL1	203230_at	**1.628244**	**2.893519**
FZD7	203705_s_at	**1.729794**	**3.858025**
PAFAH1B1	211547_s_at	**1.482621**	**3.858025**
WNT10B	206213_at	**1.087355**	**3.858025**
AXIN2	222696_at	**1.194988**	**4.822531**
CSNK1E	222015_at	**1.154453**	**4.822531**
DKK1	204602_at	**2.476747**	**4.822531**

DKK2	219908_at	**1.283061**	**4.822531**
DKK3	221127_s_at	**1.25915**	**4.822531**
FRAT1	219889_at	**1.310318**	**4.822531**
FZD3	219683_at	**1.325252**	**4.822531**
FZD7	203706_s_at	**1.448601**	**4.822531**
PAFAH1B1	200813_s_at	**1.280911**	**4.822531**
TCF7L2	216511_s_at	**1.442822**	**4.822531**
TCF7L2	212759_s_at	**1.225253**	**4.822531**
WNT4	1556689_a_at	**1.205825**	**4.822531**

Table 2.3 Significant differentially expressed WNT genes in SUM225

Gene Symbol	Probeset ID	Fold Change	q-value(%)
APC	203525_s_at	**6.057196**	**0**
APC	216933_x_at	**2.169045**	**0**
BCL9	204129_at	**1.323798**	**0**
CSNK1E	226858_at	**3.687441**	**0**
CSNK1E	225756_at	**1.577529**	**0**
CSNK1E	222015_at	**1.230732**	**0**
CTNNB1	223679_at	**2.762147**	**0**
DKK1	204602_at	**11.25073**	**0**
DKK3	230508_at	**0.664939**	**0**
DKK4	206619_at	**0.526069**	**0**
DVL1	203230_at	**2.73491**	**0**
DVL2	57532_at	**2.135484**	**0**
DVL3	201908_at	**7.646926**	**0**
FBXW2	235195_at	**3.579538**	**0**
FBXW2	241736_at	**0.76398**	**0**
FRAT1	219889_at	**1.426774**	**0**
FZD1	204451_at	**5.947582**	**0**
FZD1	204452_s_at	**1.556699**	**0**
FZD3	227499_at	**1.661159**	**0**
FZD3	219683_at	**1.659379**	**0**
FZD6	203987_at	**12.95946**	**0**
FZD7	203705_s_at	**2.378315**	**0**
FZD7	203706_s_at	**4.391103**	**0**
LRP5	229591_at	**0.551967**	**0**
LRP6	225745_at	**4.805578**	**0**
NKD2	232201_at	**0.672158**	**0**
PAFAH1B1	200816_s_at	**2.173113**	**0**
PAFAH1B1	200815_s_at	**0.541757**	**0**
ROR2	205578_at	**1.371724**	**0**

RSPO1	241450_at	**0.697006**	**0**
RSPO4	237423_at	**0.562388**	**0**
SOSTDC1	213456_at	**5.66075**	**0**
TCF7L2	212761_at	**5.207148**	**0**
WNT2B	206459_s_at	**0.619857**	**0**
WNT5A	213425_at	**2.623568**	**0**
WNT5B	223537_s_at	**0.626067**	**0**
WNT6	71933_at	**0.534937**	**0**
WNT6	221609_s_at	**1.902601**	**0**
WNT7A	210248_at	**0.67367**	**0**
AXIN2	224498_x_at	**0.701802**	**1.399177**
AXIN2	224176_s_at	**0.604779**	**1.399177**
AXIN2	222695_s_at	**0.634325**	**1.399177**
AXIN2	222696_at	**1.99963**	**1.399177**
CSNK1E /// LOC400927	234943_at	**0.716845**	**1.399177**
FBXW2	218941_at	**0.63113**	**1.399177**
FZD5	206136_at	**0.704201**	**1.399177**
FZD9	207639_at	**0.613408**	**1.399177**
LRP4	212850_s_at	**0.606795**	**1.399177**
LRP5	209468_at	**0.664687**	**1.399177**
LRP6	205606_at	**0.710998**	**1.399177**
PYGO2	239666_at	**0.724729**	**1.399177**
TCF7L2	212762_s_at	**3.431922**	**1.399177**
WNT10A	223709_s_at	**0.668815**	**1.399177**
WNT10B	206213_at	**0.681931**	**1.399177**
WNT16	221113_s_at	**0.669338**	**1.399177**
WNT2	205648_at	**0.720831**	**1.399177**
WNT4	230751_at	**0.686089**	**1.399177**
WNT5B	221029_s_at	**0.736215**	**1.399177**
FBXW2	1560752_at	**0.743755**	**1.499118**
PAFAH1B1	211547_s_at	**1.467588**	**1.499118**
RSPO3	228186_s_at	**0.693411**	**1.499118**
WNT4	1556689_a_at	**0.796031**	**1.499118**
WNT6	222086_s_at	**0.751168**	**1.499118**
WNT5A	205990_s_at	**2.160168**	**1.967593**
TCF7L2	216037_x_at	**1.401197**	**2.698413**
DKK3	214247_s_at	**0.810754**	**2.73752**
WNT11	206737_at	**0.746879**	**2.73752**
WNT3	221455_s_at	**0.735102**	**2.73752**
WNT3	231743_at	**0.79694**	**2.73752**
WNT7B	238105_x_at	**0.727763**	**2.73752**

DKK3	221126_at	**0.785168**	**3.881279**
LOC100289775 /// WNT7B	217681_at	**0.837705**	**3.881279**
NKD1	1553115_at	**0.795197**	**3.881279**
PAFAH1B1	200813_s_at	**1.331175**	**3.881279**
TCF7L2	216511_s_at	**1.405792**	**3.881279**
RSPO2	1554012_at	**0.905963**	**4.088504**
TCF7L2	236094_at	**0.844567**	**4.088504**

Table 2.2. and 2.3 WNT pathway specific genes differentially expressed in DCIS.COM and SUM225 MIND xenografts during transition from 2 to 6 weeks. Significant differentially expressed genes between the 2 to 6 week time-point in both DCIS.COM and SUM225 cell lines were further analyzed using QIAGEN's Ingenuity Pathway Analysis® (IPA). The WNT/β-catenin canonical pathway was identified as a significantly upregulated pathway in both cell lines MIND xenografts during transition from 2 to 6 weeks.

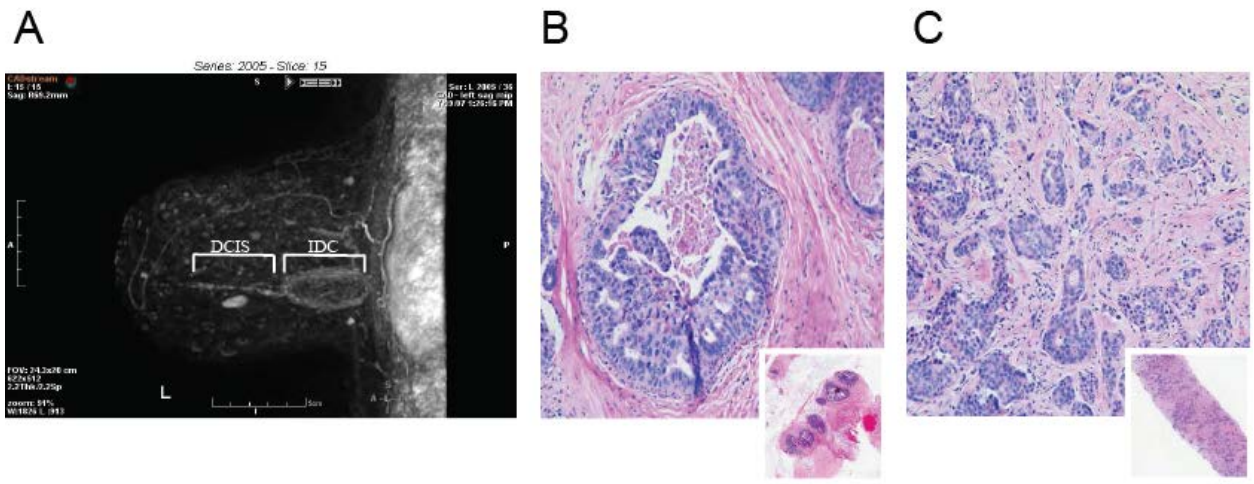

Figure 2.5. Radiographic (A) and H&E stain (B & C) images of a patient's DCIS/IDC tandem lesion. A: 3-D ultrasound image of a tandem lesion. (B) H&E of a biopsy taken from the DCIS and (C) the IDC regions. Insets: Lower magnification of B. & C. respectively, demonstrating that the biopsies were highly pure and composed of either DCIS or IDC.

A

Tandem Lesion Pair	DCIS	IDC
1	9.3	11
2	10.21	10.92
5	9.58	9.93
4	9.9	12.42
3	8.61	9.62
12	10.01	9.59

B

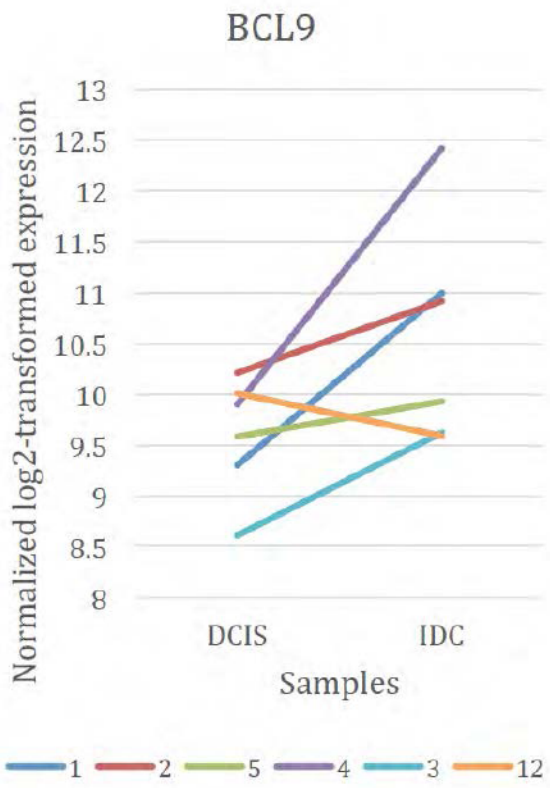

Figure 2.6. BCL9 expression in DCIS/IDC tandem samples. Normalized log2-transformed expression of BCL9 was plotted and tandem lesions between paired DCIS and IDC are connected by a line to indicate their relationship. The results indicate a significant increase in BCL9 expression in IDC samples compared to the DCIS lesions (*P*=0.01).

To confirm the microarray analysis, RT-qPCR was performed on EpCAM-positive cells sorted from an independent set of DCIS cell line MIND xenografts as they progressed from 2 to 10 weeks. BCL9 gene expression showed a significant increase at 10 compared to 2 weeks in both SUM225 and DCIS.COM MIND xenografts (62 ± 14 and 35 ± 12 -fold increase, respectively; mean ± s.e.m, $P<0.05$) (**Figure 2.7**). Furthermore, immunofluorescence (IF) staining of the MIND xenografts demonstrated increased nuclear BCL9 expression as DCIS lesions progressed to invasion (**Figure. 2.8**). There have been a few reports on the role of BCL9L (BCL9-2 or B9L), BCL9 homolog, in breast cancer. One study showed nuclear BCL9L expression to be significantly associated with high nuclear grade and expression of HER2 in breast cancers [106]. Another study reported that BCL9L induced ER positive breast cancers *in vivo* by regulating expression of ER through a ß-catenin independent mechanism and predicted therapeutic response to tamoxifen [107]. Human *BCL9* and its homolog *BCL9L* reside on chromosome 1q21 and 11q23.3, respectively. Both BCL9 and BCL9L function as co-activators of β-catenin-LEF/TCF mediated transcription [108]. Expression patterns of BCL9 and BCL9L were compared in DCIS cell line MIND xenografts as well as on tissue sections obtained from 23 DCIS with IDC patients and 14 pure DCIS patients. As shown in **Figure. 2.9**, BCL9L expression was mainly cytoplasmic, while BCL9 expression was primarily nuclear. Furthermore, RT-qPCR showed no significant increase in BCL9L expression in DCIS MIND xenografts during invasive transition from 2 to 10 weeks (**Figure 2.10**). A Western blot on cell lysates obtained from DCIS cell lines also showed no change in BCL9L expression with BCL9 KD (**Figure 2.10**). Therefore, results in both MIND and tandem lesions support the hypothesis that increased BCL9 expression is associated with DCIS transition to invasion, while the data do not show a change in BCL9L expression associated with DCIS progression.

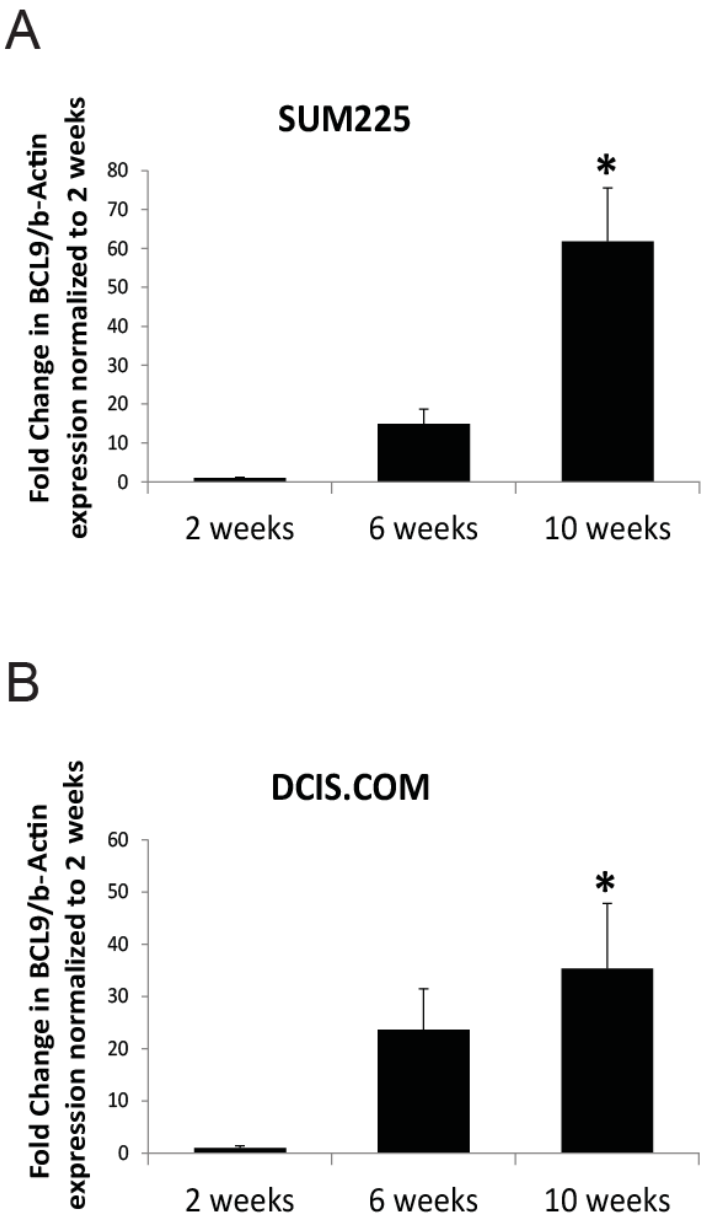

Figure 2.7. RT-qPCR of BCL9 in EpCAM-positive epithelial cells sorted from SUM225 (A) and DCIS.COM (B) MIND xenografts at 2, 6, and 10 weeks post-intraductal injection. Bar graphs represent fold change normalized to 2 weeks. Data are mean values ± s.e.m (n=3, *P<0.05).

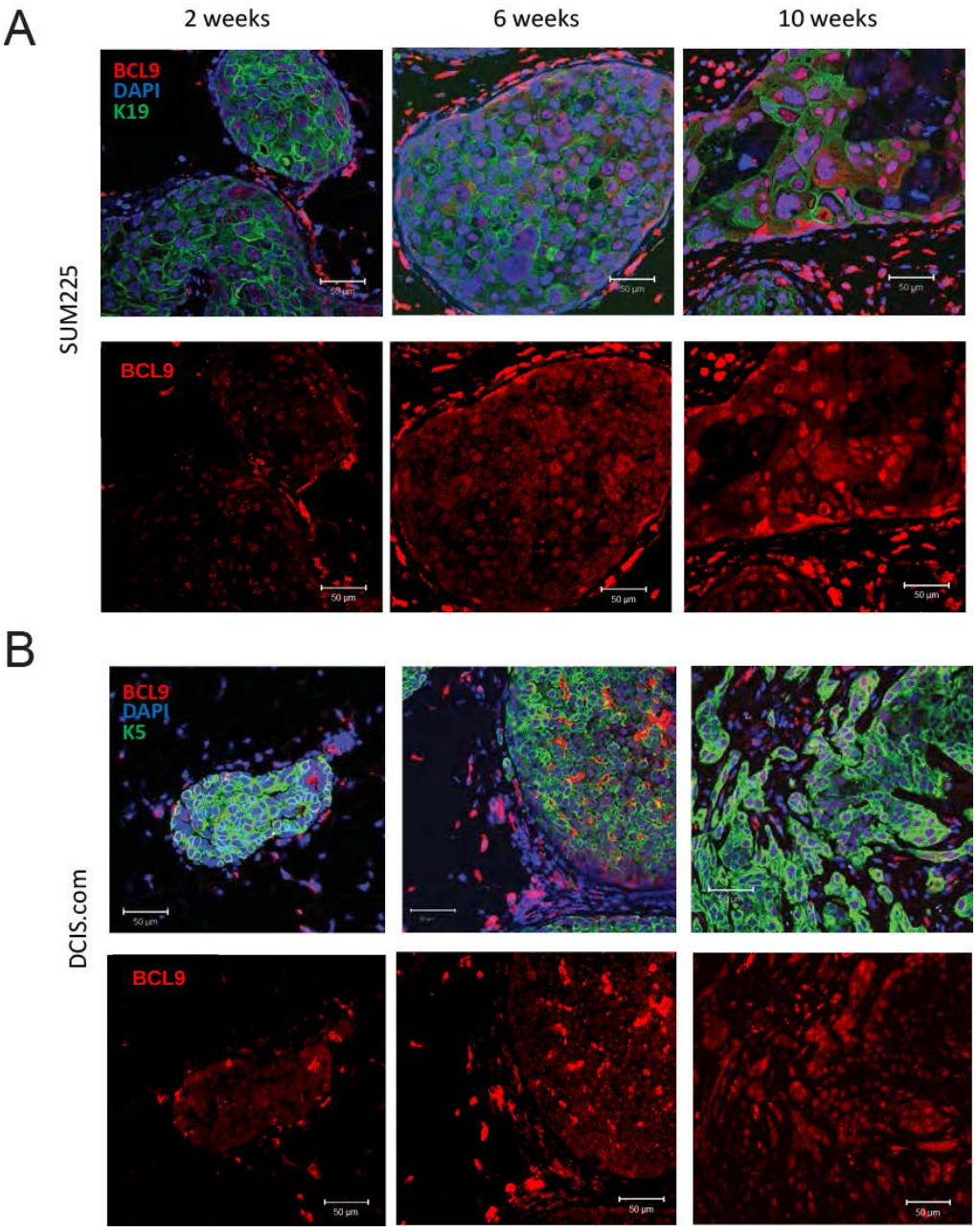
A
2 weeks
6 weeks
10 weeks
SUM225
BCL9
DAPI
K19
BCL9
B
DCIS.com
BCL9
DAPI
K5
BCL9

Figure 2.8. Enhanced BCL9 nuclear expression in DCIS cell line MIND xenografts that progress to invasive lesions. IF staining of BCL9, K5/K19, and DAPI in SUM225 (A) and DCIS.COM (B) MIND xenografts at 2, 6, and 10 weeks post-intraductal injection, merged channels are shown in the upper panels and BCL9 only channels are shown in the lower panel. BCL9 is conjugated to Alexa-Fluor 594, shown in red, and keratin 5/keratin 19 are conjugated to Alexa-Fluor 488, shown in green. Nuclei are counterstained with DAPI. Scale bars are 50 μm; 40x objective was used.

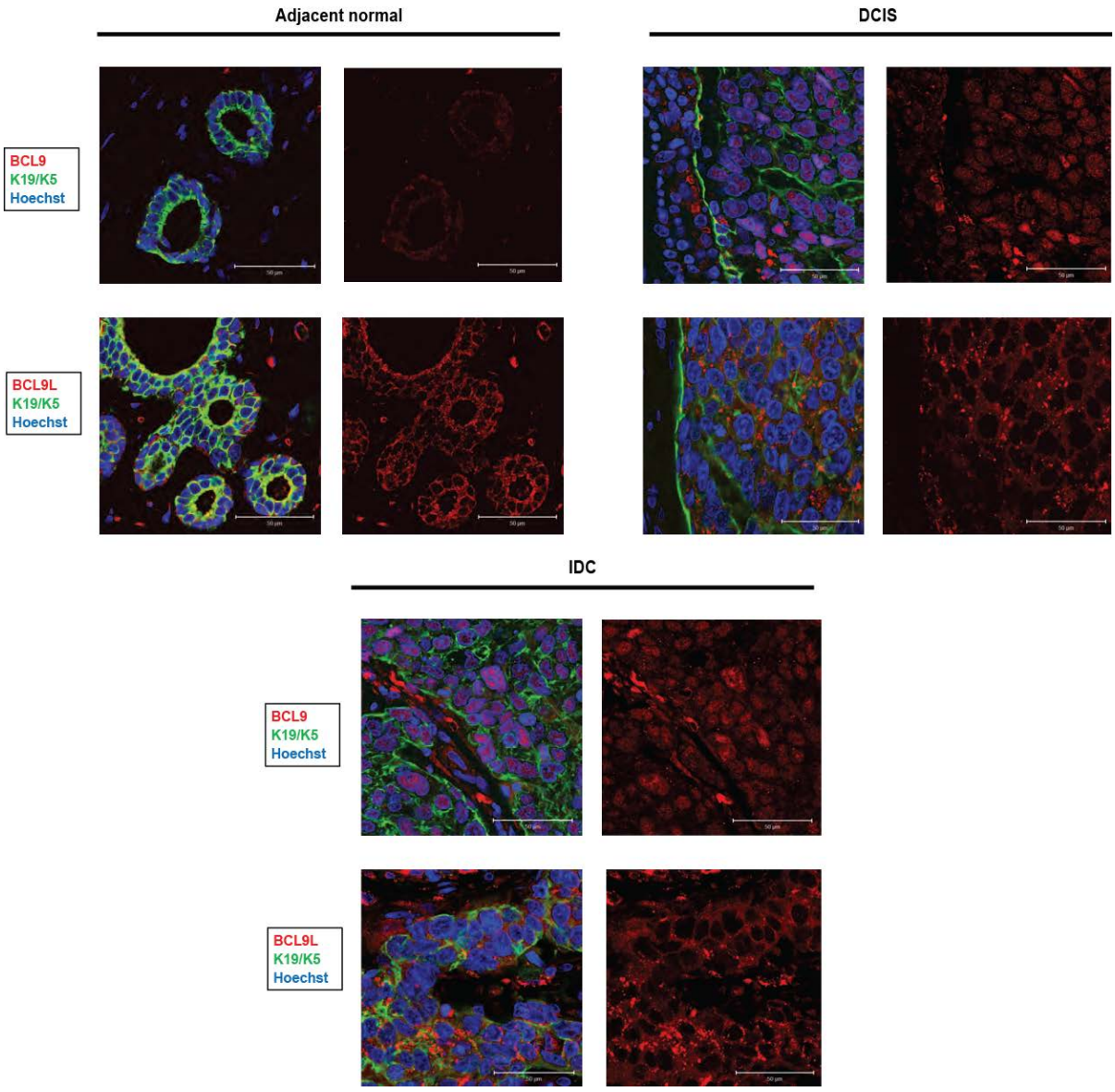

Figure 2.9. BCL9 showed increased nuclear expression, while BCL9L expression remained cytoplasmic during DCIS invasive transition. (A) Immunofluorescence staining of BCL9 (red; top panel), BCL9L (red; bottom panel), K5/K19 (green), and Hoechst (blue) in a primary sample that represents: Adjacent normal glands (Left), DCIS lesions (middle), and IDC (right). BCL9 and BCL9L are conjugated to Alexa-Fluor 594 (red) and K5/K19 are conjugated to Alexa-Fluor 488 (green). Nuclei are counterstained with Hoechst. Scale bars 50 μm, 40x objective was used.

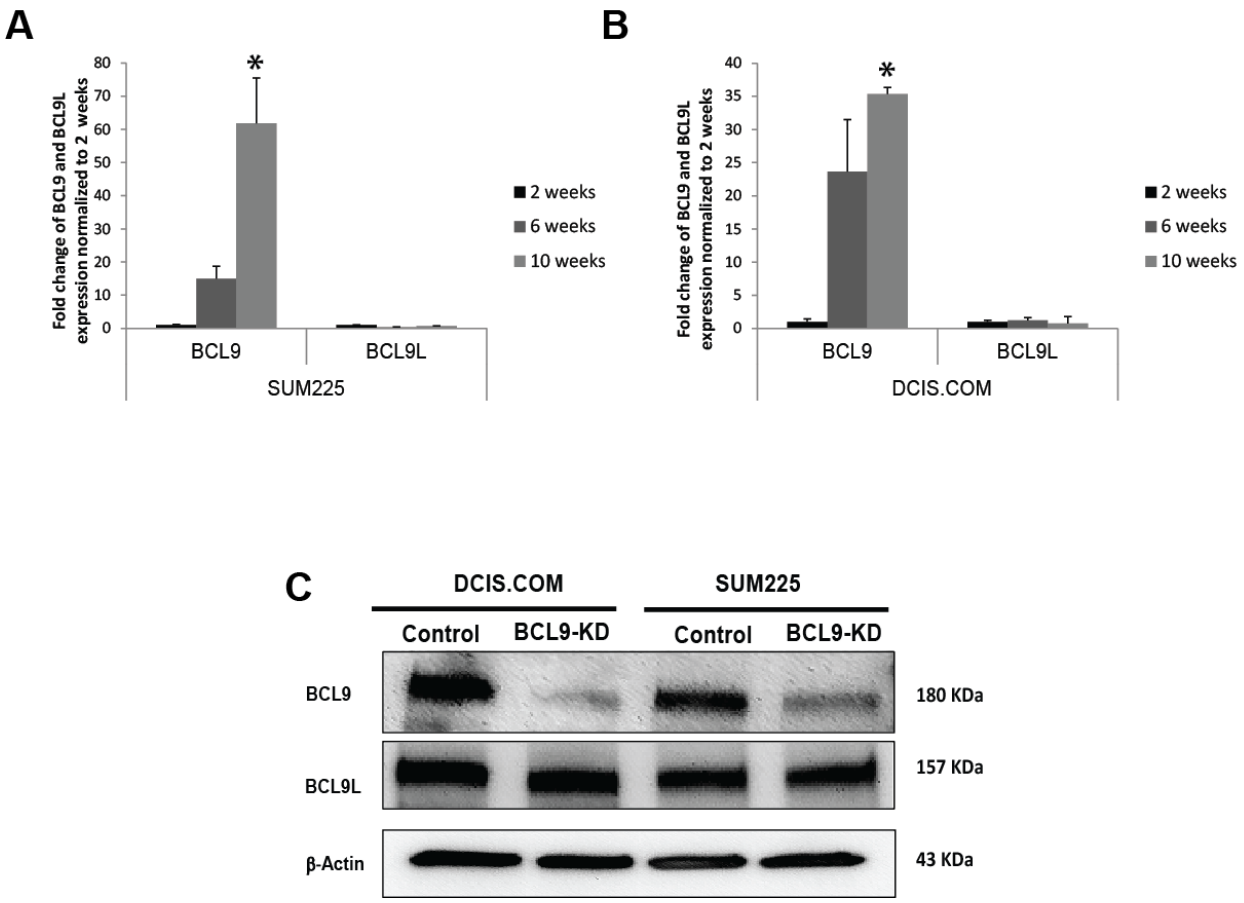

Figure 2.10. BCL9L mRNA and protein levels compared to BCL9. (A & B) RT-qPCR of BCL9 and BCL9L mRNA in EpCAM-positive epithelial cells sorted from SUM225 (A) and DCIS.COM (B) MIND xenografts at 2, 6, and 10 weeks post-intraductal injection. Bar graphs represent fold change normalized to 2 weeks. Data are mean values ± s.e.m (n=3, *P<0.05). (C) Representative western blot analysis of cell lysates from control and BCL9-KD-SUM225 and DCIS.COM blotted with anti-BCL9, and anti-BCL9L antibodies. β-actin was used as a loading control. The analysis shows no change in BCL9L protein levels in BCL9-KD cells compared to control cells.

BCL9 knockdown (KD) inhibits the proliferative, migratory, and invasive activity of DCIS cells *in vitro* and *in vivo.* The canonical WNT pathway is required for normal development and tissue homeostasis [108]. However, aberrant activation of canonical WNT signaling has been implicated in the development and progression of many cancers including breast cancer [86]. BCL9 overexpression has been proposed as one mechanism that may contribute to aberrant WNT activation [78]. BCL9 possesses a potent transcription activation domain and might function as an oncogene by providing an alternative pathway for β-catenin activation and subsequent tumor progression [71].

To assess the role of BCL9 in promoting DCIS invasive progression, two shRNA-based BCL9 constructs have been utilized: shRNA1 [78] and shRNA2, as well as their corresponding scrambled controls (Control 1 and Control 2). Since the results for both shRNAs were similar, only values for the shRNA1 groups are listed here. Western blot confirmed that shRNA1 efficiently silences BCL9 expression in both DCIS.COM (**Figure 2.11A**; left panel) and SUM225 (**Figure. 2.11A**; right panel). MTS assay was performed to assess the role of BCL9 on cell growth *in vitro* (**Figure 2.11B**). As shown in **Figure 2.11B**, knockdown of BCL9 significantly suppressed growth by 0.55 ± 0.01 fold ($P<0.05$; compared to 1.02 ± 0.02 in control) in DCIS.COM and by 0.62 ± 0.01 fold in SUM225 ($P<0.05$; compared to 0.76 ± 0.004 in control). To assess the role of BCL9 on cell migration and invasion, fibronectin and reconstituted basement membrane (Matrigel) assays were performed, respectively (**Figure 2.12**). BCL9 KD reduced invasion of DCIS.COM cells (0.23 ± 0.03 fold, $P<0.05$) compared to control (0.81 ± 0.07), and in SUM225 cells (0.62 ± 0.04 fold, $P<0.05$) compared to control (1.06 ± 0.05). In addition, cell migration in DCIS.COM BCL9 KD cells was significantly lower (0.2 ± 0.03 fold, $P<0.05$) compared to control cells (1.00 ± 0.11, $P<0.05$). However, there was no significant

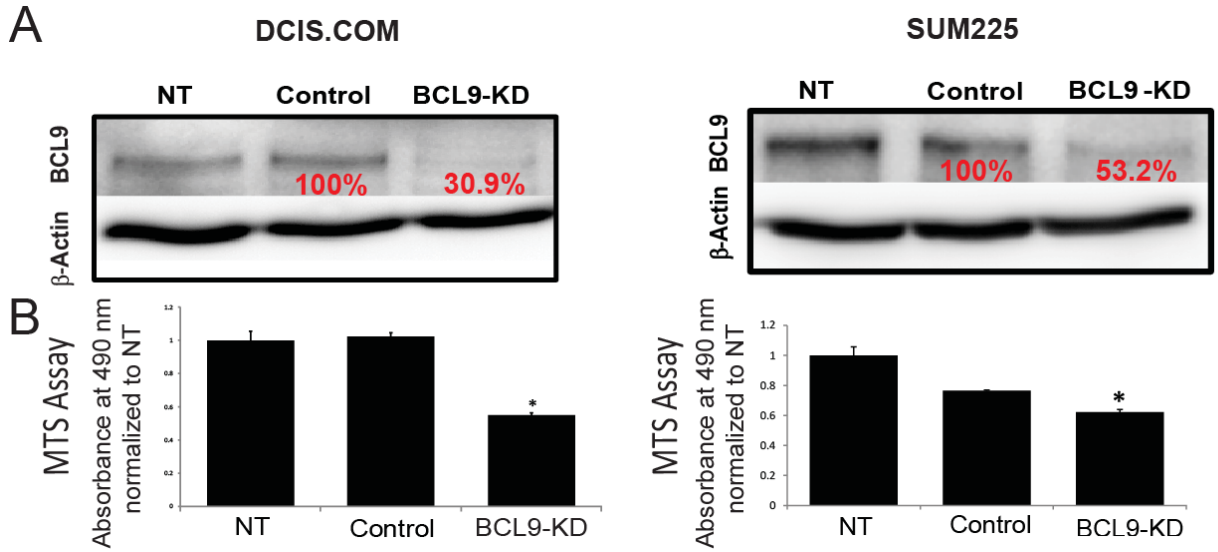

Figure 2.11. BCL9-KD decreases proliferative activity of DCIS cell lines *in vitro*. (A) Western blot analysis using anti-BCL9 antibody and anti-β-actin as a loading control (top), and (B) MTS assays of NT, scrambled control (control) and BCL9-KD in DCIS.COM (left panels) and SUM225 (right panels). Bar graphs represent mean absorbance at 490 nm normalized to NT ± s.e.m (n=3, **P*<0.05).

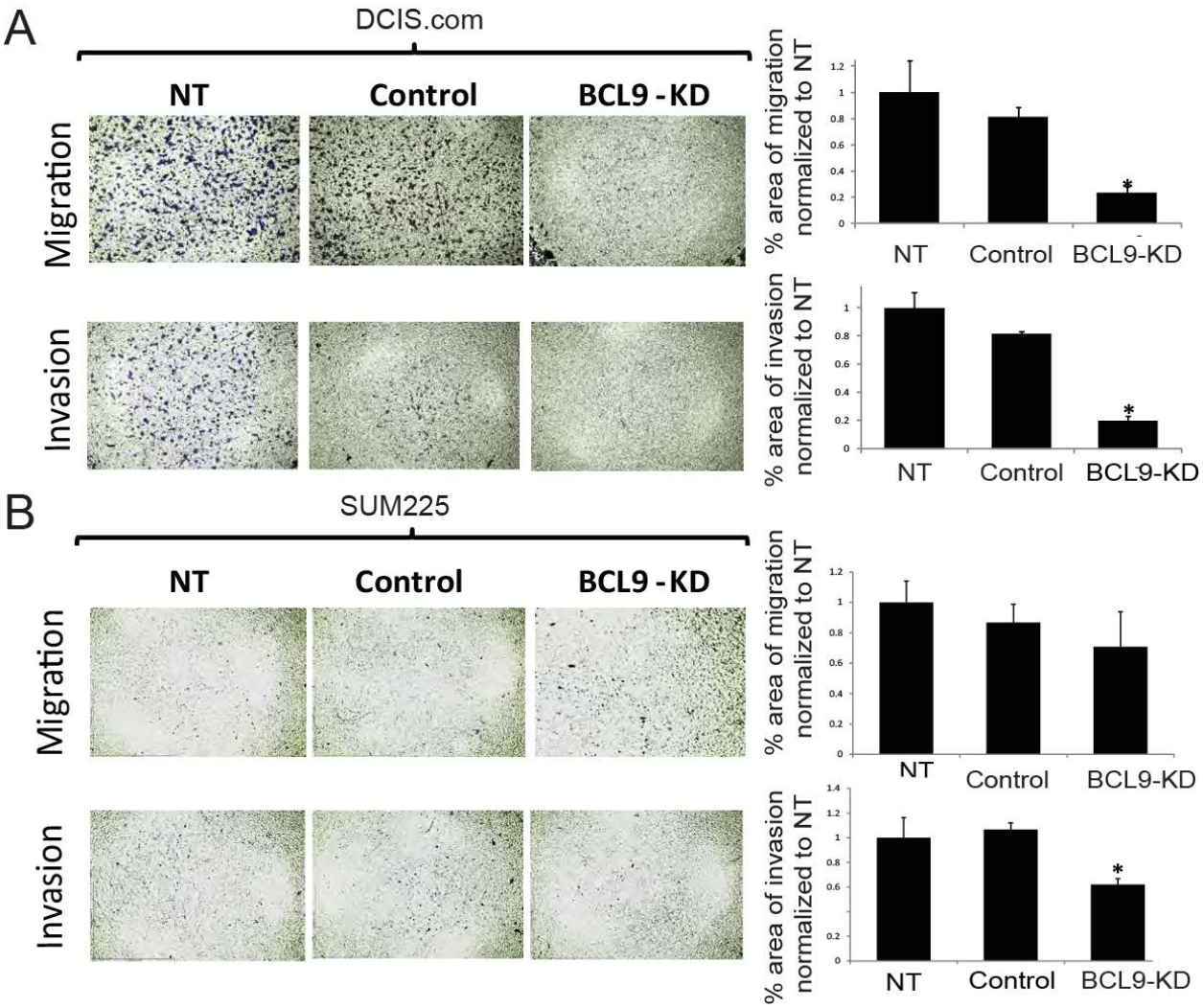

Figure 2.12. BCL9-KD decreases migratory and invasive activity of DCIS cell lines *in vitro*. (A and B) Show representative images of the migration and invasion assays in NT, scrambled control (control) and BCL9-KD in DCIS.COM (A) and SUM225 (B). Bar graphs represent % area of cells migrated (top) and invaded (bottom) under the membrane after 24 h for DCIS.com and 96 h for SUM225. Invasion and migration were determined by imageJ analysis of microscopic images per sample, data are mean values normalized to NT ± s.e.m (n=3, **P*<0.05).

reduction in SUM225 BCL9 KD cells (0.70 ± 0.23 fold, P>0.05) migration compared to control (1.00 ± 0.14 fold). Furthermore, re-expression of BCL9 in DCIS.COM BCL9 KD cells using a BCL9-overexpression lentiviral vector resulted in a significant increase in proliferation, migration and invasion *in vitro* (**Figure 2.13**) (P<0.05).

To examine the role of BCL9 in invasive progression *in vivo*, BCL9 KD DCIS.COM and SUM225 cells, and control cells, were transplanted as MIND xenografts (**Figure 2.14**). Glands were collected at 10 weeks post-transplantation for DCIS.COM, and at 14 weeks for SUM225, and prepared for IF using antibodies for BCL9 to confirm *in vivo* KD, human cytokeratin 5 and 19 (K5 and K19) to detect *in vivo* growth of human DCIS like lesions, smooth muscle actin (SMA) to detect the myoepithelial layer, phospho-histone 3 (phosphoH3) to detect cell proliferation, and cleaved caspase 3 to detect apoptosis. As shown (**Figure 2.14A**), successful *in vivo* KD was achieved in both DCIS.COM and SUM225. Extent of invasion was analyzed by measuring maximum distance traveled by invasive cells past the myoepithelial layer of each mammary duct, and by counting the number of invasive lesions per gland (**Figure 2.14B**). As shown in **Figure 2.14C**, BCL9 KD DCIS.COM and SUM225 MIND lesions showed a significant reduction in maximum distance of invasion (DCIS.COM= 78.0 ± 22.3 μm in KD compared to 302.7 ± 12.4 μm in control and for SUM225=75.5 ± 18.9 μm in KD compared to 338.3 ± 18.8 μm in control; *P*<0.05) and in the number of invasive lesions per field compared to control (DCIS.COM=1.4 ± 0.5 in KD compared to 4.3 ± 0.9 in control and for SUM225= 3.0 ± 3.0 invasive lesions in KD compared to 11.7 ± 1.2 invasive lesions in control; *P*<0.05). As shown in **Figure 2.15**, BCL9 KD DCIS.COM and SUM225 showed a significant reduction in phosphoH3 compared to control DCIS.COM and SUM225 (DCIS.COM= 3.25 ± 0.01 cells per

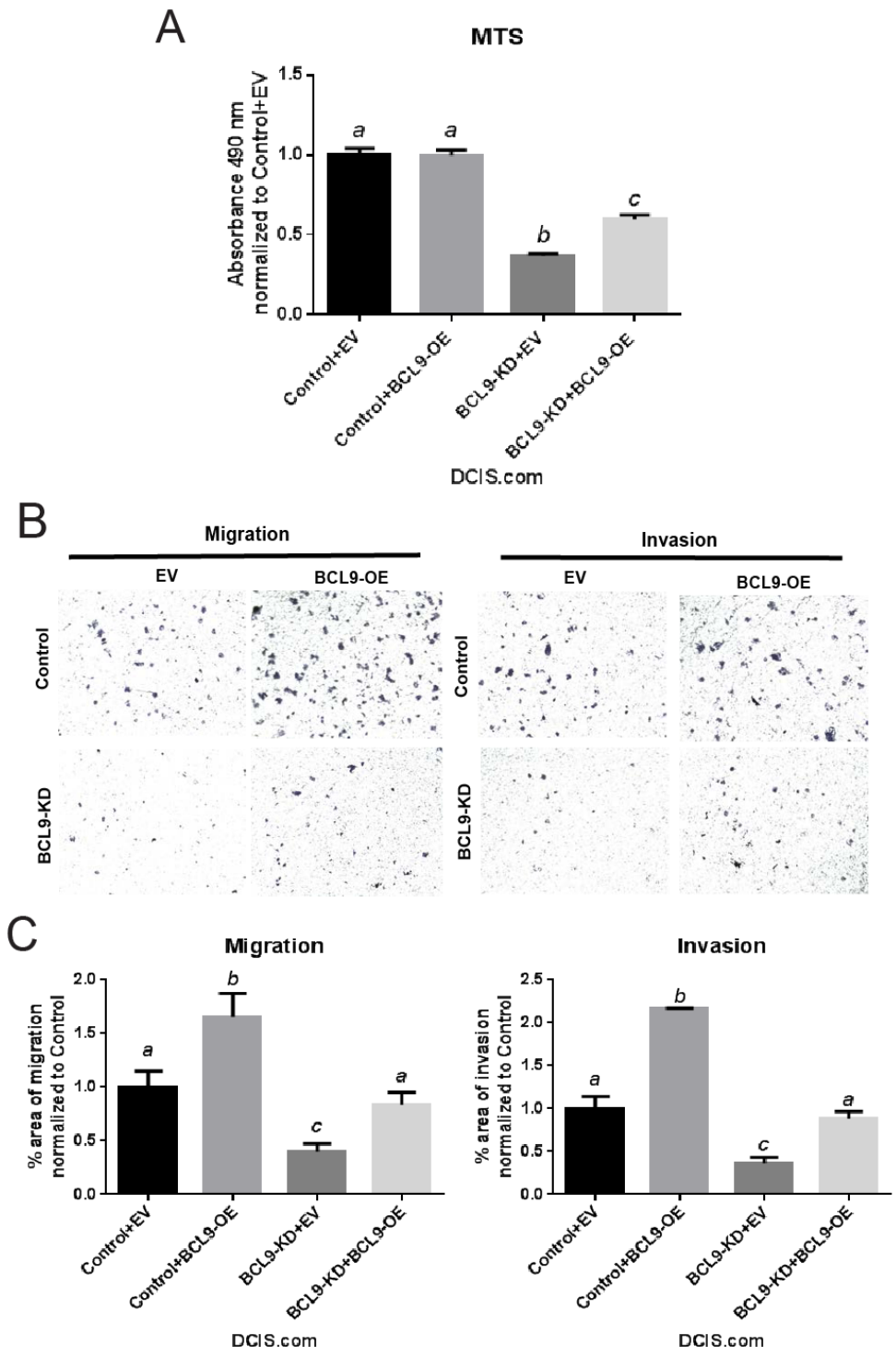
A
MTS
Absorbance 490 nm normalized to Control+EV
1.5
1.0
0.5
0.0
a
a
b
c
Control+EV
Control+BCL9-OE
BCL9-KD+EV
BCL9-KD+BCL9-OE
DCIS.com
B
Migration
Invasion
EV
BCL9-OE
EV
BCL9-OE
Control
BCL9-KD
Control
BCL9-KD
C
Migration
Invasion
% area of migration normalized to Control
% area of invasion normalized to Control
2.0
1.5
1.0
0.5
0.0
2.5
2.0
1.5
1.0
0.5
0.0
a
b
c
a
a
b
c
a
Control+EV
Control+BCL9-OE
BCL9-KD+EV
BCL9-KD+BCL9-OE
DCIS.com
DCIS.com

Figure 2.13. MTS, migration and invasion assays in DCIS.COM cells that were previously transduced with scrambled control (Control) or BCL9 KD shRNA. The control cells and BCL9 KD cells were re-transduced with empty vector (EV), BCL9 overexpression (BCL9-OE) and BCL9 KD. BCL9-OE was achieved by transduction using the PCDH-BCL9 (BCL9-OE) acquired from Dr. Carrasco. (A) MTS assay on control cells transduced with EV (control+EV), or BCL9-OE (control+BCL9-OE), BCL9-KD transduced with EV (BCL9 KD+EV), and BCL9-KD transduced with BCL9-OE (BCL9 KD+BCL9-OE). Bar graphs represent mean absorbance at 490 nm normalized to control ± s.e.m (n=6). (B and C) Show representative images of the migration and invasion assays. Bar graph represent % area of cells migrated (left) and invaded (right) under the membrane after 24 h. Invasion and migration were determined by image J analysis of microscopic images per sample, the data are mean values normalized to control ± s.e.m (n=3).

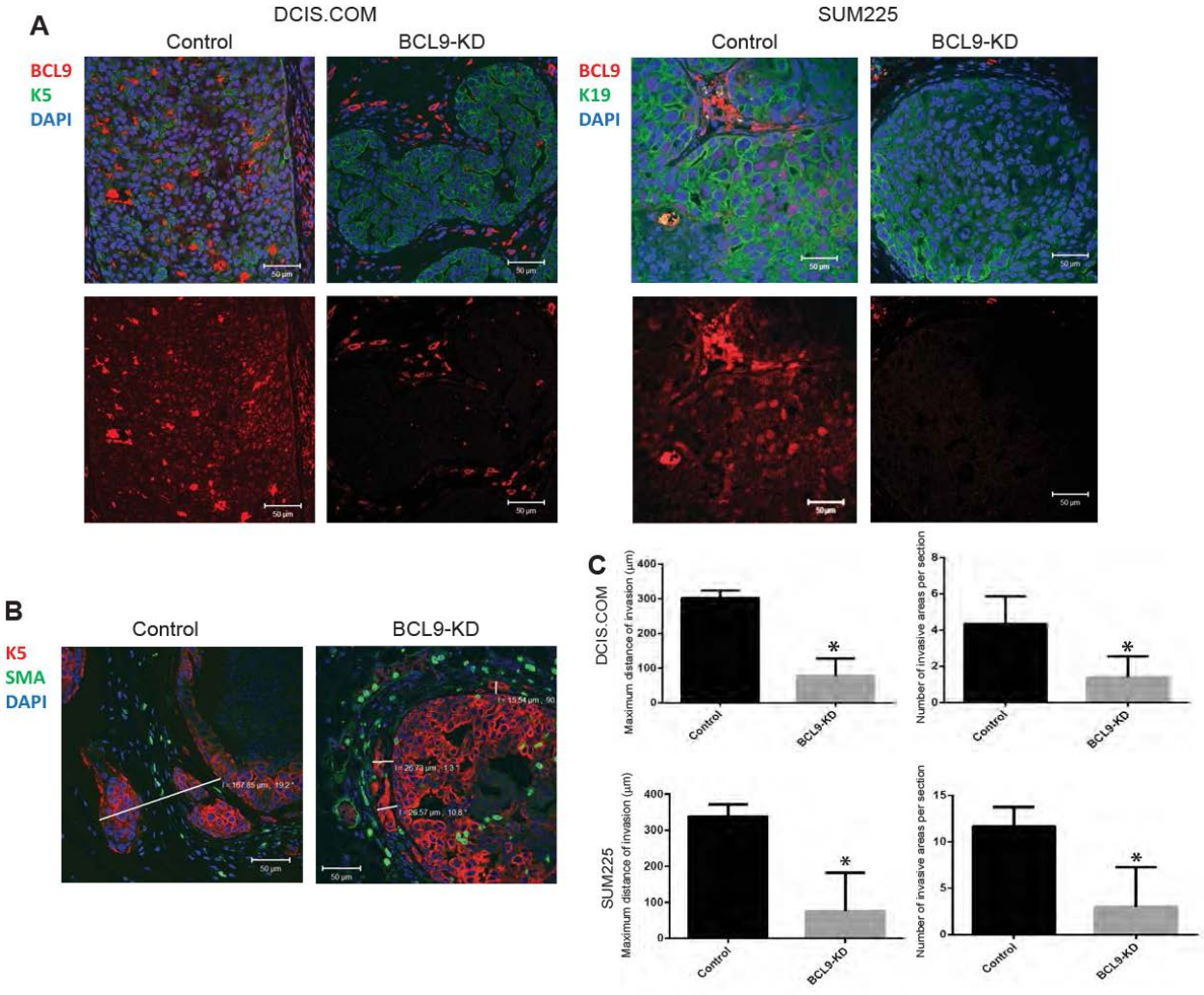

Figure 2.14. BCL9-KD inhibits invasion in DCIS cell line MIND xenografts. (A) IF staining of BCL9 (red), K5/K19 (green), and DAPI (blue) in DCIS.COM (left) and SUM225 (right), control and BCL9-KD MIND xenografts at 10 and 14 weeks post-intraductal injection, respectively. (B) IF staining of K5 (red), SMA (green), and DAPI in DCIS.COM cells demonstrating how distance of invasion was measured. Scale bars=50 μm, 40x magnification. (C) Bar graphs represent the maximum distance of invasion and number of invasive lesions in control and BCL9-KD for DCIS.COM and SUM225 MIND xenografts. Data represent the mean ± s.e.m (n=4, **P*<0.05).

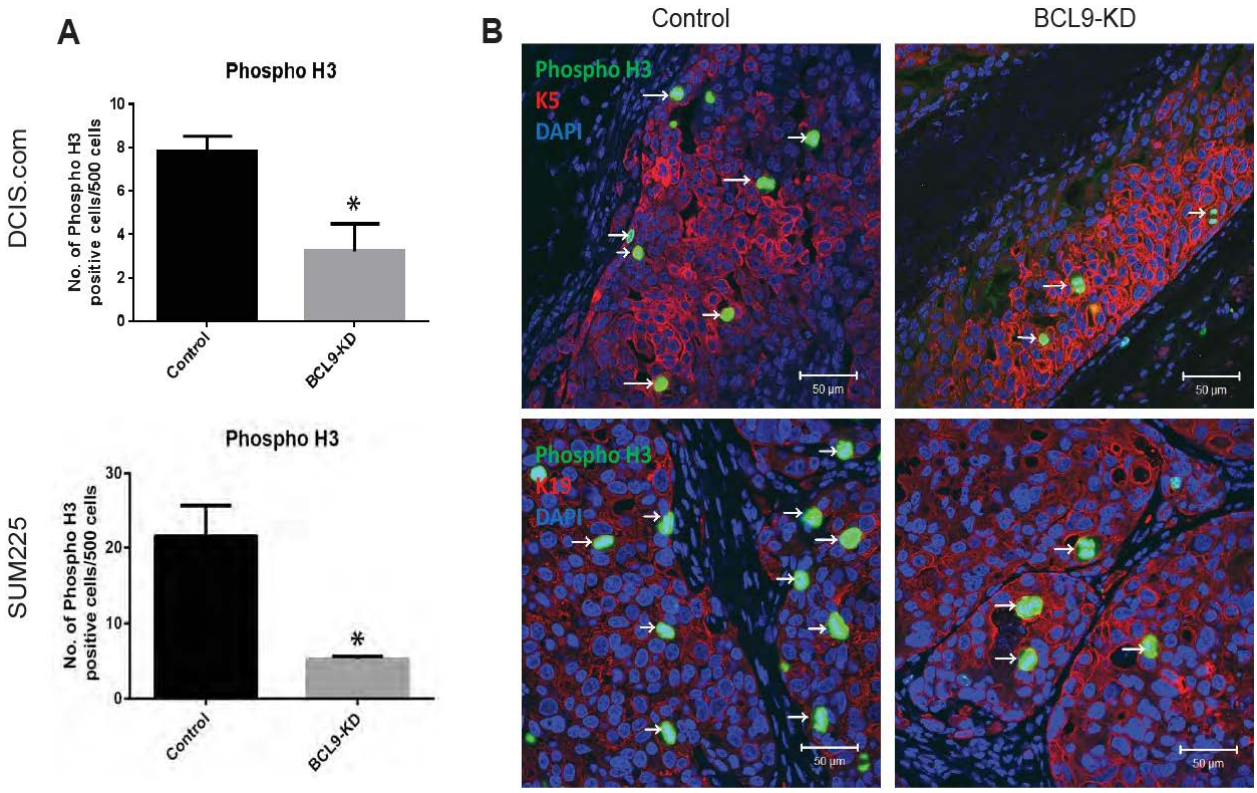

Figure 2.15. BCL9-KD decreases epithelial cell proliferation *in vivo*. (A) Bar graphs represent the number of phosphoH3-positive cells per 500 cells. Data represent the mean ± s.e.m (n=4, **P*<0.05). (B) IF staining of control and BCL9-KD DCIS.COM and SUM225 MIND xenografts stained with the proliferation marker phosphoH3 -green, and K5/K19 -red, and DAPI. White arrows point to cells with positive staining.

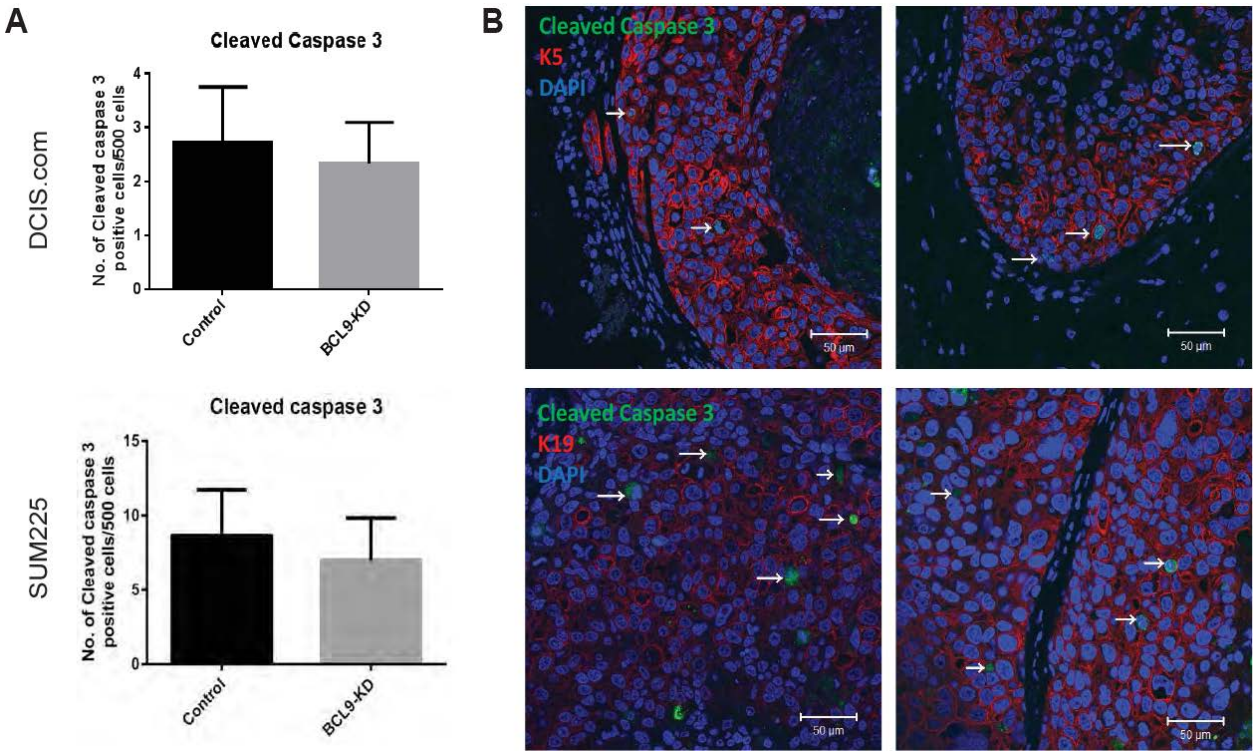

Figure 2.16. BCL9-KD causes no significant change in epithelial cell death *in vivo*. (A) Bar graphs represent the number of cleaved caspase 3-positive cells per 500 cells. Data represent the mean ± s.e.m (n=4, **P*<0.05). (B) IF staining of control and BCL9-KD DCIS.COM and SUM225 MIND xenografts stained with cleaved caspase 3 green, and K5/K19 -red, and DAPI. White arrows point to cells with positive staining.

500 KD cells compared to 5.25 ± 0.25 cells per 500 control cells counted; SUM225=7.83 ± 0.01 cells per 500 KD cells compared to 21.5 ± 2.36 per 500 control cells counted; $P<0.05$). However, there was no change in the number of cleaved caspase 3 positive cells (**Figure 2.16**). These data demonstrate that BCL9 promotes *in vivo* cellular proliferation and invasion, while BCL9 is not involved in cell survival and viability.

BCL9 regulates expression of EMT biomarkers. Previous studies in colon carcinoma and multiple myeloma models showed that tumors with BCL9 KD exhibited altered expression and distribution of mesenchymal and epithelial markers, vimentin, β-catenin and E-cadherin, indicative of reduced EMT [78]. Likewise, Deka, J and Colleagues [79] showed that mice with conditionally deleted *Bcl9/Bcl9l* in intestinal cells exposed to a carcinogen (dimethylhydrazine followed by DSS) showed higher expression of both WNT target genes that regulate EMT (vimentin, fibronectin and β-catenin) and stem cell related genes such as Sox6 compared to wild type. Based on these data, we assessed the role of BCL9 on expression of EMT biomarkers in our DCIS cell lines. A western blot was performed on cell lysates derived from DCIS.COM and SUM225 cells that were NT, expressed a scrambled shRNA control, or BCL9-KD using antibodies for vimentin as a mesenchymal marker and E-cadherin as an epithelial marker. BCL9 KD in DCIS.COM cells exhibited reduced vimentin and increase epithelial marker E-cadherin (**Figure 2.17**). SUM225 also showed an increase in E-cadherin, but control cells did not express vimentin, so as expected, BCL9 KD did not change vimentin expression. Overexpression of BCL9 (BCL9 OE) on the other hand, reduced E-cadherin and increased vimentin expression in DCIS.COM cells (Figure 2.17) To confirm our findings *in vivo*, IF staining of BCL9 KD DCIS.COM and SUM225 MIND xenografts, and their controls were performed using anti-vimentin, anti-E-cadherin, and anti-K5/K19 antibodies. Images were analyzed using imageJ for

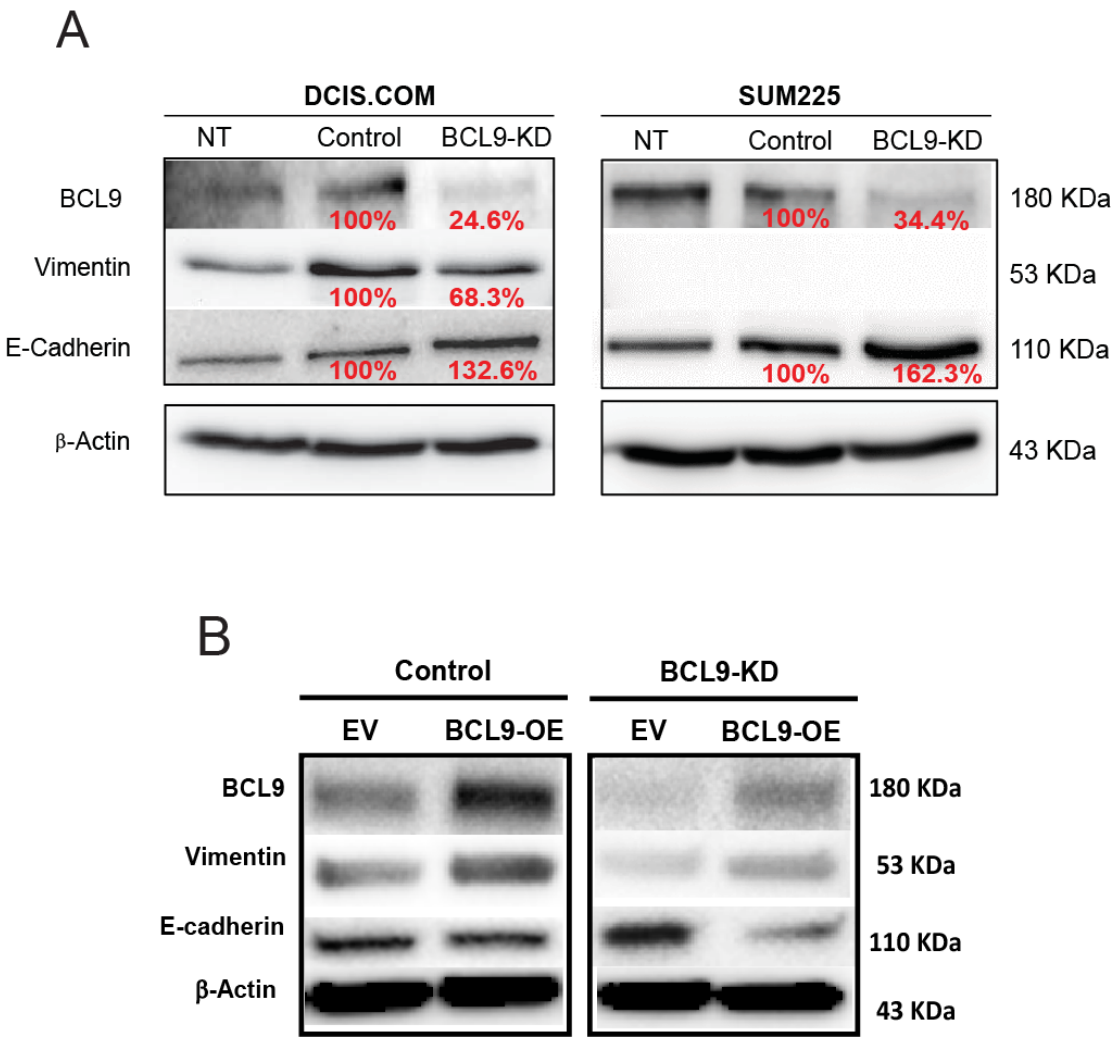

Figure 2.17. BCL9-KD reduces the mesenchymal markers and increases the luminal markers in DCIS cell lines. (A) Representative western blot analysis of cell lysates from NT, control and BCL9-KD DCIS.COM and SUM225 cells blotted with anti-BCL9, anti-vimentin, and anti-E-cadherin antibodies. *B*-actin was used as a loading control. The labels show percent change in BCL9-KD protein compared to control. (B) Western blot analysis with E-cadherin and vimentin on DCIS.COM control cells transduced with EV (control+EV), or BCL9-OE (control+BCL9-OE), BCL9-KD transduced with EV (BCL9 KD+EV), and BCL9-KD transduced with BCL9-OE (BCL9 KD+BCL9-OE).

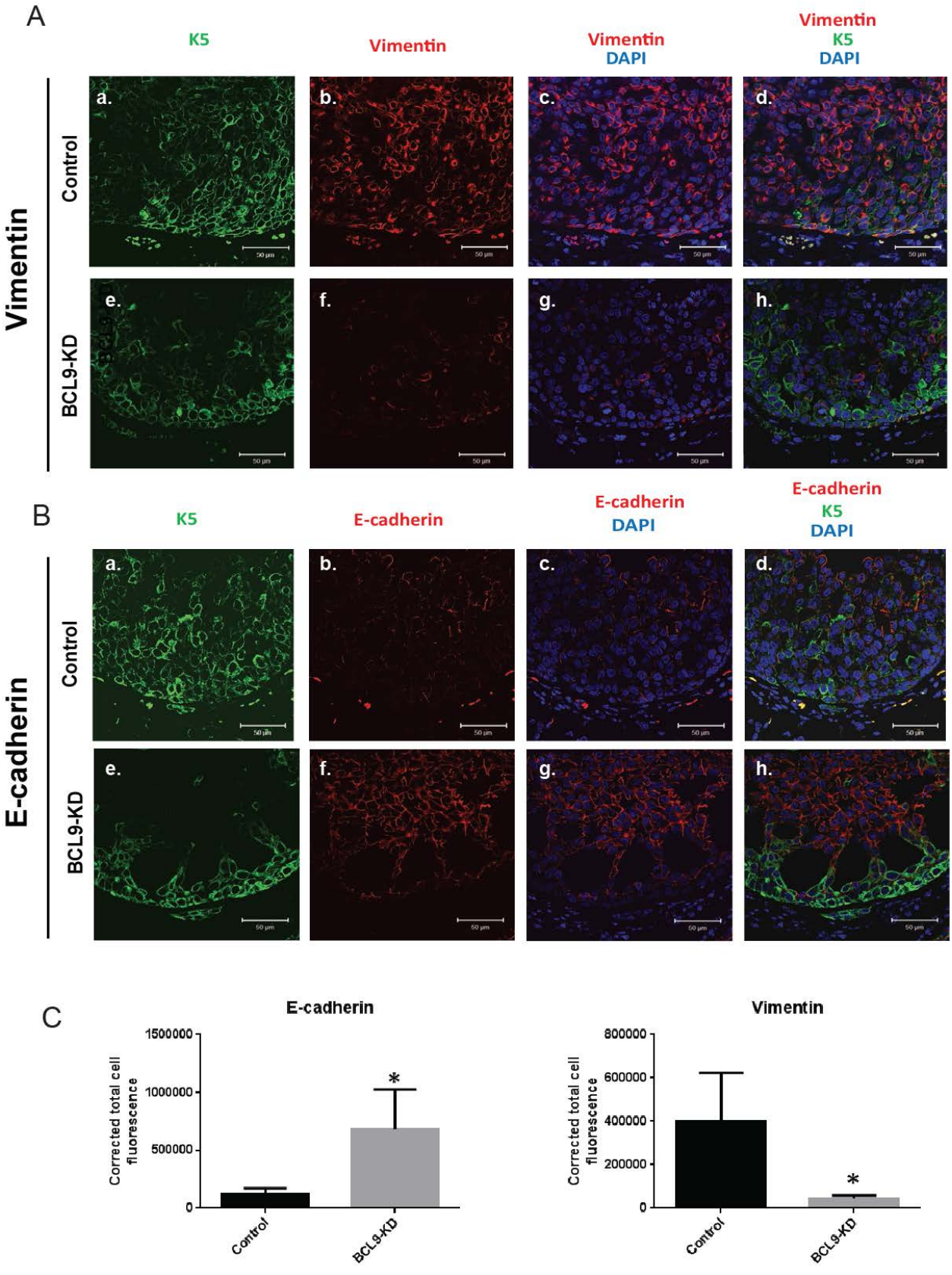
A
K5
Vimentin
Vimentin
DAPI
Vimentin
K5
DAPI
Vimentin
Control
BCL9-KD
a.
b.
c.
d.
e.
f.
g.
h.
B
K5
E-cadherin
E-cadherin
DAPI
E-cadherin
K5
DAPI
E-cadherin
Control
BCL9-KD
C
E-cadherin
Corrected total cell fluorescence
1500000
1000000
500000
0
Control
BCL9-KD
Vimentin
800000
600000
400000
200000
0

Figure 2.18. BCL9-KD reduced mesenchymal markers and increases luminal markers in DCIS cell lines. (A and B) show IF images of control (a-d) and BCL9-KD DCIS.COM (e-h) xenografts stained with vimentin (A) and E-cadherin (B) shown in red, and K5 shown in green, and DAPI in blue. Scale bars=50 μm, 40x magnification. (C) Bar graphs of cell fluorescence intensity units for E-cadherin and vimentin in control and BCL9 KD DCIS.COM cells. Measurements were obtained by imageJ. Corrected cell fluorescence was calculated by subtracting the background mean density from the total integrated density. Data represent the mean ± s.e.m (n=4, *P<0.05).

fluorescence intensity. As shown in **Figure 2.18**, in our DCIS.COM MIND xenografts exhibited a significant increase in E-cadherin expression in BCL9 KD compared to the control (681207 ± 198349 U compared to 120994 ± 25258 U; $P<0.05$) and a significant reduction in vimentin expression in BCL9 KD compared to control (44967 ± 5402 U compared to 400345 ± 111633 U; $P<0.05$). DCIS.COM cells generated Basal like DCIS like lesions *in vivo*. However, in our SUM225 xenografts, there was not a significant reduction in vimentin and or upregulation in E-cadherin expression. SUM225 cells generate luminal like DCIS lesions *in vivo*. These data suggest that BCL9 may have a more significant effect on EMT-like phenotype in basal cells compared to luminal cells. The effects of BCL9-KD on the luminal marker CD24 and the basal marker CD44 in DCIS.COM and SUM225 were also assessed by flow cytometry analysis of NT, control and BCL9-KD cells. As seen in **Figure 2.19**, BCL9-KD cells showed an increase in expression of luminal marker CD24 compared to control in DCIS.COM (77.27% ± 0.20% vs. 90.77% ± 3.26%; $P<0.05$), while there was no change in SUM225 cells (data not shown). CD44 expression levels did not change in either cell line, DCIS.COM or SUM225 (**Figure 2.19B**; SUM225 data not shown). These data confirm our previous findings that BCL9 may contribute to maintenance of an EMT program in some but not all cancer cell types.

BCL9 interacts with β-catenin and enhances WNT/β-catenin signaling. BCL9 and its homolog BCL9L and pygopus (PYGO) were identified as co-activators for WNT/β-catenin transcription in *Drosophila* and in mammalian cells [71] [78]. To examine BCL9 and β-catenin interactions in our DCIS cell line models, BCL9 was immunoprecipitated from whole cell extracts of DCIS.COM and SUM225 cells using anti-BCL9 antibody, followed by western blot using anti β-catenin antibody. As shown in **Figure 2.20**, BCL9 interacts with β-catenin in both

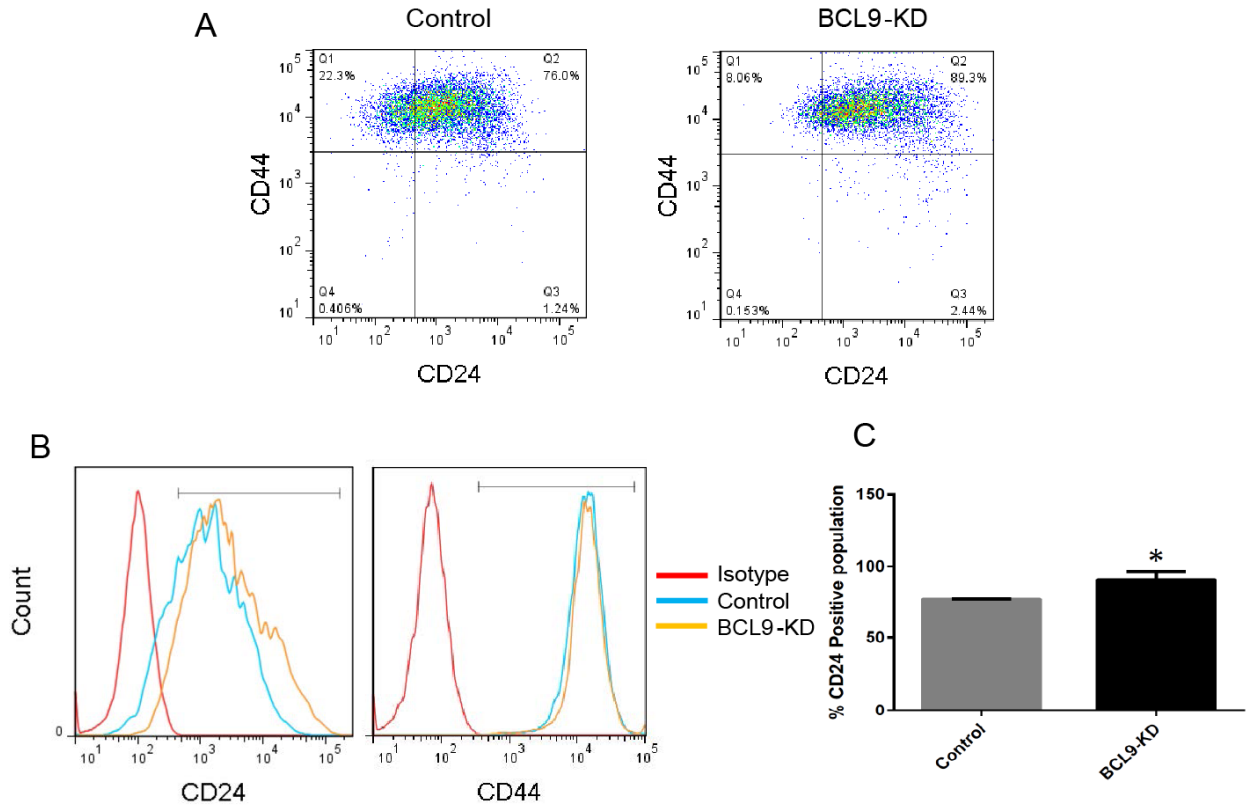

Figure 2.19. BCL9-KD increased CD24 positive population in DCIS.COM. (A) Representative flow analysis of control and BCL9-KD DCIS.COM cells for CD24 and CD44 (top), representative histogram showing changes in CD24 (left) and CD44 (right) in control (blue line), BCL9-KD DCIS.com cells (yellow line) compared to isotype control (red line). (C) Bar graphs show the percentage of CD24 positive population in BCL9 KD and control. Data represent the mean ± s.e.m (n=3, $P<0.05$).

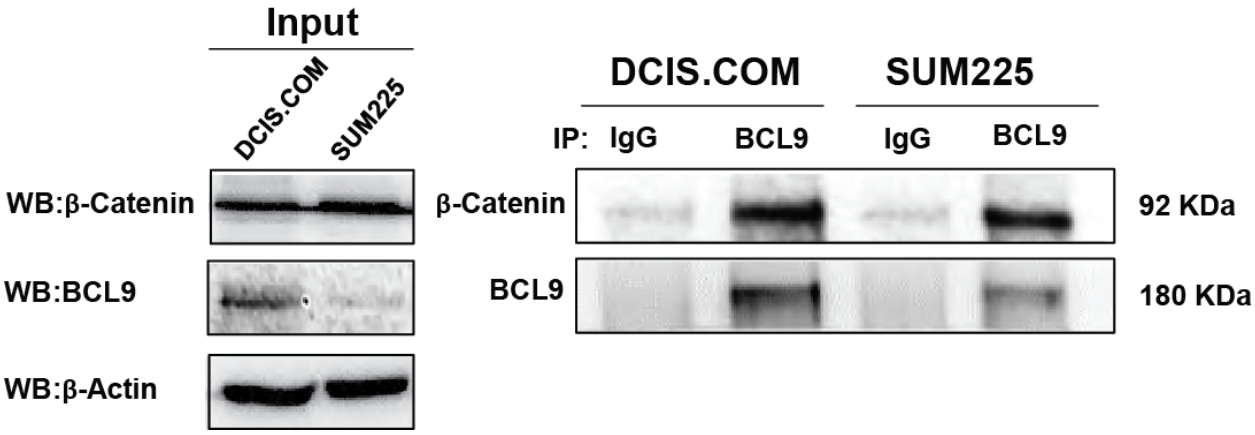

Figure 2.20. BCL9 interacts with β-catenin in DCIS cell lines. Whole cell extracts of DCIS.COM and SUM225 cells were immunoprecipitated for BCL9 using an anti-BCL9 antibody, followed by western blot analysis using anti-β-catenin and anti-BCL9 antibody. IgG antibody was used as a negative control for IP and 2 μg of whole cell lysate was used as input.

of our DCIS cell lines, DCIS.COM (**Figure 2.20**, left panel) and SUM225 (**Figure 2.20**, right panel). To explore whether BCL9 modulates WNT/β-catenin-mediated transcription, the SuperTopFlash (STopflash), a luciferase reporter assay that measures β-catenin/LEF-TCF-mediated transcription, along with the FopFlash reporter with mutated LEF/TCF binding sites as a control were used. Non-transduced, control, and BCL9-KD DCIS.COM and SUM225 cells were transiently transfected along with STopFlash and FopFlash reporters, and treated with control or WNT3A conditioned medium (CM) 4 hours following transfection. Twenty-four hours following transfection, luciferase activity was measured. As shown in **Figure 2.21A**, KD of BCL9 significantly reduced β-catenin/TCF-mediated transcription ($P<0.05$) in DCIS.COM, both in the presence and absence of WNT3A stimulation, compared to similarly treated NT and controls, but not in SUM225 cells with or without WNT3a stimulation (Figure 2.21B). In order to assess whether BCL9 enhances β-catenin mediated transcription, BCL9 and constitutively active β-catenin were overexpressed in human embryonic kidney (HEK) 293T cells, which express low endogenous levels of BCL9 (data not shown). As expected, constitutively active β-catenin expression increased transcription, both in the absence and presence of WNT3a stimulation, compared to non-transduced controls (NT; $P<0.05$; **Figure 2.21C**). Overexpression of BCL9 enhanced β-catenin/TCF-mediated transcription induced by WNT3A by about 2-fold compared to NT control ($P<0.05$). Furthermore, cells that overexpressed both BCL9 and constitutively active β-catenin showed significantly higher β-catenin/TCF-mediated transcription compared to β-catenin overexpression alone and in response to WNT3A stimulation (~1.7-fold increase; $P<0.05$). In addition, canonical WNT activation was analyzed in BCL9 KD DCIS.COM cells after re-expression of BCL9 (BCL9-KD/OE). As shown in **Figure 2.21D**, BCL9 KD/OE showed a significant increase in reporter activity compared to BCL9 KD with and

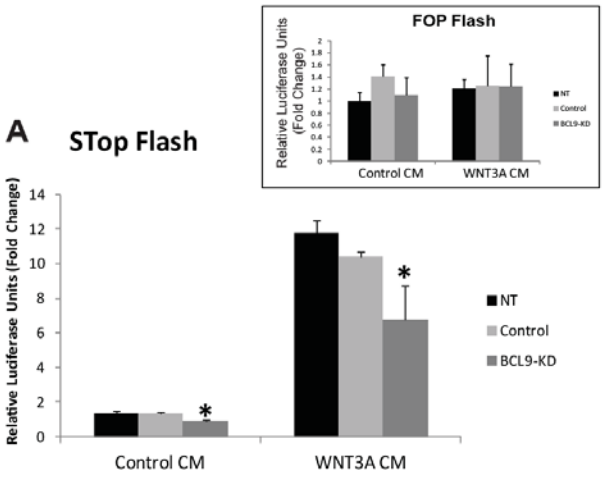
A
STop Flash
FOP Flash
Relative Luciferase Units (Fold Change)
Control CM
WNT3A CM
NT
Control
BCL9-KD

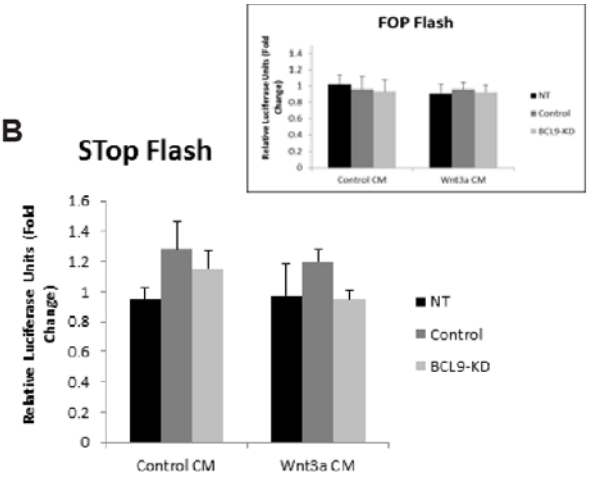
B
STop Flash
FOP Flash
Relative Luciferase Units (Fold Change)
Control CM
Wnt3a CM
NT
Control
BCL9-KD

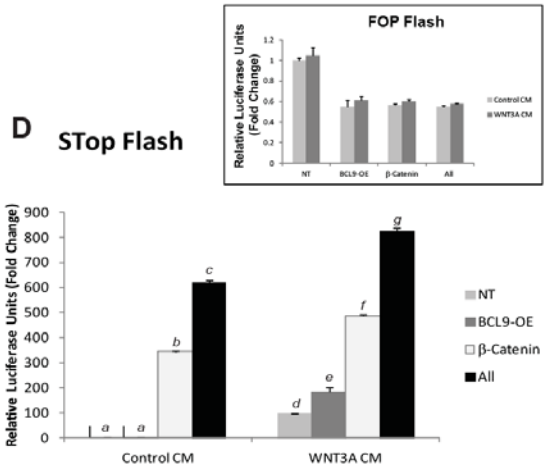
D
STop Flash
FOP Flash
Relative Luciferase Units (Fold Change)
Control CM
WNT3A CM
NT
BCL9-OE
β-Catenin
All

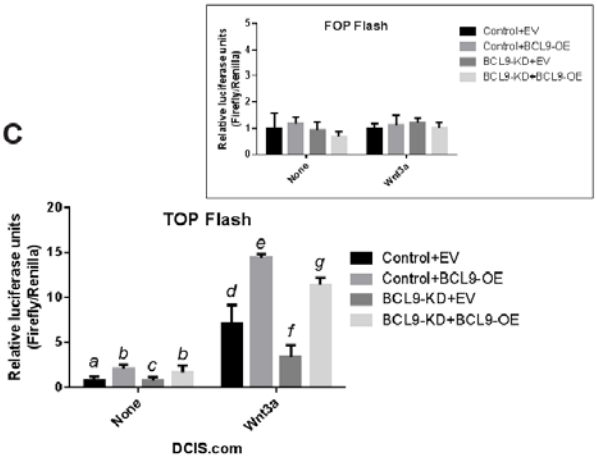
C
FOP Flash
TOP Flash
Relative luciferase units (Firefly/Renilla)
None
Wnt3a
Control+EV
Control+BCL9-OE
BCL9-KD+EV
BCL9-KD+BCL9-OE
DCIS.com

Figure 2.21. BCL9 KD inhibits WNT/β-catenin signaling activity in DCIS.COM. STopFlash reporter activity in DCIS.COM (A) and SUM225 (B) NT, control, and BCL9-KD, that were either treated with WNT3A or control CM. (A and B-inset) FopFlash in these cells with control or WNT3A CM. (C) STopFlash reporter activity in 293T cells NT, BCL9-OE, constitutively active β-catenin, or all combined that were either treated with WNT3A or control CM. (C-inset) FopFlash in these cells with control or WNT3A CM. Data represents mean ± s.e.m (n=3, **P*<0.05, letters indicate statistical difference). (D) TopFlash and FopFlash reporter activity in DCIS.COM control cells transduced with EV (control+EV), or BCL9-OE (control+BCL9-OE), BCL9-KD transduced with EV (BCL9 KD+EV), and BCL9-KD transduced with BCL9-OE (BCL9 KD+BCL9-OE). They were either treated with WNT3A or control CM. Data represents mean ± s.e.m (n=3, letters indicate statistical difference).

without WNT3a (1.7 ± 0.28 vs. 0.6 ± 0.13) in untreated and after treatment with WNT3a (11.42 ± 0.46 vs. 3.3 ± 0.76; $P<0.05$). These data demonstrate that BCL9, by binding to β-catenin, enhances canonical WNT activation in DCIS.COM cells (a basal cell line). While BCL9 still binds β-catenin in SUM225 (luminal HER2 overexpressing) it does not activate WNT canonical signaling that can be assessed by luciferase reporter assay.

2.4.Discussion

Canonical WNT signaling can be constitutively activated in cancer by a variety of mechanisms including mutations in APC, Axin, and β-catenin [109]. These mutations enable β-catenin to escape destruction and drive oncogenic WNT signaling [109]. However, in breast cancer, where mutations in APC or β-catenin are not commonly reported, BCL9 overexpression may be a molecular mechanism contributing to aberrant WNT activation and progression [78]. The mechanism by which BCL9 is overexpressed in some cancers is not entirely understood, but cancer genome analysis via GISTIC reveals copy number alterations in 13% of all breast cancer cases examined [110]. BCL9 resides on chromosome 1q (1q21). Chromosome 1q amplification is a common finding in several cancers including breast [111]. BCL9 is a nuclear co-factor that, by binding β-catenin and PYGO, modulates canonical WNT signaling and promotes β-catenin-mediated transcription. Formation of a quaternary complex consisting of LEF/TCF, β-catenin, BCL9 and PYGO enhances β-catenin-dependent WNT transcriptional activity [71]. Indeed, BCL9 is recognized as an adaptor that helps PYGO recognize modified histone H3 tails by their plant homeodomain (PHD) fingers [112]. Human *BCL9* and its paralog *BCL9L* reside on chromosome 1q21 and 11q23.3 respectively. Thus, the molecular regulation of these two genes

may be very different. One study reported BCL9L to regulate ER transcription by interaction with Sp1 through the proximal ESR1 gene promoter and to be highly expressed in patients with ER-positive breast cancers [107]. The exact role of BCL9 vs. BCL9L in normal mammary gland development has not been studied. In addition, we did not find BCL9L upregulation to be associated with invasive progression in our DCIS MIND models. Therefore, role of BCL9L in breast cancer remains unknown.

Here BCL9 was identified by analysis of molecular profiling of DCIS at distinct stages of *in situ* to invasive transition. Initial findings suggested that BCL9 expression and activity in DCIS cells are important risk factors for breast cancer progression. This is based on the enhanced nuclear expression of BCL9 in DCIS epithelia that progressed to invasion. Silencing of BCL9 in the invasive DCIS cell line led to *in vivo* and *in vitro* inhibition of both cell growth and invasion, as well as down-regulation of vimentin, a biomarker of epithelial-mesenchymal transition (EMT). The role of BCL9 in progression of other types of cancers has been reported previously. However, to our knowledge, there are currently no data on the contribution of BCL9 in breast cancer progression. Mani and colleagues [78] showed that KD of BCL9 by shRNA in a colon cancer cell line (colo320) and a multiple myeloma cell line (MM1S) reduced proliferation and colony formation. On the contrary, overexpression of BCL9 increased colo320 and MM1S migration in transwell migration assays and *in vitro* Matrigel coated invasion assays. Immunocompromised mice injected with colo320 KD of BCL9 showed significant increase in survival and reduced lung metastasis. Likewise, mice injected with MM1S cells KD BCL9 also showed improved survival and reduced metastasis to long bone, spine, and head. BCL9 KD tumors also showed reduced EMT markers such as vimentin, E-cadherin and β-catenin.

It also been demonstrated in this chapter that BCL9 KD suppressed WNT signaling as assessed by TOP-FLASH WNT reporter assays in the basal DCIS cell line (DCIS.COM), while BCL9 KD in SUM225 (luminal HER2 overexpressing) did not affect the canonical WNT signaling. This result may indicate that the canonical WNT pathway is involved in the progression of certain subtypes of breast cancers, i.e. basal subtypes. This observation is interesting since the TCGA breast cancer data shows that BCL9 is significantly amplified in basal subtypes of breast cancers [110, 113]. However, there is also the possibility that TopFlash used in our study did not detect WNT activity since this reporter does not detect all transcriptional effects in WNT signaling.

2.5. Conclusion:

Collectively, the findings in this chapter suggest that BCL9, by enhancing canonical WNT signaling and initiating EMT, serves as an important molecular driver in invasive transition of human DCIS. Therefore, BCL9 may serve as a potential therapeutic target for prevention of IDC. However, the results obtained from the luminal DCIS cell line (SUM225) show that BCL9 is promoting invasion without affecting canonical WNT signaling. In chapter three we investigate other possible signaling pathways that BCL9 may regulate.

CHAPTER THREE

Novel Role of BCL9 in the Activation of Other Oncogenic Signaling Pathways

3.1. Introduction:

In the previous chapter, BCL9 was shown to promote DCIS progression to invasion in two representative DCIS cell lines, DCIS.COM and SUM225, *in vitro* and *in vivo*. In DCIS.COM cells, BCL9 promoted tumorigenesis by mediating canonical WNT signaling. However, in SUM225 cells, we observed lack of response to WNT3a ligand, and BCL9-KD had no effect on WNT reporter activity. Therefore, the mechanism by which BCL9 promotes invasion in SUM225 is not fully understood. Previous studies showed that the C-terminal region of BCL9 has two homology domains (HD4 and HD5) that are highly conserved between human, mouse and zebrafish, and these HD4-5 regions contain a transactivation domain that can activate transcription independently [72]. Interestingly, there are no known binding partners identified for these domains [72]. We explored the possibility that BCL9 might interact with other transcription factors and could be mediating crosstalk between WNT and other signaling pathways. Here, we performed reverse phase protein analysis (RPPA) to screen BCL9-KD and control DCIS cells for changes in protein expression. This screening revealed a novel role of BCL9 in activating Signal transducer and activator of transcription 3 (STAT3) signaling.

STAT3 is constitutively active in 50% of breast cancers [114]. STAT3 signaling is shown to activate targets directly involved in proliferation, cell cycle progression and survival such as Cyclin D1 and C-Met, while its inhibition can impair tumor growth [115]. Furthermore, STAT3 signaling has other biological functions in cancer such as, preparing pre-metastatic niches for disseminating tumor cells to colonize and metastasize [116] and promoting development of obesity-associated cancer through activation of inflammatory immune responses [117]. In addition, STAT3 signaling expands the cancer stem cell (CSC) population in breast cancer cells and maintains the expression of genes important for eliciting stem cell phenotype [118, 119].

Traditionally, STAT3 signaling is activated mainly by cytokines such as interleukin-6 (IL6), IL11, and Leukemia inhibitory factor (LIF), and by growth factor receptors such as Epidermal Growth Factor Receptor (EGFR), and HER2 receptor. Newly discovered activators of STAT3 pathway, such as Toll-like receptors (TLRs) and G-protein-coupled receptors (GPCRs), have also been reported [118]. The signaling cascade differs within these upstream activators. For instance, unlike receptor tyrosine kinases, IL6 receptor and TLRs lack kinase activity, they instead rely on Janus kinases (JAKs) to phosphorylate and activate STAT3. Upon binding of these ligands to their receptors, a conformational change occurs, which activates JAK. STAT3 is then recruited to the receptor and phosphorylated at Tyr705 which leads to its dimerization and translocation into the nucleus. In addition, serine/threonine kinases mediate Ser727 phosphorylation, of which enhances STAT3 transcriptional activity (**Figure 3.1**).

As described above, STAT3 has a complex role in tumorigenesis. Discovering new mechanisms by which this pathway exerts its cancer promoting effects will help us design and develop novel and effective therapeutic strategies.

3.2. Materials and methods

Cell Culture: LentiX 293T, DCIS.COM and SUM225 were purchased from Asterand, Inc. (Detroit, MI) in 2007 and were maintained according to the supplier's guidelines.

Immunofluorescence staining (IF): IF was performed as previously described [33]. In addition to mouse anti phospho (Ser727) STAT3 (Millipore # 07-703) other antibodies are listed in Table 2.1. Imaging was performed on a laser-scanning confocal microscope (Model 510; Carl Zeiss MicroImaging, Inc., Thornwood, NY, USA). The acquisition software used was Pascal (Carl Zeiss MicroImaging, Inc.).

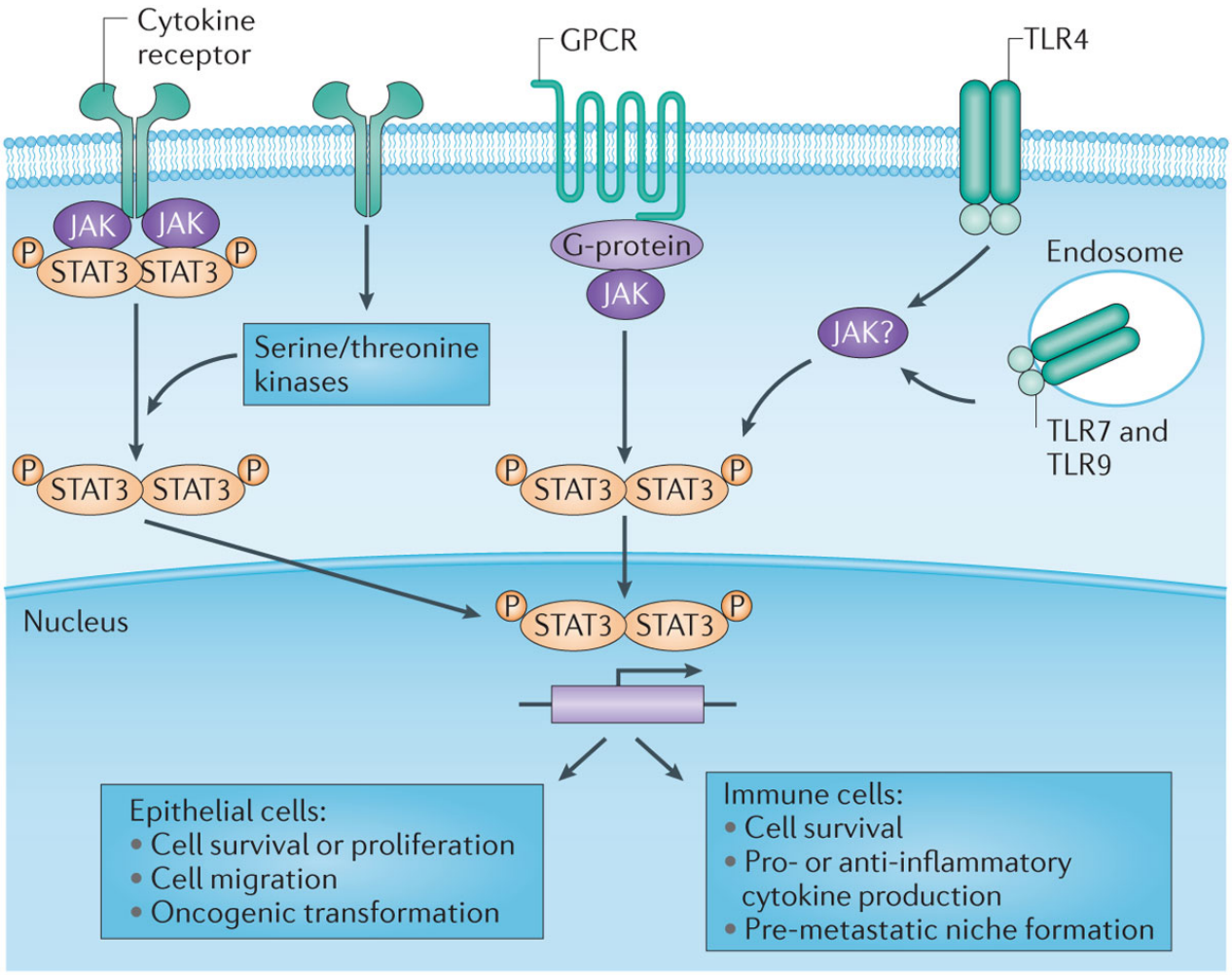

Figure 3.1. Pathways activating STAT3 signaling in cancer. The figure was obtained from Yu, et al 2014. STAT3 signaling is activated by diverse receptors, which cause activation of JAKs and phosphorylation of STAT3 at Tyr705. Serine/Threonine kinases mediate STAT3 phosphorylation at Ser727. STAT3 dimerizes and translocates to the nucleus; STAT3 binds promoters of genes required to promote tumorigenesis.

Plasmids, transfection, and luciferase reporter assay: Plasmids for BCL9 KD were described in chapter two. For STAT3 signaling activity, Cignal STAT3 Reporter (luc) kit (Qiagen # CCS-9028L) was used. Plasmid constructs: Constitutively active STAT3 overexpression, EF.STAT3C.Ubc.GFP (Addgene plasmid 24983) was provided by Linzhao Cheng via Addgene [120]. HEK293T cells were transfected using Lipofectamine 2000 reagent (Invitrogen #11668-027) according to manufacturer's protocols. Luciferase assays were performed using Dual-Luciferase® Reporter Assay System (Promega #E1910).

Western blot analysis and co-immunoprecipitation: For co-immunoprecipitation, 1,000 μg of protein was incubated with antibodies at 4^{o}C overnight followed by centrifugation at 3000 rpm for 1 min in 4^{o}C. Supernatants were incubated with Protein A/G PLUS-Agrose beads (Santa Cruz #sc-2003) at 4°C for 1 hour, followed by a wash in PBS. Proteins bound to beads were eluted with SDS-loading buffer at 99°C for 5 min and then loaded for western blot. Two micrograms whole cell lysates were loaded as input. Western blots analysis was carried out as previously described [103]. For western blots, 25 μg of DCIS.COM and 50 μg of SUM225 cell lysates were loaded into each lane. Rabbit polyclonal anti-STAT3 (Clone:K15, Santa Cruz # sc483) antibody was used. The antibodies used to detect BCL9, β-catenin are listed in **Table 2.1**.

Reverse Phase Protein Array (RPPA)

RPPA lysis buffer, protease inhibitors, phosphatase inhibitors, and SDS Sample Buffer were provided by Cancer Proteomic and Metabolomic Core Facility at the Cancer Prevention and Research Institute of Texas (CPRIT). To prepare cell lysates, cells were harvested by trypsinization, and washed twice with cold PBS and centrifuged at 400xg for 5 minutes. The pellet ($5x10^6$ cells) was resuspended in 300 μl RPPA working solution (composed of 1 ml

protease Inhibitors, 1 ml phosphatase inhibitors, and 3 ml RPPA lysis buffer). Proteins were incubated on ice and vortexed every 10 minutes for 30 minutes. Lysates were centrifuged at 14,000xg for 15 minutes at 4^{o}C, and the supernatant was transferred to a fresh tube. BCA was used to determine protein concentration.

To prepare lysates for RPPA analysis, each lysate was combined with 70 µl of 2xSDS Sample Buffer 3.5 µl β-mercaptoethanol, and RPPA Working Solution was added to a total volume of 140 µl. Samples were heated for 8 minutes at 100^{o}C, brought to room temperature, and centrifuged for 2 minutes at 14,000 xg. Supernatant was collected and aliquoted into three tubes and shipped to CPRIT (Cancer Proteomic and Metabolomic Core Facility) for RPPA (https://www.bcm.edu/centers/cancer-center/research/shared-resources/cprit-cancer-proteomics-and-metabolomics/reverse-phase-proteinarray).

3.3. Results

BCL9 knockdown cells showed a significant reduction in EGFR and STAT3 signaling: To address whether or not BCL9 regulates other oncogenic pathways, RPPA of 200 validated antibodies was performed on cell lysates from DCIS.COM and SUM225 BCL9-KD or control cells. The array covers multiple total proteins and phosphoproteins in the following protein pathways or functional protein groups: epithelial-mesenchymal transition, stem cells, apoptosis, DNA damage, proliferation and cell cycle, growth factor receptors, cytokines/STATs, and nuclear receptors/transcriptional regulatory proteins. BCL9 KD decreased expression of proteins involved in pro-tumorigenic pathways in both DCIS cell lines. Interestingly, total and phosphorylated EGFR and STAT3 protein levels were also down-regulated in our dataset (Table 3.1).

DCIS.COM	KD vs NS	SUM225	KD vs NS
c-Jun	**-1.54**	c-Jun (60A8)	-1.53
Cox-2	**-1.35**	ILK1	-1.29
FGFR1	**2.20**	Integrina4	-1.12
HER2/c-ErbB2	**1.23**	KLF4	-1.18
Integrina4	**-1.21**	p-AKT	-1.52
Integrinb3	-2.22	p-ALK (384)/Y1586)	-1.41
MEK6	1.22	p-AMPKb1 (S108)	-1.41
p70S6K	**-1.09**	p-Chk1 (S345)	-1.51
p-Akt (T308)	-1.70	p-Chk2 (S33/35)	-1.21
p-ALK (Y1604)	-1.26	p-EGFR	-1.25
p-AuroraA (T288)/B(T232)/C(T198)	-1.50	p-HER2/ErbB2 (Y1248)	-1.24
p-c-Jun (S63)	-1.33	p-HER2/ErbB2 (Y877)	-1.34
p-EGFR	**-1.28**	p-Jak1 (Y1022/1023)	-1.31
p-EGFR	**-1.13**	p-MEK1/2 (S217/221)	-1.37
p-MEK1/2	1.90	p-p70S6K (T389)	-1.25
p-p44/42MAPK (Erk1/2)(T202/Y204)	1.95	p-Ret (Y905)	-1.17
p-p70S6K (T389)	**-1.24**	p-SHC (2431)(Y317)	-1.21
p-Rb (S807/811)	-1.97	p-Src (Y527)	-1.44
p-SAPK/JNK (T183/Y185)	1.50	p-STAT3 (S727)	-1.15
p-Src (Y527)	**-1.60**	p70S6K	-1.18
p-STAT3 (S727)	**-1.30**	Sox2	-1.22
STAT3	**-1.27**	Sox9	-1.33
		Src-2 (TIF2)	-1.18
		STAT3	-1.21

Table 3.1: BCL9 regulates expression of several tumorigenic factors. Reverse Phase Protein Array (RPPA) was performed on DCIS.COM and SUM225 cells KD of BCL9 or control. The table shows significant fold change (bold) values comparing KD to non-silencing control. Factors common to both cell lines are in green. BCL9 KD decreased expression of several protumorigenic factors. In DCIS.COM, BCL9 KD enhanced expression of some factors (FGFR and HER2) and are shown in red.

To determine whether or not STAT3 correlates with BCL9 in breast cancers, TCGA analysis of breast cancers that had alterations in *BCL9* gene was performed. Data included 962 breast cancers, 26% of which showed BCL9 mRNA upregulation (described in chapter four). As shown in **Figure 3.2**, TCGA data showed a significant correlation between BCL9 expression and phosphor(Tyr705)STAT3 (P= 0.03). These data suggest that BCL9 may regulate and activate STAT3 either through a direct interaction, or indirectly by controlling STAT3 upstream regulators.

STAT3 upregulation is associated with DCIS that progressed to invasive breast cancer: Before addressing the role of BCL9 in STAT3 signaling, STAT3 was evaluated in the DCIS.COM and SUM225 MIND models described in chapter two. As shown in Figure 3.3. microarray analysis revealed that STAT3 was upregulated from 2 to 6 week time point post intraductal injection in both cell lines (**Figure 3.3**). Ingenuity Pathway Analysis (IPA) of microarray data from DCIS.COM and SUM225 MIND xenografts, showed that genes in the STAT3 signaling pathway were upregulated (**Figure 3.4**). To confirm the microarray results, IF staining of DCIS.COM and SUM225 MIND xenografts with anti-phosphor(Ser727)STAT3 antibody was performed, These studies showed BCL9 and phosphor(Ser727)STAT3 co-localizion in nuclei of DCIS lesions (**Figure 3.5**).

A

Protein	Residue	Unaltered	Altered	p-value
RPS6KA1	pT359	-0.11	0.36	▲ **4.66E-05**
RB1	pS807	-0.12	0.29	▲ **4.56E-04**
SHC1	pY317	-0.07	0.25	▲ **9.82E-04**
ARAF	pS299	-0.07	0.27	▲ **0.005**
MAPK1/MAPK3	pT202	-0.06	0.19	▲ **0.02**
ESR1	pS118	-0.07	0.21	▲ **0.03**
MAP2K1	pS217	-0.04	0.19	▲ **0.036**
STAT3	pY705	-0.06	0.17	▲ **0.036**
NFKB1	pS536	-0.06	0.19	▲ **0.039**
RPS6	pS240	0.05	-0.16	▼ **0.049**

B

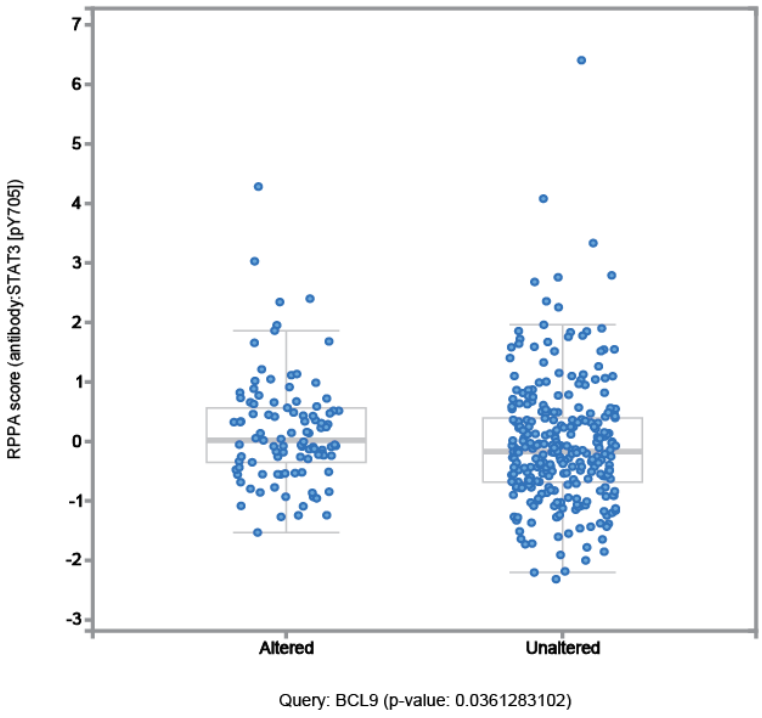

Figure 3.2: TCGA data showed a significant correlation between BCL9 expression and p-STAT3. The data included 962 breast cancers, 26% of which showed BCL9 upregulation.

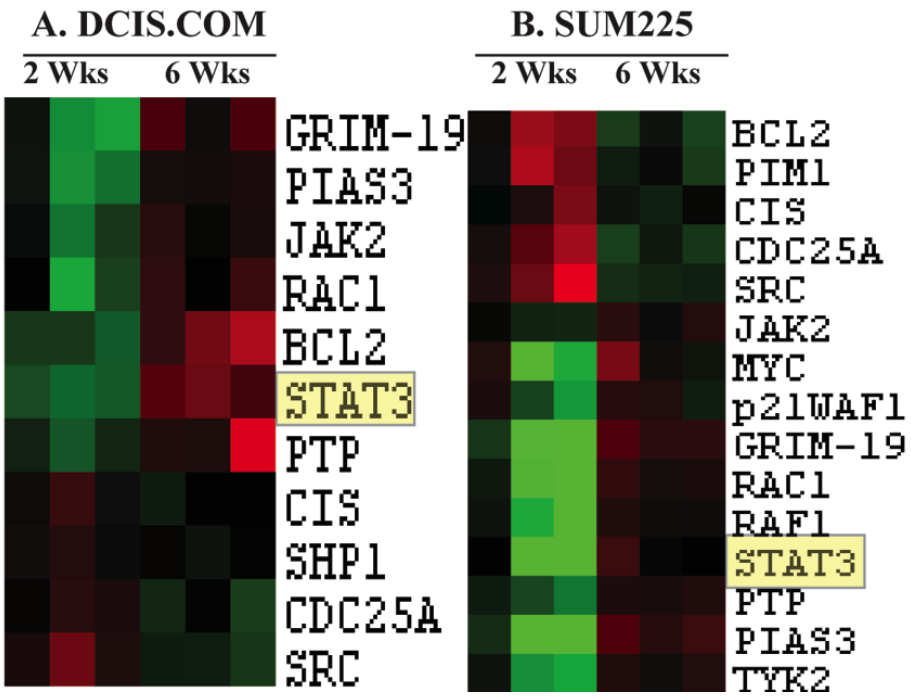

Figure 3.3. STAT3 is upregulated in DCIS.COM and SUM225 MIND xenografts during progression. Microarray data obtained from DCIS.COM (A), and SUM225 (B)-MIND xenografts from 2 to 6 weeks post intraductal injection show upregulation of STAT3 expression.

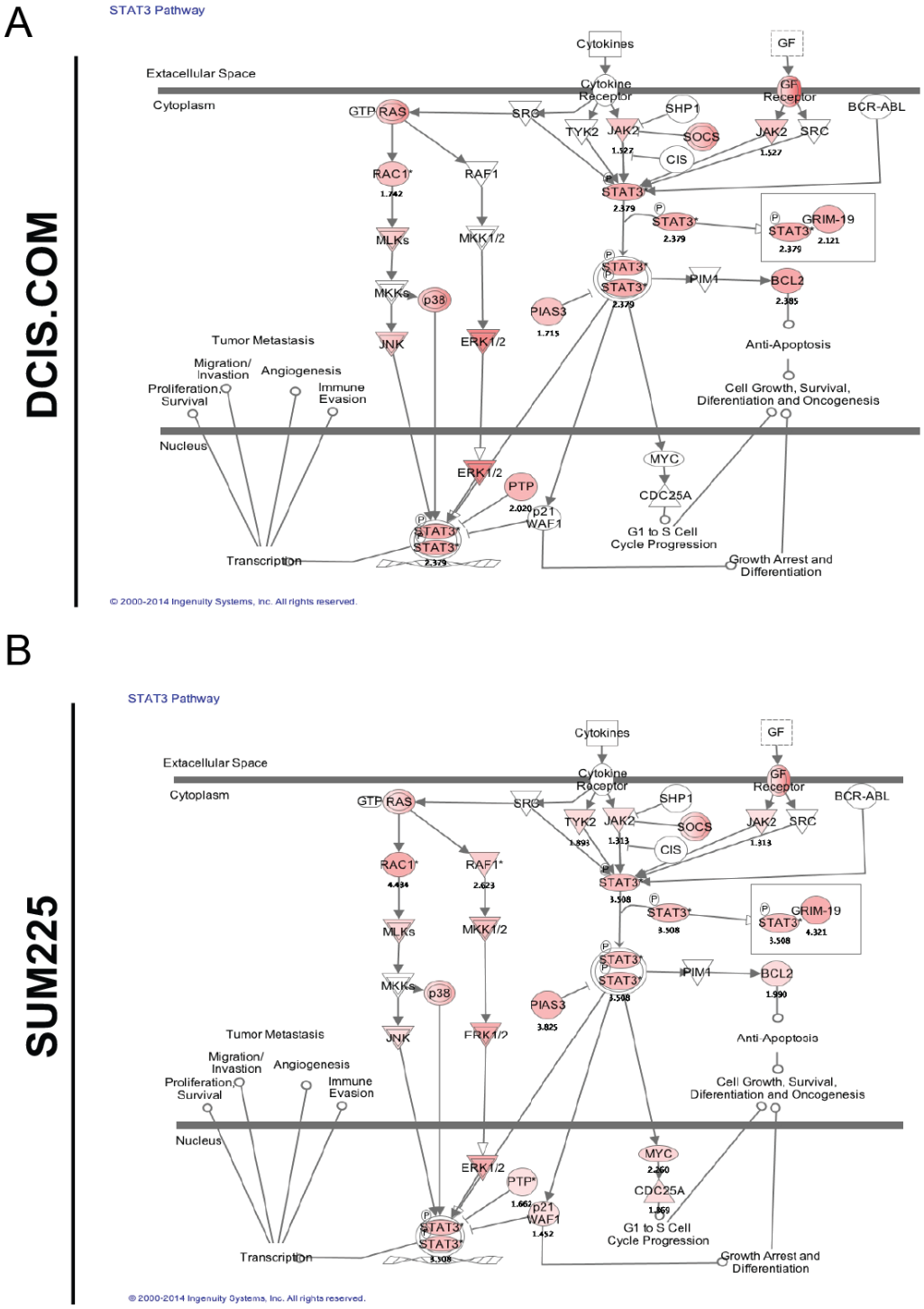

Figure 3.4. IPA analysis of DCIS.COM and SUM225 MIND xenografts microarray data. IPA analysis of the microarray data obtained from DCIS.COM (A), and SUM225 (B)-MIND xenografts from 2 to 6 weeks post intraductal injection show upregulation of STAT3 expression as well as other genes involved in STAT3 signaling pathway.

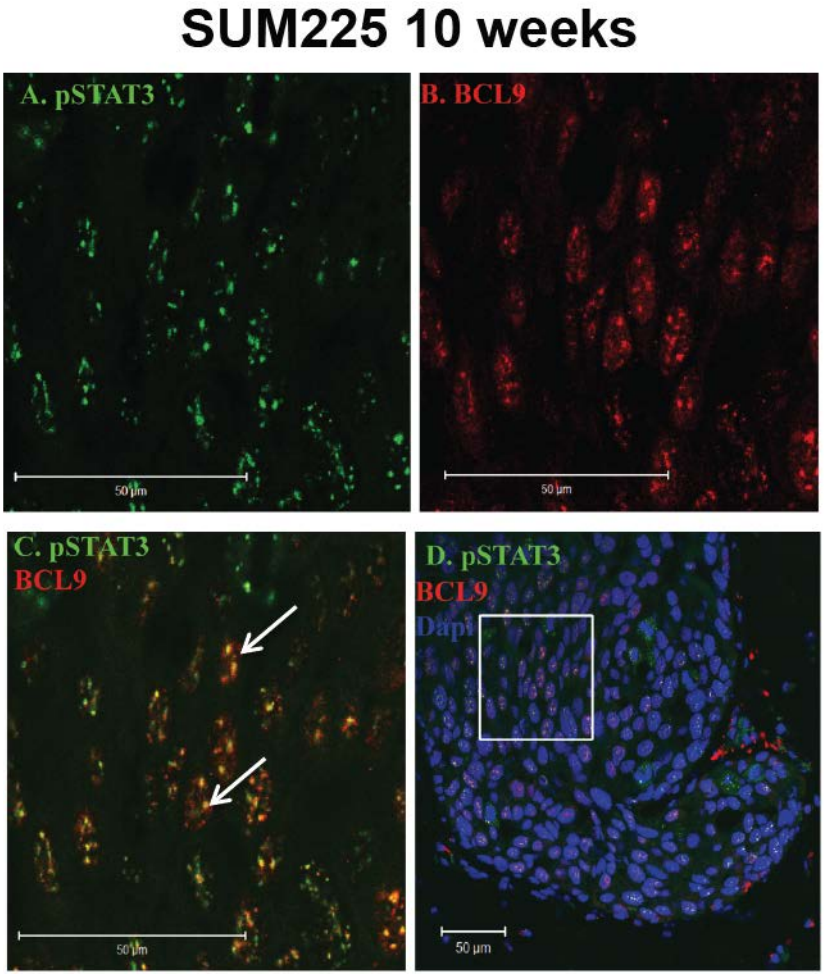

Figure 3.5. Phosphorylated STAT3 co-localizes with BCL9 in DCIS MIND xenografts during progression. Immunofluorescence staining of SUM225 at 10 weeks post-intraductal injection. BCL9 is conjugated to Alexa-Fluor 594, shown in red, and p(Ser727)STAT3 is conjugated to Alexa-Fluor 488, shown in green. Merged BCL9 and pSTAT3 shows co-localization points in yellow (white arrows). Nuclei are counterstained with DAPI. Scale bars 50 µm, 40x objective was used.

BCL9 binds STAT3 and enhances STAT3 signaling: To test if BCL9 interacts with STAT3, whole cell extracts of DCIS.COM and SUM225 were co-immunoprecipitated with anti-BCL9 antibody followed by Western blot with anti-STAT3 antibody. As shown in **Figure 3.6**, BCL9 and STAT3 interacted with each other in both cell lines. In addition, an inducible STAT3-responsive firefly luciferase construct was utilized to measure STAT3 signaling activity in 293T cells that were non-transfected (control) or transiently transfected with: constitutively active STAT3 (CA-STAT3), pCDH-BCL9-overexpression vector (BCL9), or both (CA-STAT3+BCL9). As seen in **Figure 3.7**, BCL9 overexpression significantly enhanced STAT3 signaling compared to control (4.54 ± 0.22 fold vs. 1.0 ± 0.07 fold; $P<0.05$), and BCL9+CA-STAT3 significantly increased STAT3 activity compared to CA-STAT3 alone ($P<0.01$). These findings support that BCL9 regulates STAT3 signaling. Furthermore, Western blot analysis of BCL9-KD and control DCIS.COM and SUM225 cells with phosphor(Ser727)STAT3 showed reduced phosphorylated STAT3 levels with BCL9 KD, suggesting that BCL9 does not only bind STAT3 but also mediates STAT3 activation (**Figure 3.8**).

3.4. Discussion

In chapter two, it was demonstrated that BCL9 is upregulated in both DCIS models, and that BCL9 knockdown inhibited proliferation, migration and invasion in both cell lines *in vitro* and *in vivo*. It was also shown that these effects were mediated through the WNT signaling pathway in case of the basal cell line (DCIS.COM), while the HER2 overexpressing cell line (SUM225) lacked WNT signaling. In this chapter, RPPA, and TCGA data analysis provide evidence that BCL9 levels correlate with phosphor(Tyr705)STAT3 and phosphor-EGFR protein levels . These data support the hypothesis that BCL9 mediates the activation of STAT3 signaling activity.

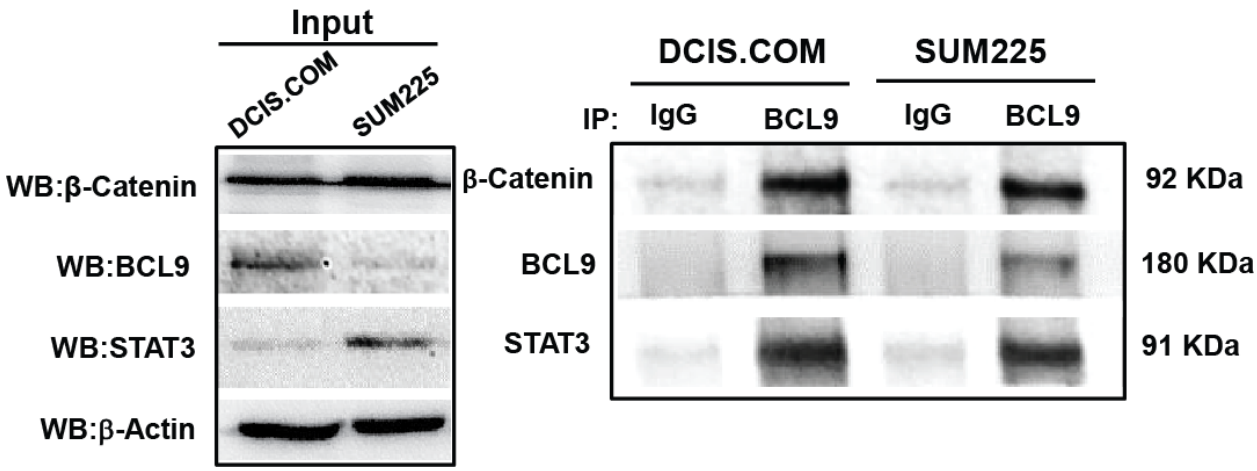

Figure 3.6. BCL9 IP followed by Western blotting demonstrated binding of BCL9 to β-catenin and STAT3 in DCIS.COM and SUM225.

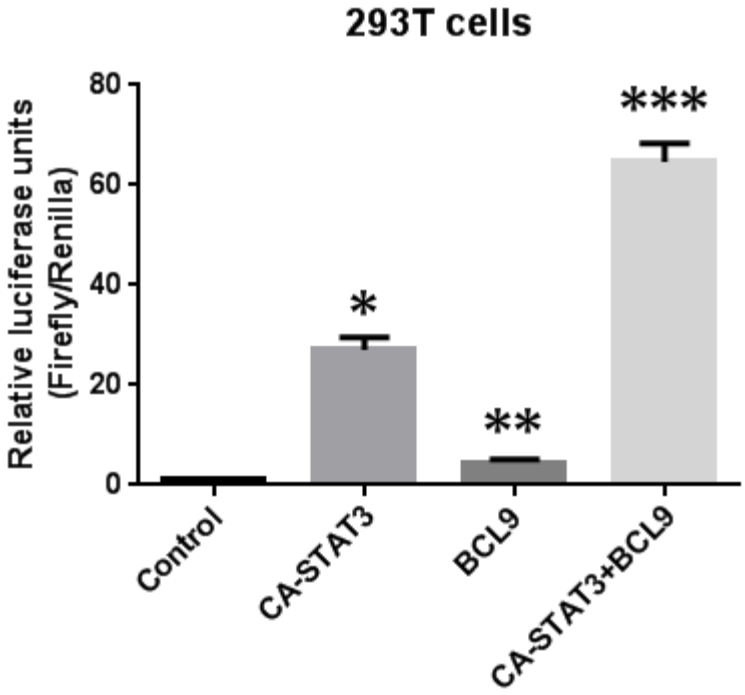

Figure 3.7. BCL9 overexpression enhances STAT3 signaling activity in 293T cells. Bar graph represent STAT3 reporter activity in 293T cells non-transfected (control) or transiently transfected with: constitutively active STAT3 (CA-STAT3), pCDH-BCL9-overexpression vector (BCL9), or both (CA-STAT3+BCL9). The reporter is a mixture of inducible STAT3-responsive firefly luciferase construct and constitutively expressing Renilla luciferase construct (40:1) obtained from Qiagen (CCS-9028L). Data represent mean ± s.e.m (n=3, **P*<0.05).

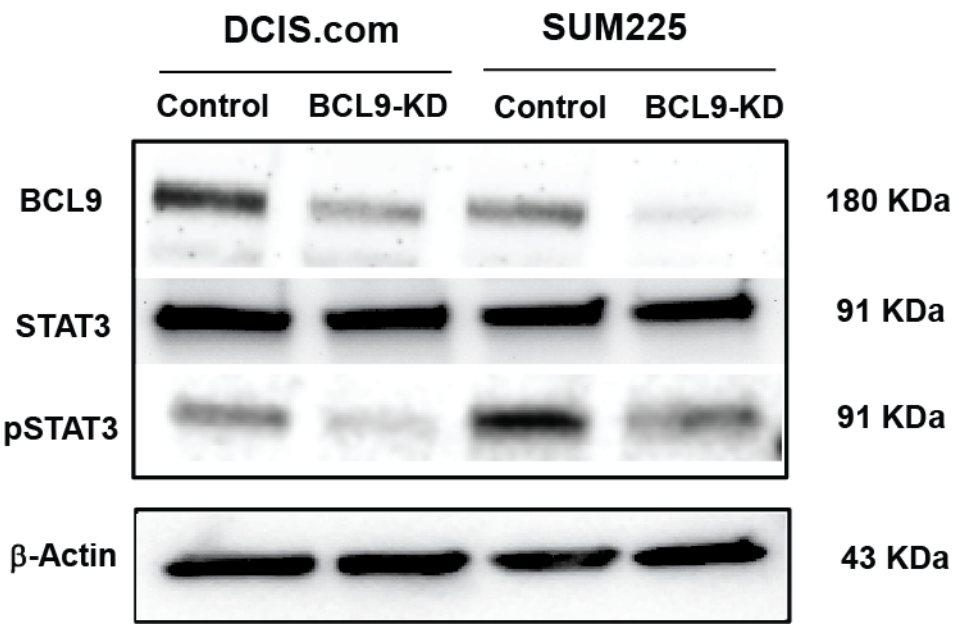

Figure 3.8. BCL9 KD cells showed reduced STAT3 activation. Representative Western blot analysis of cell lysates from control and BCL9-KD cells blotted with anti-BCL9, anti-STAT3 and anti-phospho(Ser727) STAT3 antibodies. β-actin was used as a loading control.

The mechanism for BCL9 mediated activation of STAT3 signaling maybe by enhancement in the transcription of tyrosine/serine kinases. STAT3 tyrosine phosphorylation occurs by receptor associated JAK kinases, and Src-family members, and is associated with STAT3 activation. Previous studies showed that inhibition of Src and JAKs decreased STAT3 activity and thus growth and survival of human breast cancer cells [121]. STAT3 serine phosphorylation is mediated by MAPK, p53, and JNK [122]. Further studies will need to assess levels of these kinases in BCL9 knockdown DCIS cells. Table 3.1, already showed downregulation of Src in BCL9-KD DCIS.COM and SUM225 cells, which supports that BCL9 may modulate this kinase. However, results need confirmation by Western blot analysis for phospho-proteins.

Another mechanism by which BCL9 might be regulating STAT3 is through secreted cytokines and growth factors, growth factor receptors. Interestingly, Zhu, et al. 2015 showed that BCL9 mediated the expression and secretion of Cyclophillin-A from bone marrow endothelial cells. Cyclophillin-A binds CD147 on multiple myeloma cells thereby increasing STAT3 expression and tumor colonization and growth [123]. EGFR is an activator of STAT3 signaling, and it serves as transcriptional coactivator that binds STAT3 in the nucleus [124]. Studies also showed EGFR to be a direct target of WNT/β-catenin signaling pathway [125]. EGFR was down regulated in the RPPA analysis, which might be a direct result of inhibition of β-catenin/BCL9 mediated transcriptional activity.

Co-immunoprecipitation experiments and IF co-staining revealed a novel interaction between BCL9 and STAT3. As described in the introduction, BCL9 possesses a potent transactivation domain in the HD4-HD5 region that enables it to activate transcription independent of Pygo [72]. This observation suggests that STAT3 may also serve as a binding partner for BCL9 either

directly or as part of a complex. Further studies will be necessary to evaluate BCL9-STAT3 interactions, these would include *in vitro* coupled transcription/translation reactions, and Chromatin Re-Immunoprecipitation (Re-ChIP) assays.

3.5. Conclusion

The working model derived from these results is illustrated in **Figure 3.9.** When BCL9 is altered in a subset of DCIS lesions, the concept is that it will either bind β-catenin or STAT3 to activate transcription of an upstream STAT3 signaling activator that will in turn cause further STAT3 activation. Activation of STAT3 signaling will induce transcription of protumorigenic genes. Future studies will identify these secreted factors/kinases. Disrupting this positive feedback cycle by inhibiting BCL9 to STAT3 interaction could be a new powerful and effective strategy to prevent DCIS to IDC transition.

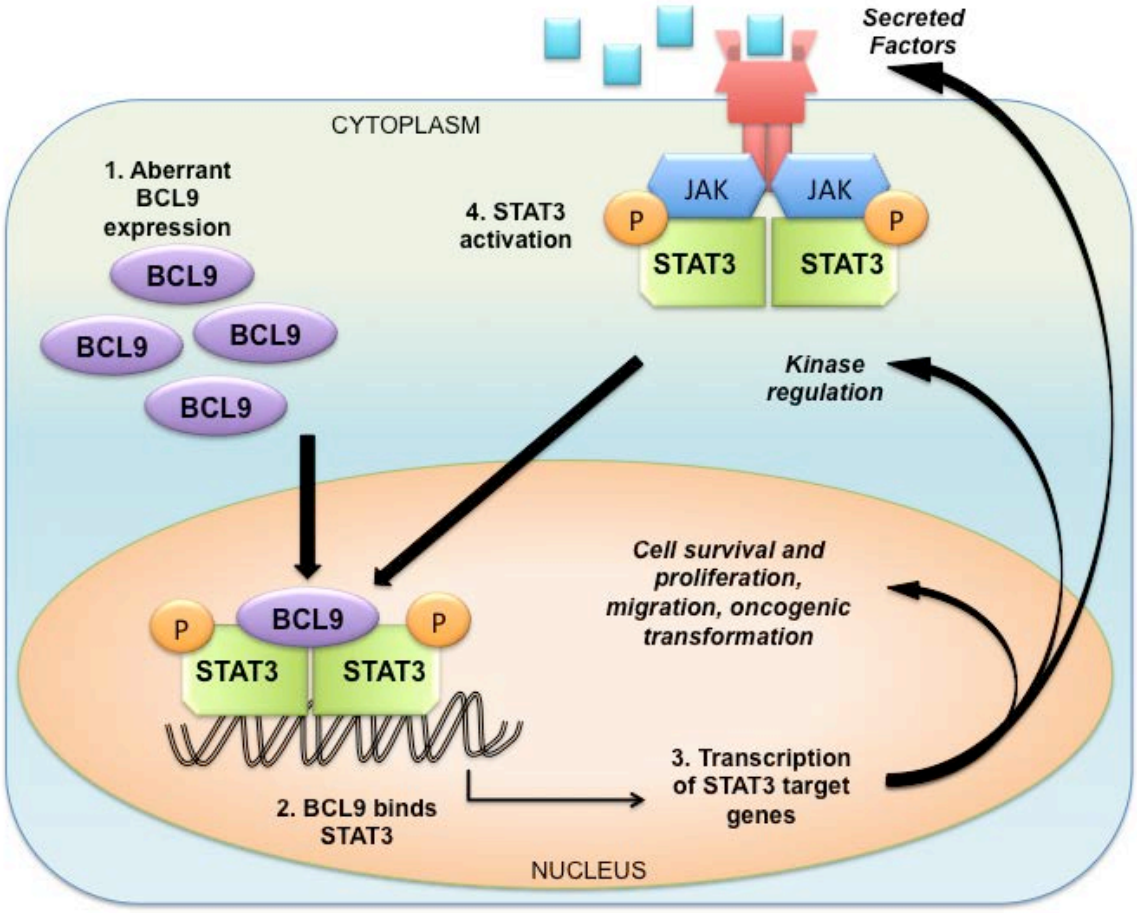

Figure 3.9. A model of BCL9 and STAT3 collaboration demonstrating how BCL9 and STAT3 may interact to promote tumorigenesis.

CHAPTER FOUR

BCL9 as a Potential Biomarker of High Risk DCIS

4.1. Introduction

Various risk stratification methods have been developed to identify DCIS patients at low, intermediate, and high risk of recurrence after breast conserving surgery, and who will benefit from radiotherapy after surgery. These methods are based on clinical, radiological, and pathological risk stratification systems, but none has shown value in predicting invasive recurrence. Molecular profiling is a new strategy to classify DCIS lesions into subgroups based on their risk of recurrence. There are several studies that involve gene expression profiling in DCIS to understand the molecular changes linked to development of invasion from DCIS [126]. However, few of these studies focus on the association between gene expression changes and risk of local recurrence. One retrospective study utilized DCIS lesions from 327 patients who had undergone surgery but not radiation; in this study, genomic profiling correlated with local recurrence rate, and yielded a DCIS recurrence score based on seven cancer genes and five reference genes [11]. Recent studies demonstrated some utility in using expression of a limited gene set for predicting DCIS recurrence; however, general use of this system is controversial [126]. Thus, finding biomarkers of DCIS high risk for recurrence is still a research priority in breast cancer.

As shown in chapter two, total BCL9 expression in human breast cancer samples correlated with progression to invasion, and preliminary studies showed heterogeneous BCL9 expression patterns in pure DCIS. Thus, it has been hypothesized that BCL9 alone or as part of an expression signature can mark DCIS lesions that have higher risk of invasion. In this chapter, the expression pattern of BCL9 in primary pure DCIS and DCIS associated with IDC was evaluated.

4.2. Materials and Methods

Patient samples for analysis of BCL9 as a potential biomarker of high risk: Tissue sections for BCL9 analysis were provided by Dr. Jeffrey Marks (Duke University) as a part of the NIH's Early Detection Research Network (EDRN) GYN/Breast working group initiative to validate biomarkers that may predict a greater risk of invasive breast cancer or bad prognosis disease. These samples were identified, procured, and sectioned, stored, and maintained under a Duke approved protocol (eIRB Pro00027811, J. Marks, PI). Two categories were defined: cases of DCIS that progressed to invasive cancer in the same breast between 1.8 and 17.6 years after initial diagnosis and controls of DCIS that did not progress (either recurrent DCIS or invasive cancer) over a minimum of 10 year follow-up. Controls were further selected based on size and nuclear grade to match or exceed case size. The Van Nuys index (Silverstein, Lancet 1995) for controls had a higher median value than that of the cases (p=0.04).

Statistical analysis: Data are presented as mean normalized expression ± s.e.m. Unless otherwise noted, one-way analysis of variance (ANOVA) was used for statistical comparisons. A value of $P \leq 0.05$ was considered significant.

Immunofluorescence staining (IF): IF was performed as previously described [33]. Antibodies are listed in Table 2.1. The acquisition software used was Pascal (Carl Zeiss MicroImaging, Inc). Fluorescence quantitation and analysis was done using MetaMorph® Microscopy Automation & Image Analysis Software (Molecular Devices, Inc.,Sunnyvale, CA ,USA).

4.3. Results

Enhanced BCL9 nuclear expression in DCIS with invasive component. To evaluate BCL9 as a potential biomarker for DCIS with high risk of recurrence, the pattern of BCL9 expression was initially examined using a tissue microarray (TMA) composed of eight patient DCIS samples: 3 DCIS with IDC and 5 pure DCIS. **Figure 4.1** illustrates the 3 patterns of staining observed: weak cytoplasmic staining (adjacent normal; **Figure 4.1A,** left panel); mixed nuclear and cytoplasmic (**Figure 4.1A,** middle panel and **Figure 4.1B,** lower panel); and enhanced nuclear expression (**Figure 4.1A,** right panel and **Figure 4.1B,** top panel). All adjacent normal breast epithelial cells expressed weak cytoplasmic BCL9 expression (similar to **Figure 4.1A,** left panel). Strikingly, all DCIS with IDC cases exhibited >90% enhanced nuclear expression (similar to **Figure 4.1A** right panel). Interestingly, enhanced BCL9 nuclear expression was associated with a loss of cytokeratin expression, which is indicative of EMT (as seen in **Figure 4.1A**, right panel). Although increased expression of BCL9 was also observed in stromal macrophages (**Figure 4.1A**, right panel), the role of BCL9 in these cells is beyond the scope of this study. Among the pure DCIS cases, comedo or cribriform DCIS exhibited enhanced BCL9 nuclear expression; papillary DCIS cases showed mixed nuclear and cytoplasmic BCL9 expression (data not shown).

To quantify BCL9 protein expression, IF staining with anti-BCL9, anti-K5/K19 and DAPI was performed on tissue microarrays from 30 pure DCIS and 62 DCIS with IDC patients. Nuclear and cytoplasmic median integrated density was quantified using Metamorph® Microscopy Automation and Image Analysis Software. As shown in **Figure 4.2**, pure DCIS lesions have a wider range of nuclear BCL9-median integrated density values, which reflects the heterogeneity of pure DCIS lesions. In addition, DCIS lesions with IDC have significantly higher

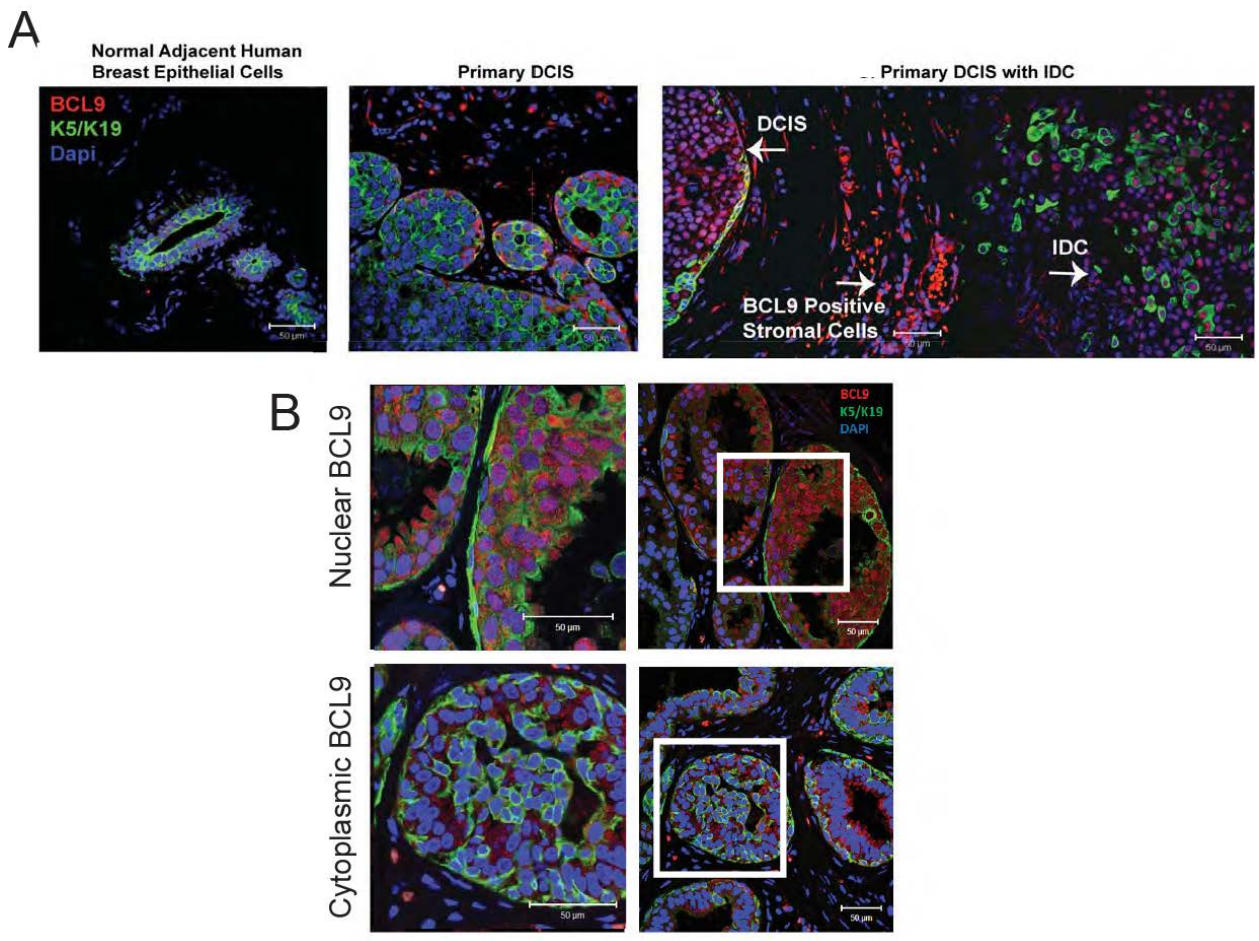

Figure 4.1. BCL9 may serve as a biomarker of high risk DCIS. (A) IF staining using anti-BCL9 antibody (red), anti-K5/K19 (green), and counterstained with DAPI (blue) in patient DCIS samples with and without invasion, and in normal adjacent human breast epithelial cells. (B) Representative IF images for patient DCIS samples with the above antibodies, demonstrating nuclear (top) and cytoplasmic (bottom) BCL9 expression patterns. Scale bars=50 μm

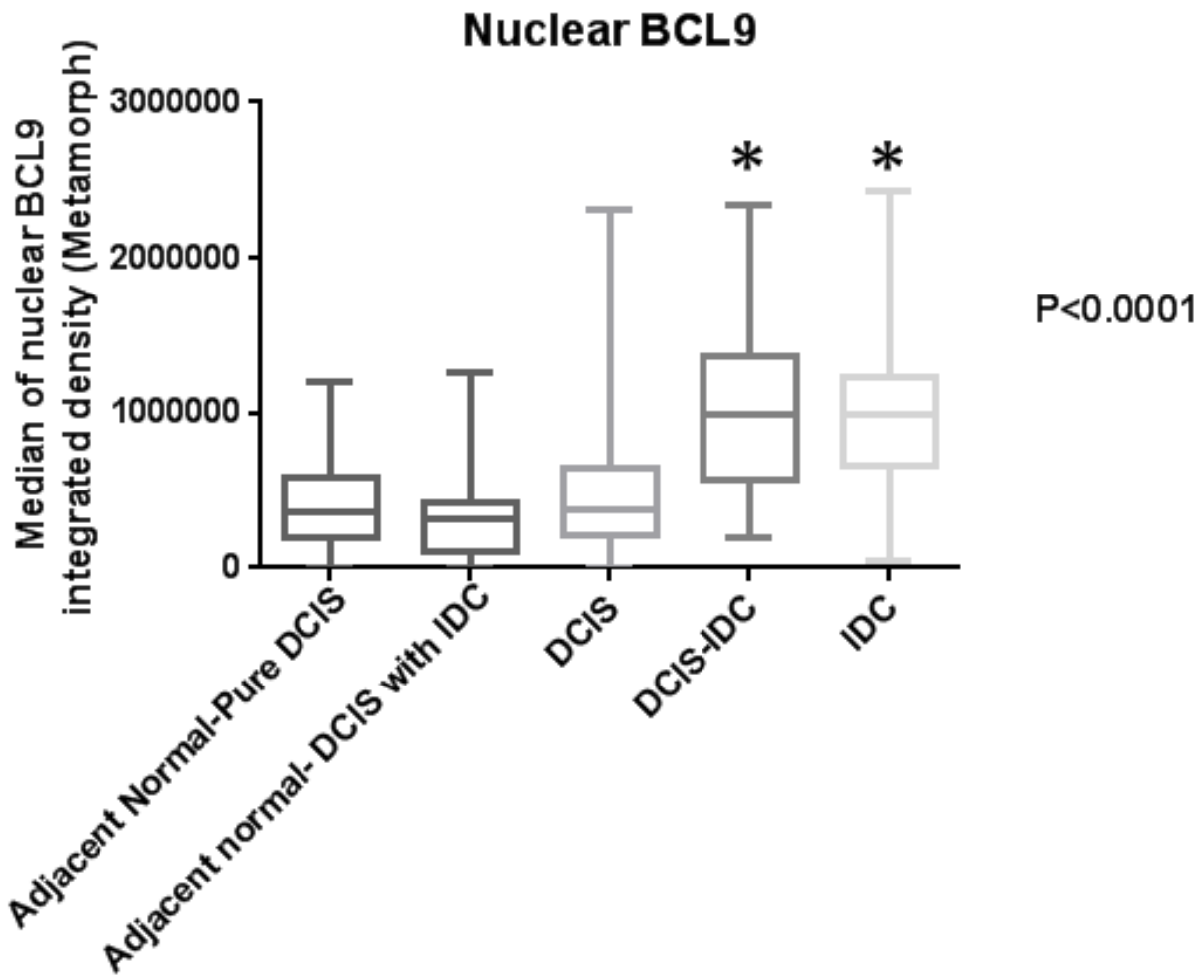

Figure 4.2. BCL9 nuclear expression is higher in DCIS/IDC than in pure DCIS cases. Representative box plots of median nuclear BCL9 integrated density measured by Metamorph software in pure DCIS and DCIS/IDC cases. The groups represent measurements from adjacent normal tissue and DCIS in pure DCIS cases, and adjacent normal tissue, DCIS component and IDC component in DCIS/IDC cases. The box plots represent means and the bars represent standard deviation from the mean, *P<0.0001.

integrated density values than pure DCIS (1,007,000 ± 58,940 compared to 519,531 ± 91,248; Mean ± s.e.m, P<0.0001). Furthermore, there was no significant difference between BCL9 expression in the DCIS component and IDC component of DCIS with IDC cases. These data suggest that BCL9 pattern is more useful in sub-classifying pure DCIS lesions before they become invasive.

Enhanced BCL9 nuclear expression in high risk DCIS. Since high nuclear BCL9 expression is present in DCIS with concurrent IDC, it may mean that this pattern predicts aggressive behavior; however, we do not know whether the pure DCIS cases will recur, nor do we know whether or not the lesions were completely excised, which could of course ensure a favorable outcome, even if the pure DCIS lesions with nuclear BCL9 were more aggressive. To begin to address this question the pattern of BCL9 expression, was examined in a patient set comprised of 28 pure DCIS samples with over 10 year followup (**Figure 4.3**). In this set, BCL9 localization was compared with pathologic variables that correlated with aggressive behavior and high risk for recurrence: nuclear grade, hormone receptor status and human epidermal growth factor receptor 2 (HER2) expression [127]. This analysis showed that DCIS lesions expressing higher numbers of nuclear BCL9 positive cells were more likely to be ER negative (*P*=0.004; Wilcoxon rank-sum test), PR negative (*P*=0.003; Wilcoxon rank-sum test), high nuclear grade (Spearman correlation=0.49; *P*=0.008), and high HER2 expressing (Spearman correlation=0.56; *P*=0.002; **Figure 4.3**). Based on these data, BCL9 may serve as a biomarker if validated in a larger dataset of DCIS patients with known outcome.

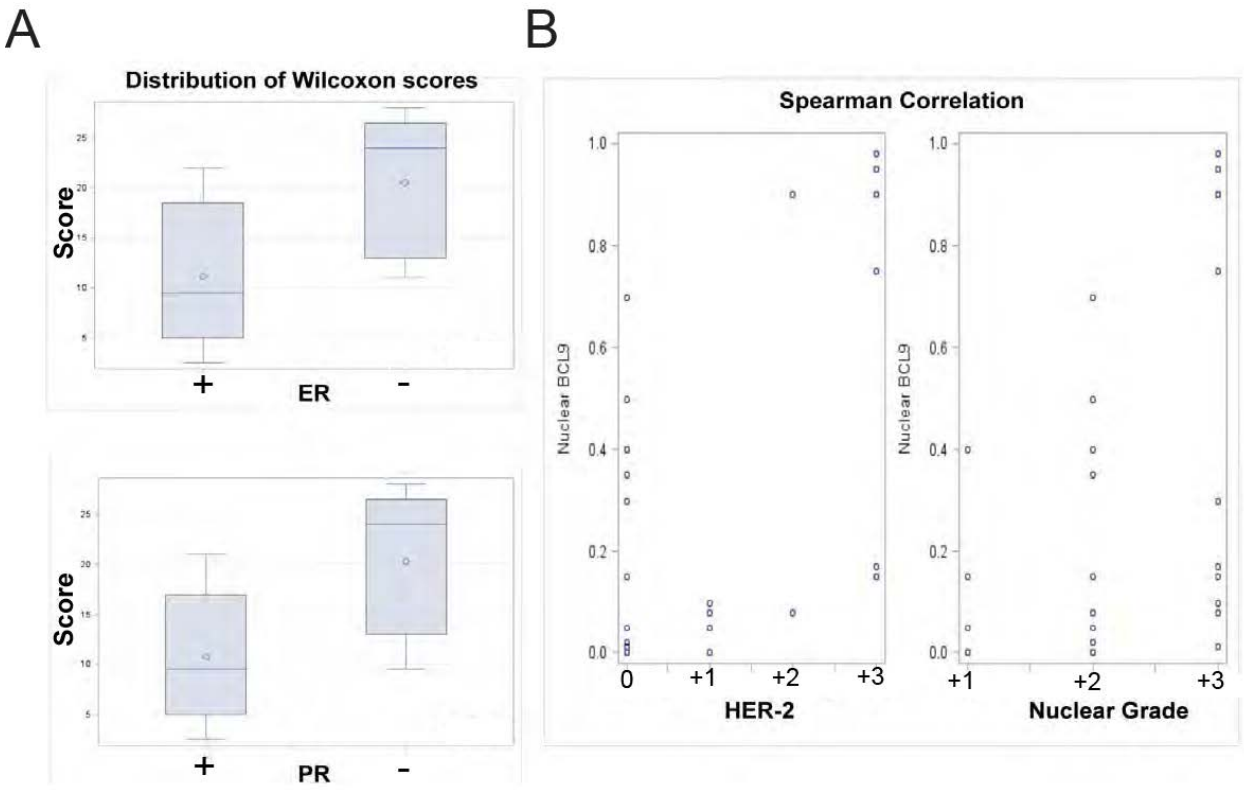

Figure 4.3. Statistical analysis of tissue sections from 28 patients with pure DCIS analyzed by IF using anti-BCL9 antibody. This analysis showed that the percent of cells expressing nuclear BCL9 was significantly higher in DCIS that were ER negative (*P*=0.004; Wilcoxon rank-sum test), PR negative (*P*=0.003; Wilcoxon rank-sum test) (A), high HER2 (Spearman correlation =0.56; *P*=0.002), and high nuclear grade (Spearman correlation=0.49; *P*=0.008) (B). Median percent of cells positive for nuclear BCL9 (IQR=interquartile range) for ER positive samples = 8% (1%, 40%); for PR positive = 8% (1%, 35%); ER negative = 90% (15%, 95%); PR negative = 90% (15%, 95%).

***BCL9* gene is altered in breast cancers.** Interestingly, analysis of TCGA data (provisional TCGA; 959 cases) (http://cancergenome.nih.gov/) showed that 26% of invasive breast cancers contain *BCL9* gene alterations. The majority of these alterations include amplification (13%) and mRNA upregulation (17%). This is a significant level of gene alteration compared to *ESR1* (8%), *ERBB2* (19%) and *BCL9L* (5%) (**Figure 4.4**). Furthermore, *BCL9* amplification is observed in a significantly higher proportion of invasive basal breast cancer (BLBC) subtypes compared to other subtypes (**Figure 4.5**) [110, 113]. Moreover, there is a significant association between *BCL9* gene amplification and mRNA upregulation (**Figure 4.6**). These data suggest that BCL9 may predispose to development of basal like invasive breast cancers. The TCGA data were also analyzed for the expression of differentially expressed genes in breast cancers that showed BCL9 mRNA upregulation. BCL9 upregulation was defined as BCL9 expression levels above the range observed by normal samples. IPA analysis on the differentially expressed genes showed WNT/β-catenin pathway to be significantly upregulated in BCL9 high compared to BCL9 low breast cancers [128].

A.

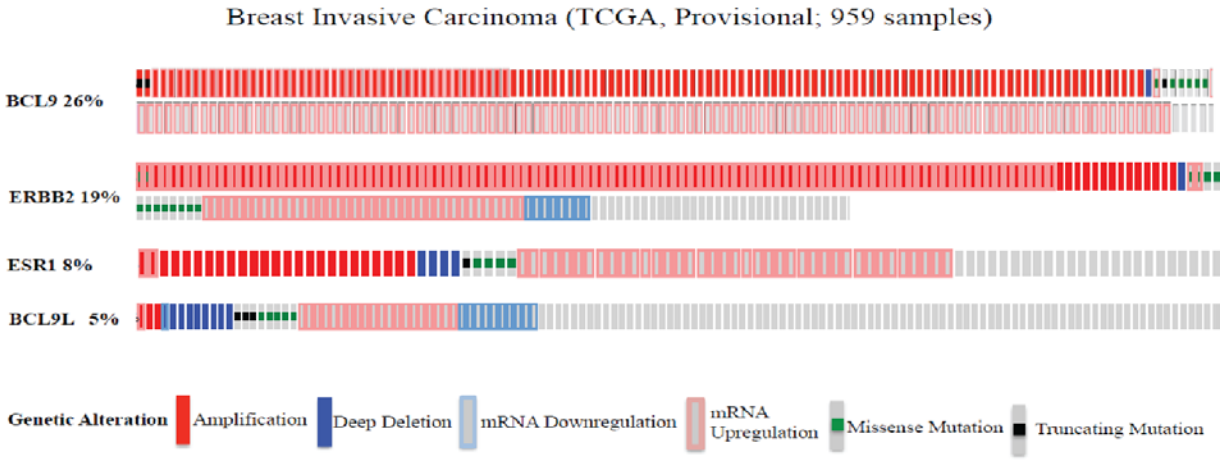

B.

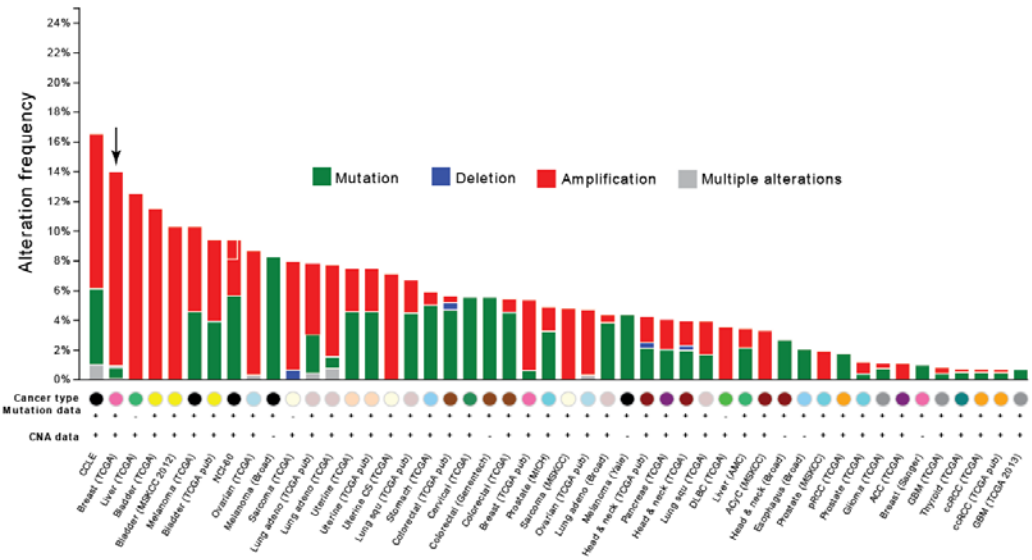

Figure 4.4. A significant proportion of breast cancers show *BCL9* gene alteration. (A) TCGA Provisional data shows that 26% of invasive breast cancers (total of 959 cases) contain a genetic alteration in *BCL9* gene; the majority of these consist of gene amplification and mRNA up-regulation. This is a significant level of genetic alteration when compared to *ERBB2* (19%), *ESR1* (8%) and *BCL9L* (5%). (B) *BCL9* gene alterations across all cancers. *BCL9* gene is altered in many cancers including breast, liver and bladder. The arrow points to invasive breast cancers showing 14% gene alteration (135 in 962 cases).

A.

	All tumors	*Basal*	*Luminal A*	*Luminal B*	*HER2 enriched*
No. Cases	825	81	235	133	58
No. Amplified	37	15	5	3	3
% Amplified	4.5%	18.5%	2.1%	2.3%	5.2%
95% CI	3.2%,6.1%	10.8%, 28.7%	0.7%, 4.9%	0.5%, 6.5%	1.1%, 14.4%

B.

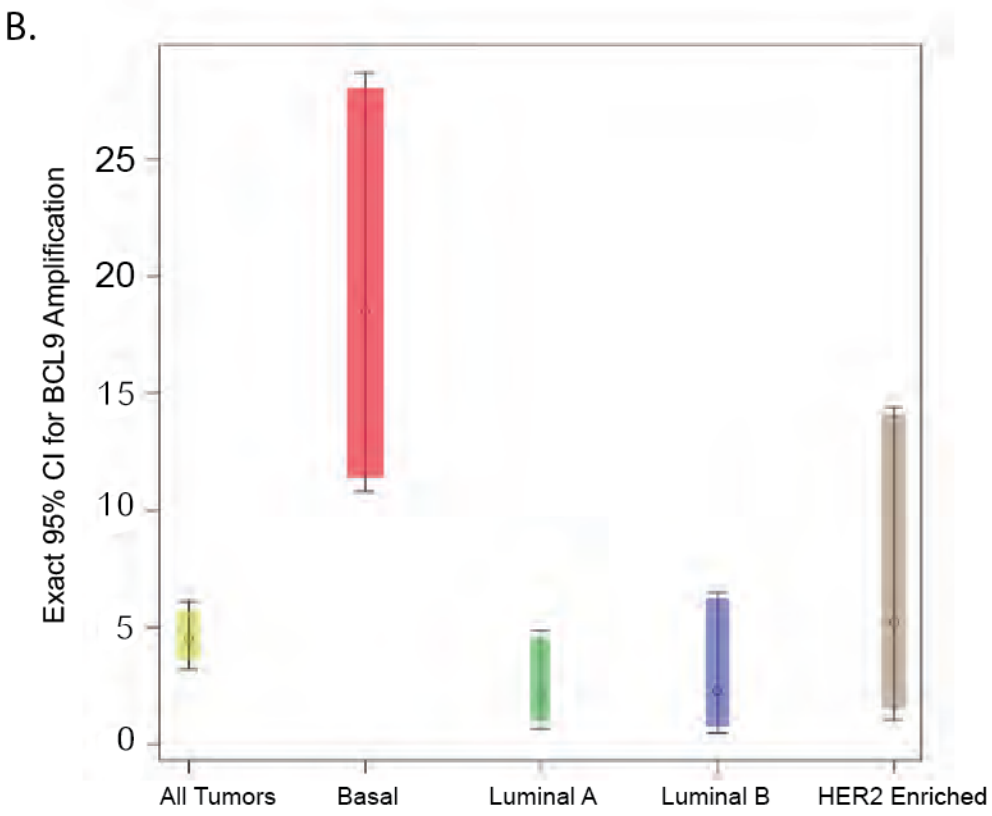

Figure 4.5. *BCL9* genomic alteration is higher in basal breast cancers. TCGA data shows that a significantly higher proportion of basal breast cancers contain *BCL9* genomic amplification compared to other subtypes (total of 825 cases).

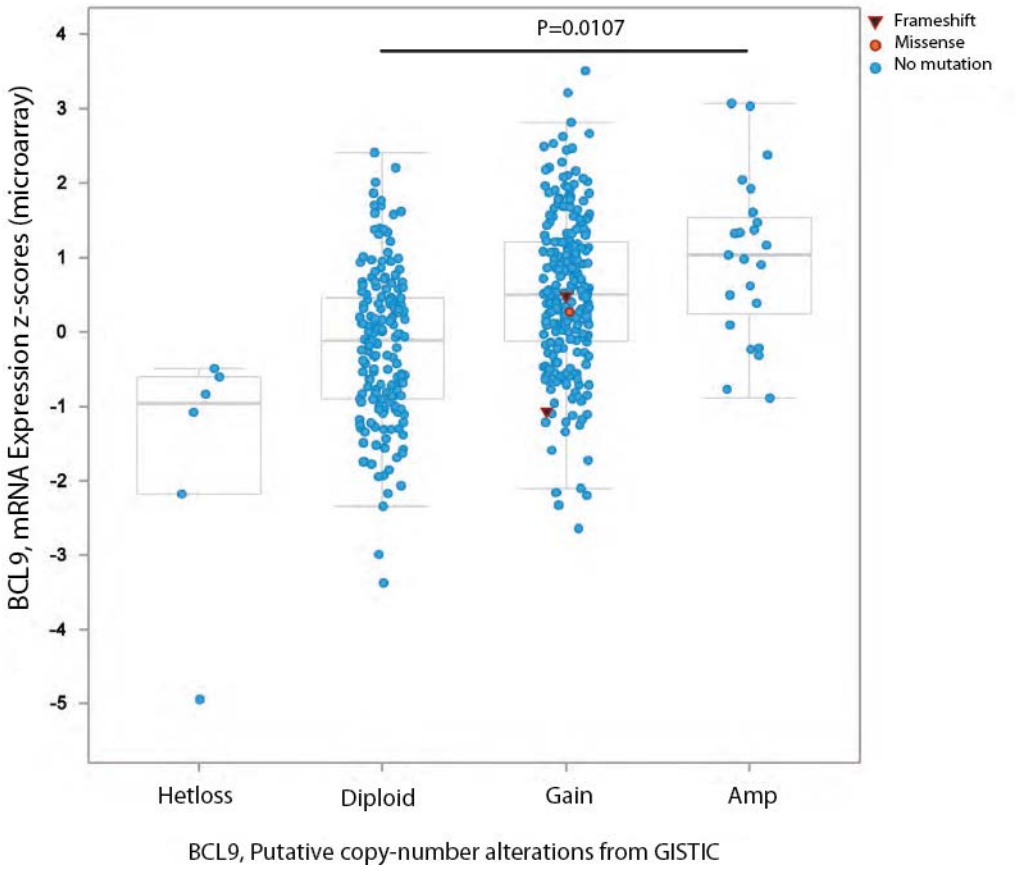

Figure 4.6. Correlation between *BCL9* mRNA expression and *BCL9* amplification. The gene expression data was available as z-score. Diploid classification was used to identify median gene expression value, and this value was used as the cut off for dichotomizing gene expression as low (<= median) or high (>median) for *BCL9* expression. Contingency tables were created for diploid vs amplified or gain vs amplified against low or high *BCL9* expression. Chi-square analysis indicates significant association between *BCL9* amplification and high levels of *BCL9* gene expression compared to diploid samples.

4.4. Discussion

In this chapter, evaluation of pure DCIS, and DCIS with IDC revealed different BCL9 expression patterns within the same patient and between different DCIS cases. BCL9 staining was observed to be nuclear, or cytoplasmic or both. This pattern is consistent with a study by Hyeon, et al. 2013 in hepatocellular carcinoma (HCC) patients [81], where BCL9 expression had cytoplasmic weak to moderate intensity in normal hepatocytes, while in HCC BCL9 was observed in nuclei with or without cytoplasmic expression [81]. Our hypothesis is that BCL9 nuclear expression is associated with risk of invasion. By analysis of 28 DCIS patient samples, It has been demonstrated that DCIS lesions expressing higher nuclear BCL9 (% cells expressing nuclear BCL9) were more likely to be ER negative, PR negative, high nuclear grade, and high in HER2 expression. These characteristics are associated with higher recurrence rate in DCIS [127]. In chapter two, we described that BCL9 expression pattern was different from that of BCL9 homolog-BCL9L during progression, which was predominantly cytoplasmic. This finding was different from what other studies described. Toya et al. 2007 demonstrated that BCL9L expression was nuclear in invasive lesions and was associated with high nuclear grade and HER2 positivity [106]. Another study showed overexpression of BCL9L in ER positive tumors and that tamoxifen treated patients had better survival rates [107]. However, no studies had evaluated BCL9 staining in DCIS patients.

Interestingly, TCGA data analysis revealed that BCL9 gene alterations were found in 26% of all breast cancers, the majority of which were gene amplifications (13%) or overexpression (17%). For future studies, Fluorescence in situ hybridization (FISH) will be performed on DCIS tissue microarrays to evaluate the association between BCL9 copy numbers in DCIS lesions and risk of recurrence.

4.5. Conclusion

Here, the prognostic significance of BCL9 was evaluated in primary DCIS cases. Analysis of 30 pure DCIS and 62 DCIS with IDC patient samples revealed that BCL9 expression is significantly higher in DCIS/IDC than in pure DCIS cases. It was shown that nuclear BCL9 was associated with low ER, PR, and high HER2. Therefore, BCL9 may serve as a potential future biomarker of high risk DCIS if validated in a large dataset of DCIS patients with known outcome. Furthermore, evaluation of the adjacent normal mammary tissue for BCL9 protein expression, as well as BCL9 copy number by FISH will be considered for future analyses.

CHAPTER FIVE

Summary, Conclusions, and Future Directions

DCIS is the most common premalignant lesion of the breast. With the development of advanced breast cancer screening methods, diagnosis of DCIS cases is increasing. DCIS patients are treated with lumpectomy alone or lumpectomy with radiotherapy. Hormonal therapy is also added to the treatment regimen depending on the ER status of the DCIS lesions. The major problem in DCIS management is lack of risk stratification methods to separate patients who benefit from lumpectomy alone from other patients who require radiotherapy and surgery. As a result, many DCIS patients are potentially over-treated. The aims of our studies was to identify new and more effectivetherapeutic strategies to prevent recurrence, and to identify biomarkers for DCIS patients who have potential risk of invasive progression.

Toward these aims, we utilized two *in vivo* models to perform gene expression profiling and to screen for molecular changes during progression from DCIS to IDC. This led to discovery of a novel role of BCL9 in breast cancer tumorigenesis.

In chapter two, we showed that BCL9 knockdown inhibited proliferation, migration and invasion, and regulated EMT biomarkers in our DCIS cell lines. We confirmed that BCL9 exerts its pro-tumorigenic effects through activating β-catenin mediated WNT signaling. Future studies will focus on identifying small molecule or peptide inhibitors that target BCL9 by disrupting its binding with β-catenin and other binding partners such as PYGO. Takada *et al.* developed a stabilized α helix of BCL9 (SAH-BCL9). SAH-BCL9 disrupts β-catenin/BCL9 binding, and selectively suppresses WNT transcription, and thus exhibits mechanism-based antitumor effects [86]. Similarly, a recent study by de la Roche and colleagues screened for small molecular inhibitors of β-catenin binding to BCL9 [88]. Their screen identified that carnosic acid (CA), a natural compound found in rosemary, inhibited BCL9/β-catenin binding and attenuated β-catenin dependent transcription [88]. CA inhibited the growth of MCF7 human breast cancer cells [129].

CA is orally bioavailable and may be administered by oral gavage and or by administration of a compounded flavored tablet to mice. If our studies demonstrate efficacy for prevention of DCIS-IDC transition, CA may serve as a future therapy to prevent IDC recurrence following DCIS treatment.

In chapter three, we shed light on a new mechanism by which BCL9 might promote DCIS invasion through STAT3 signaling. BCL9 showed an interaction with STAT3 and increased STAT3 signaling activity. Interestingly, BCL9 protein levels correlated with phosphorylated STAT3 protein levels in TCGA analysis of 959 breast cancers. This finding suggests that BCL9 indirectly activates and phosphorylates STAT3 either at the receptor level or by modulating kinase activity. However, the mechanism by which BCL9 contributes to STAT3 signaling requires further investigation. Future studies will identify BCL9-mediated secreted factors that stimulate STAT3 signaling, and screen for kinases that are regulated by BCL9. In addition, future experiments will evaluate the transcriptional activity of the STAT3/BCL9 complex.

In chapter four, we evaluated BCL9 as a biomarker for high risk DCIS. BCL9 nuclear expression was higher in DCIS cases that were associated with IDC when compared with pure DCIS. Nuclear BCL9 levels were higher in DCIS lesions that exhibited characteristics of high-risk DCIS, such as ER-negative, PR-negative, HER2-positive, and high nuclear grade. For the future, these studies will be validated in a larger group of patients with appropriately matched cases and controls based on age at DCIS diagnosis (+/- 5 years), year of DCIS diagnosis (+/- 2.5 years), surgical treatment (in the following categories: biopsy only, lumpectomy without or without nodal dissection, and mastectomy), and radiation (yes vs. no). Associations between nuclear BCL9 in the DCIS lesion and invasive outcome will be analyzed.

In addition, we observed BCL9-expressing macrophages recruited to DCIS lesions in our DCIS cell line MIND xenografts and in primary patient DCIS. There is growing evidence that macrophages promote tumor initiation and progression. Macrophages are recruited to the sites of invasion by a number of chemokines and growth factors secreted by tumor epithelial cells such as colony stimulating factor-1 and CCL2. Macrophages in turn produce growth factors, EGF, VEGF, and MMP7/9 that promote tumor cell growth and invasion [130]. Furthermore, Oguma *et al.* have demonstrated that the release of TNF-α by macrophages enhanced canonical WNT signaling in gastric cancer epithelial cells [131]. These studies [132] suggested that interactions of BCL9-expressing macrophages with DCIS epithelia promote cancer progression. Although studying the role of BCL9 in recruiting macrophages is outside the scope of this dissertation, it would be interesting to evaluate BCL9-mediated macrophage-DCIS interactions.

By studying BCL9 in DCIS we hope to identify new therapeutic opportunities to prevent DCIS progression and recurrence. Finding biomarkers such as BCL9 that alone or in combination with other existing biomarkers can predict future risk of DCIS/IDC development will spare many patients from unnecessary therapies.

References

1. Erbas, B., et al., *The natural history of ductal carcinoma in situ of the breast: a review.* Breast Cancer Res Treat, 2006. **97**(2): p. 135-44.

2. Allred, D.C., et al., *Adjuvant tamoxifen reduces subsequent breast cancer in women with estrogen receptor-positive ductal carcinoma in situ: a study based on NSABP protocol B-24.* J Clin Oncol, 2012. **30**(12): p. 1268-73.

3. Allred, D.C., et al., *Ductal carcinoma in situ and the emergence of diversity during breast cancer evolution.* Clin Cancer Res, 2008. **14**(2): p. 370-8.

4. Fisher, B., et al., *Lumpectomy and radiation therapy for the treatment of intraductal breast cancer: findings from National Surgical Adjuvant Breast and Bowel Project B-17.* J Clin Oncol, 1998. **16**(2): p. 441-52.

5. Wapnir, I.L., et al., *Long-term outcomes of invasive ipsilateral breast tumor recurrences after lumpectomy in NSABP B-17 and B-24 randomized clinical trials for DCIS.* J Natl Cancer Inst, 2011. **103**(6): p. 478-88.

6. Baxter, N.N., et al., *Trends in the treatment of ductal carcinoma in situ of the breast.* J Natl Cancer Inst, 2004. **96**(6): p. 443-8.

7. Dignam, J.J. and B. Fisher, *Occurrence of stroke with tamoxifen in NSABP B-24.* Lancet, 2000. **355**(9206): p. 848-9.

8. Leonard, G.D. and S.M. Swain, *Ductal carcinoma in situ, complexities and challenges.* J Natl Cancer Inst, 2004. **96**(12): p. 906-20.

9. Gilleard, O., et al., *The significance of the Van Nuys prognostic index in the management of ductal carcinoma in situ.* World J Surg Oncol, 2008. **6**: p. 61.

10. Bartlett, J.M., S. Nofech-Moses, and E. Rakovitch, *Ductal carcinoma in situ of the breast: can biomarkers improve current management?* Clin Chem, 2014. **60**(1): p. 60-7.

11. Nuyten, D.S., et al., *Predicting a local recurrence after breast-conserving therapy by gene expression profiling.* Breast Cancer Res, 2006. **8**(5): p. R62.

12. Nuyten, D.S. and M.J. van de Vijver, *Gene expression signatures to predict the development of metastasis in breast cancer.* Breast Dis, 2006. **26**: p. 149-56.

13. Solin, L.J., et al., *A multigene expression assay to predict local recurrence risk for ductal carcinoma in situ of the breast.* J Natl Cancer Inst, 2013. **105**(10): p. 701-10.

14. Marshall, E., *Breast cancer. Dare to do less.* Science, 2014. **343**(6178): p. 1454-6.

15. Ma, X.J., et al., *Gene expression profiling of the tumor microenvironment during breast cancer progression.* Breast Cancer Res, 2009. **11**(1): p. R7.

16. Ma, X.J., et al., *Gene expression profiles of human breast cancer progression.* Proc Natl Acad Sci U S A, 2003. **100**(10): p. 5974-9.

17. Schuetz, C.S., et al., *Progression-specific genes identified by expression profiling of matched ductal carcinomas in situ and invasive breast tumors, combining laser capture microdissection and oligonucleotide microarray analysis.* Cancer Res, 2006. **66**(10): p. 5278-86.

18. Luzzi, V., V. Holtschlag, and M.A. Watson, *Expression profiling of ductal carcinoma in situ by laser capture microdissection and high-density oligonucleotide arrays.* Am J Pathol, 2001. **158**(6): p. 2005-10.

19. Yao, J., et al., *Combined cDNA array comparative genomic hybridization and serial analysis of gene expression analysis of breast tumor progression.* Cancer Res, 2006. **66**(8): p. 4065-78.

20. Liao, S., et al., *Differential copy number aberrations in novel candidate genes associated with progression from in situ to invasive ductal carcinoma of the breast.* Genes Chromosomes Cancer, 2012. **51**(12): p. 1067-78.

21. Dang, T.T., A.M. Prechtl, and G.W. Pearson, *Breast cancer subtype-specific interactions with the microenvironment dictate mechanisms of invasion.* Cancer Res, 2011. **71**(21): p. 6857-66.

22. Orimo, A., et al., *Stromal fibroblasts present in invasive human breast carcinomas promote tumor growth and angiogenesis through elevated SDF-1/CXCL12 secretion.* Cell, 2005. **121**(3): p. 335-48.

23. Cichon, M.A., et al., *Microenvironmental influences that drive progression from benign breast disease to invasive breast cancer.* J Mammary Gland Biol Neoplasia, 2010. **15**(4): p. 389-97.

24. Hu, M., et al., *Regulation of in situ to invasive breast carcinoma transition.* Cancer Cell, 2008. **13**(5): p. 394-406.

25. Allinen, M., et al., *Molecular characterization of the tumor microenvironment in breast cancer.* Cancer Cell, 2004. **6**(1): p. 17-32.

26. Polyak, K. and M. Hu, *Do myoepithelial cells hold the key for breast tumor progression?* J Mammary Gland Biol Neoplasia, 2005. **10**(3): p. 231-47.

27. Cardiff, R.D., D. Moghanaki, and R.A. Jensen, *Genetically engineered mouse models of mammary intraepithelial neoplasia.* J Mammary Gland Biol Neoplasia, 2000. **5**(4): p. 421-37.

28. Frech, M.S., et al., *Deregulated estrogen receptor alpha expression in mammary epithelial cells of transgenic mice results in the development of ductal carcinoma in situ.* Cancer Res, 2005. **65**(3): p. 681-5.

29. Schulze-Garg, C., et al., *A transgenic mouse model for the ductal carcinoma in situ (DCIS) of the mammary gland.* Oncogene, 2000. **19**(8): p. 1028-37.

30. Medina, D., *Serial transplantation of carcinogen-treated mammary nodule outgrowths. 3. Dissociation of carcinogen-induced cell variants by dose and chemical structure of carcinogen.* J Natl Cancer Inst, 1973. **50**(6): p. 1555-9.

31. Medina, D., K.B. DeOme, and L. Young, *Tumor-producing capabilities of hyperplastic alveolar nodules in virgin and hormone-stimulated BALB/c f. C3H and C3Hf mice.* J Natl Cancer Inst, 1970. **44**(1): p. 167-74.

32. Behbod, F., et al., *An intraductal human-in-mouse transplantation model mimics the subtypes of ductal carcinoma in situ.* Breast Cancer Res, 2009. **11**(5): p. R66.

33. Valdez, K.E., et al., *Human primary ductal carcinoma in situ (DCIS) subtype-specific pathology is preserved in a mouse intraductal (MIND) xenograft model.* J Pathol, 2011. **225**(4): p. 565-73.

34. Logan, C.Y. and R. Nusse, *The Wnt signaling pathway in development and disease.* Annu Rev Cell Dev Biol, 2004. **20**: p. 781-810.

35. Niehrs, C., *Function and biological roles of the Dickkopf family of Wnt modulators.* Oncogene, 2006. **25**(57): p. 7469-81.

36. Kansara, M., et al., *Wnt inhibitory factor 1 is epigenetically silenced in human osteosarcoma, and targeted disruption accelerates osteosarcomagenesis in mice.* J Clin Invest, 2009. **119**(4): p. 837-51.

37. Cruciat, C.M. and C. Niehrs, *Secreted and transmembrane wnt inhibitors and activators.* Cold Spring Harb Perspect Biol, 2013. **5**(3): p. a015081.

38. Yamamoto, A., et al., *Shisa promotes head formation through the inhibition of receptor protein maturation for the caudalizing factors, Wnt and FGF.* Cell, 2005. **120**(2): p. 223-35.

39. Kagermeier-Schenk, B., et al., *Waif1/5T4 inhibits Wnt/beta-catenin signaling and activates noncanonical Wnt pathways by modifying LRP6 subcellular localization.* Dev Cell, 2011. **21**(6): p. 1129-43.

40. Takahashi, M., et al., *Isolation of a novel human gene, APCDD1, as a direct target of the beta-Catenin/T-cell factor 4 complex with probable involvement in colorectal carcinogenesis.* Cancer Res, 2002. **62**(20): p. 5651-6.

41. Carmon, K.S., et al., *R-spondins function as ligands of the orphan receptors LGR4 and LGR5 to regulate Wnt/beta-catenin signaling.* Proc Natl Acad Sci U S A, 2011. **108**(28): p. 11452-7.

42. Theodorou, V., et al., *MMTV insertional mutagenesis identifies genes, gene families and pathways involved in mammary cancer.* Nat Genet, 2007. **39**(6): p. 759-69.

43. Smallwood, P.M., et al., *Mutational analysis of Norrin-Frizzled4 recognition.* J Biol Chem, 2007. **282**(6): p. 4057-68.

44. Wu, Q.L., C. Zierold, and E.A. Ranheim, *Dysregulation of Frizzled 6 is a critical component of B-cell leukemogenesis in a mouse model of chronic lymphocytic leukemia.* Blood, 2009. **113**(13): p. 3031-9.

45. Kirikoshi, H., H. Sekihara, and M. Katoh, *Up-regulation of Frizzled-7 (FZD7) in human gastric cancer.* Int J Oncol, 2001. **19**(1): p. 111-5.

46. Ueno, K., et al., *Frizzled-7 as a potential therapeutic target in colorectal cancer.* Neoplasia, 2008. **10**(7): p. 697-705.

47. Ueno, K., et al., *Down-regulation of frizzled-7 expression decreases survival, invasion and metastatic capabilities of colon cancer cells.* Br J Cancer, 2009. **101**(8): p. 1374-81.

48. Qiang, Y.W., et al., *Wnts induce migration and invasion of myeloma plasma cells.* Blood, 2005. **106**(5): p. 1786-93.

49. Syed Khaja, A.S., et al., *Elevated level of Wnt5a protein in localized prostate cancer tissue is associated with better outcome.* PLoS One, 2011. **6**(10): p. e26539.

50. Toyama, T., et al., *Noncanonical Wnt11 inhibits hepatocellular carcinoma cell proliferation and migration.* Mol Cancer Res, 2010. **8**(2): p. 254-65.

51. Barker, N., et al., *Crypt stem cells as the cells-of-origin of intestinal cancer.* Nature, 2009. **457**(7229): p. 608-11.

52. Zurawel, R.H., et al., *Sporadic medulloblastomas contain oncogenic beta-catenin mutations.* Cancer Res, 1998. **58**(5): p. 896-9.

53. Breuhahn, K., T. Longerich, and P. Schirmacher, *Dysregulation of growth factor signaling in human hepatocellular carcinoma.* Oncogene, 2006. **25**(27): p. 3787-800.

54. Palacios, J. and C. Gamallo, *Mutations in the beta-catenin gene (CTNNB1) in endometrioid ovarian carcinomas.* Cancer Res, 1998. **58**(7): p. 1344-7.

55. Baldus, S.E., et al., *MUC1 and nuclear beta-catenin are coexpressed at the invasion front of colorectal carcinomas and are both correlated with tumor prognosis.* Clin Cancer Res, 2004. **10**(8): p. 2790-6.

56. Lin, S.Y., et al., *Beta-catenin, a novel prognostic marker for breast cancer: its roles in cyclin D1 expression and cancer progression.* Proc Natl Acad Sci U S A, 2000. **97**(8): p. 4262-6.

57. Li, Y., W.P. Hively, and H.E. Varmus, *Use of MMTV-Wnt-1 transgenic mice for studying the genetic basis of breast cancer.* Oncogene, 2000. **19**(8): p. 1002-9.

58. Candidus, S., et al., *No evidence for mutations in the alpha- and beta-catenin genes in human gastric and breast carcinomas.* Cancer Res, 1996. **56**(1): p. 49-52.

59. Sorlie, T., I. Bukholm, and A.L. Borresen-Dale, *Truncating somatic mutation in exon 15 of the APC gene is a rare event in human breast carcinomas. Mutations in brief no. 179. Online.* Hum Mutat, 1998. **12**(3): p. 215.

60. Howe, L.R. and A.M. Brown, *Wnt signaling and breast cancer.* Cancer Biol Ther, 2004. **3**(1): p. 36-41.

61. Huguet, E.L., et al., *Differential expression of human Wnt genes 2, 3, 4, and 7B in human breast cell lines and normal and disease states of human breast tissue.* Cancer Res, 1994. **54**(10): p. 2615-21.

62. Li, Y., et al., *Evidence that transgenes encoding components of the Wnt signaling pathway preferentially induce mammary cancers from progenitor cells.* Proc Natl Acad Sci U S A, 2003. **100**(26): p. 15853-8.

63. Zeng, Y.A. and R. Nusse, *Wnt proteins are self-renewal factors for mammary stem cells and promote their long-term expansion in culture.* Cell Stem Cell, 2010. **6**(6): p. 568-77.

64. Jang, G.B., et al., *Blockade of Wnt/beta-catenin signaling suppresses breast cancer metastasis by inhibiting CSC-like phenotype.* Sci Rep, 2015. **5**: p. 12465.

65. Yook, J.I., et al., *A Wnt-Axin2-GSK3beta cascade regulates Snail1 activity in breast cancer cells.* Nat Cell Biol, 2006. **8**(12): p. 1398-406.

66. Scheel, C., et al., *Paracrine and autocrine signals induce and maintain mesenchymal and stem cell states in the breast.* Cell, 2011. **145**(6): p. 926-40.

67. Tian, W., et al., *Structure-based discovery of a novel inhibitor targeting the beta-catenin/Tcf4 interaction.* Biochemistry, 2012. **51**(2): p. 724-31.

68. Pode-Shakked, N., et al., *Resistance or sensitivity of Wilms' tumor to anti-FZD7 antibody highlights the Wnt pathway as a possible therapeutic target.* Oncogene, 2011. **30**(14): p. 1664-80.

69. Ettenberg, S.A., et al., *Inhibition of tumorigenesis driven by different Wnt proteins requires blockade of distinct ligand-binding regions by LRP6 antibodies.* Proc Natl Acad Sci U S A, 2010. **107**(35): p. 15473-8.

70. Willis, T.G., et al., *Molecular cloning of translocation t(1;14)(q21;q32) defines a novel gene (BCL9) at chromosome 1q21.* Blood, 1998. **91**(6): p. 1873-81.

71. Kramps, T., et al., *Wnt/wingless signaling requires BCL9/legless-mediated recruitment of pygopus to the nuclear beta-catenin-TCF complex.* Cell, 2002. **109**(1): p. 47-60.

72. Sustmann, C., et al., *Cell-type-specific function of BCL9 involves a transcriptional activation domain that synergizes with beta-catenin.* Mol Cell Biol, 2008. **28**(10): p. 3526-37.

73. Sampietro, J., et al., *Crystal structure of a beta-catenin/BCL9/Tcf4 complex.* Mol Cell, 2006. **24**(2): p. 293-300.

74. Xu, C., et al., *BCL9 and C9orf5 are associated with negative symptoms in schizophrenia: meta-analysis of two genome-wide association studies.* PLoS One, 2013. **8**(1): p. e51674.

75. Brunetti-Pierri, N., et al., *Recurrent reciprocal 1q21.1 deletions and duplications associated with microcephaly or macrocephaly and developmental and behavioral abnormalities.* Nat Genet, 2008. **40**(12): p. 1466-71.

76. Brack, A.S., et al., *BCL9 is an essential component of canonical Wnt signaling that mediates the differentiation of myogenic progenitors during muscle regeneration.* Dev Biol, 2009. **335**(1): p. 93-105.

77. Velasco, J., et al., *Wnt pathway genes in osteoporosis and osteoarthritis: differential expression and genetic association study.* Osteoporos Int, 2010. **21**(1): p. 109-18.

78. Mani, M., et al., *BCL9 promotes tumor progression by conferring enhanced proliferative, metastatic, and angiogenic properties to cancer cells.* Cancer Res, 2009. **69**(19): p. 7577-86.

79. Deka, J., et al., *Bcl9/Bcl9l are critical for Wnt-mediated regulation of stem cell traits in colon epithelium and adenocarcinomas.* Cancer Res, 2010. **70**(16): p. 6619-28.

80. Wang, K., et al., *Genomic landscape of copy number aberrations enables the identification of oncogenic drivers in hepatocellular carcinoma.* Hepatology, 2013. **58**(2): p. 706-17.

81. Hyeon, J., et al., *Prognostic Significance of BCL9 Expression in Hepatocellular Carcinoma.* Korean J Pathol, 2013. **47**(2): p. 130-6.

82. Nancarrow, D.J., et al., *Genome-wide copy number analysis in esophageal adenocarcinoma using high-density single-nucleotide polymorphism arrays.* Cancer Res, 2008. **68**(11): p. 4163-72.

83. Jia, W., et al., *MicroRNA-30c-2* expressed in ovarian cancer cells suppresses growth factor-induced cellular proliferation and downregulates the oncogene BCL9.* Mol Cancer Res, 2011. **9**(12): p. 1732-45.

84. Zhao, J.J., et al., *miR-30-5p functions as a tumor suppressor and novel therapeutic tool by targeting the oncogenic Wnt/beta-catenin/BCL9 pathway.* Cancer Res, 2014. **74**(6): p. 1801-13.

85. Li, J., et al., *LATS2 suppresses oncogenic Wnt signaling by disrupting beta-catenin/BCL9 interaction.* Cell Rep, 2013. **5**(6): p. 1650-63.

86. Takada, K., et al., *Targeted disruption of the BCL9/beta-catenin complex inhibits oncogenic Wnt signaling.* Sci Transl Med, 2012. **4**(148): p. 148ra117.

87. Kawamoto, S.A., et al., *Design of triazole-stapled BCL9 alpha-helical peptides to target the beta-catenin/B-cell CLL/lymphoma 9 (BCL9) protein-protein interaction.* J Med Chem, 2012. **55**(3): p. 1137-46.

88. de la Roche, M., et al., *An intrinsically labile alpha-helix abutting the BCL9-binding site of beta-catenin is required for its inhibition by carnosic acid.* Nat Commun, 2012. **3**: p. 680.

89. Zhao, J.J. and R.D. Carrasco, *Crosstalk between microRNA30a/b/c/d/e-5p and the canonical Wnt pathway: implications for multiple myeloma therapy.* Cancer Res, 2014. **74**(19): p. 5351-8.

90. Miller, T.C., et al., *Competitive binding of a benzimidazole to the histone-binding pocket of the Pygo PHD finger.* ACS Chem Biol, 2014. **9**(12): p. 2864-74.

91. Betsill, W.L., Jr., et al., *Intraductal carcinoma. Long-term follow-up after treatment by biopsy alone.* JAMA, 1978. **239**(18): p. 1863-7.

92. Nielsen, M., J. Jensen, and J. Andersen, *Precancerous and cancerous breast lesions during lifetime and at autopsy. A study of 83 women.* Cancer, 1984. **54**(4): p. 612-5.

93. Porter, D., et al., *Molecular markers in ductal carcinoma in situ of the breast.* Mol Cancer Res, 2003. **1**(5): p. 362-75.

94. Hernandez, L., et al., *Genomic and mutational profiling of ductal carcinomas in situ and matched adjacent invasive breast cancers reveals intra-tumour genetic heterogeneity and clonal selection.* J Pathol, 2012. **227**(1): p. 42-52.

95. de la Roche, M., J. Worm, and M. Bienz, *The function of BCL9 in Wnt/beta-catenin signaling and colorectal cancer cells.* BMC Cancer, 2008. **8**: p. 199.

96. Barnabas, N. and D. Cohen, *Phenotypic and Molecular Characterization of MCF10DCIS and SUM Breast Cancer Cell Lines.* Int J Breast Cancer, 2013. **2013**: p. 872743.

97. Livak, K.J. and T.D. Schmittgen, *Analysis of relative gene expression data using real-time quantitative PCR and the 2(-Delta Delta C(T)) Method.* Methods, 2001. **25**(4): p. 402-8.

98. Mortazavi, A., et al., *Mapping and quantifying mammalian transcriptomes by RNA-Seq.* Nat Methods, 2008. **5**(7): p. 621-8.

99. Robinson, M.D. and G.K. Smyth, *Small-sample estimation of negative binomial dispersion, with applications to SAGE data.* Biostatistics, 2008. **9**(2): p. 321-32.

100. Veeman, M.T., et al., *Zebrafish prickle, a modulator of noncanonical Wnt/Fz signaling, regulates gastrulation movements.* Curr Biol, 2003. **13**(8): p. 680-5.

101. Kolligs, F.T., et al., *Neoplastic transformation of RK3E by mutant beta-catenin requires deregulation of Tcf/Lef transcription but not activation of c-myc expression.* Mol Cell Biol, 1999. **19**(8): p. 5696-706.

102. Stewart, S.A., et al., *Lentivirus-delivered stable gene silencing by RNAi in primary cells.* RNA, 2003. **9**(4): p. 493-501.

103. Elsarraj, H.S., et al., *A novel role of microRNA146b in promoting mammary alveolar progenitor cell maintenance.* J Cell Sci, 2013. **126**(Pt 11): p. 2446-58.

104. Savagner, P., *The epithelial-mesenchymal transition (EMT) phenomenon.* Ann Oncol, 2010. **21 Suppl 7**: p. vii89-92.

105. Hyman, E., et al., *Impact of DNA amplification on gene expression patterns in breast cancer.* Cancer Res, 2002. **62**(21): p. 6240-5.

106. Toya, H., et al., *Immunohistochemical expression of the beta-catenin-interacting protein B9L is associated with histological high nuclear grade and immunohistochemical ErbB2/HER-2 expression in breast cancers.* Cancer Sci, 2007. **98**(4): p. 484-90.

107. Zatula, N., et al., *The BCL9-2 proto-oncogene governs estrogen receptor alpha expression in breast tumorigenesis.* Oncotarget, 2014. **5**(16): p. 6770-87.

108. Katoh, M., *Networking of WNT, FGF, Notch, BMP, and Hedgehog signaling pathways during carcinogenesis.* Stem Cell Rev, 2007. **3**(1): p. 30-8.

109. Mosimann, C., G. Hausmann, and K. Basler, *Beta-catenin hits chromatin: regulation of Wnt target gene activation.* Nat Rev Mol Cell Biol, 2009. **10**(4): p. 276-86.

110. Gao, J., et al., *Integrative analysis of complex cancer genomics and clinical profiles using the cBioPortal.* Sci Signal, 2013. **6**(269): p. pl1.

111. Orsetti, B., et al., *Genetic profiling of chromosome 1 in breast cancer: mapping of regions of gains and losses and identification of candidate genes on 1q.* Br J Cancer, 2006. **95**(10): p. 1439-47.

112. Fiedler, M., et al., *Decoding of methylated histone H3 tail by the Pygo-BCL9 Wnt signaling complex.* Mol Cell, 2008. **30**(4): p. 507-18.

113. Cancer Genome Atlas, N., *Comprehensive molecular portraits of human breast tumours.* Nature, 2012. **490**(7418): p. 61-70.

114. Berishaj, M., et al., *Stat3 is tyrosine-phosphorylated through the interleukin-6/glycoprotein 130/Janus kinase pathway in breast cancer.* Breast Cancer Res, 2007. **9**(3): p. R32.

115. Avalle, L., et al., *STAT1 and STAT3 in tumorigenesis: A matter of balance.* JAKSTAT, 2012. **1**(2): p. 65-72.

116. Deng, J., et al., *S1PR1-STAT3 signaling is crucial for myeloid cell colonization at future metastatic sites.* Cancer Cell, 2012. **21**(5): p. 642-54.

117. Park, E.J., et al., *Dietary and genetic obesity promote liver inflammation and tumorigenesis by enhancing IL-6 and TNF expression.* Cell, 2010. **140**(2): p. 197-208.

118. Yu, H., et al., *Revisiting STAT3 signalling in cancer: new and unexpected biological functions.* Nat Rev Cancer, 2014. **14**(11): p. 736-46.

119. Marotta, L.L., et al., *The JAK2/STAT3 signaling pathway is required for growth of CD44(+)CD24(-) stem cell-like breast cancer cells in human tumors.* J Clin Invest, 2011. **121**(7): p. 2723-35.

120. Hillion, J., et al., *The high-mobility group A1a/signal transducer and activator of transcription-3 axis: an achilles heel for hematopoietic malignancies?* Cancer Res, 2008. **68**(24): p. 10121-7.

121. Garcia, R., et al., *Constitutive activation of Stat3 by the Src and JAK tyrosine kinases participates in growth regulation of human breast carcinoma cells.* Oncogene, 2001. **20**(20): p. 2499-513.

122. Clevenger, C.V., *Roles and regulation of stat family transcription factors in human breast cancer.* Am J Pathol, 2004. **165**(5): p. 1449-60.

123. Zhu, D., et al., *The Cyclophilin A-CD147 complex promotes the proliferation and homing of multiple myeloma cells.* Nat Med, 2015. **21**(6): p. 572-80.

124. Lo, H.W., et al., *Nuclear interaction of EGFR and STAT3 in the activation of the iNOS/NO pathway.* Cancer Cell, 2005. **7**(6): p. 575-89.

125. Hu, T. and C. Li, *Convergence between Wnt-beta-catenin and EGFR signaling in cancer.* Mol Cancer, 2010. **9**: p. 236.

126. Freedman, G.M., *Risk stratification in ductal carcinoma in situ: the role of genomic testing.* Curr Oncol Rep, 2013. **15**(1): p. 7-13.

127. Lari, S.A. and H.M. Kuerer, *Biological Markers in DCIS and Risk of Breast Recurrence: A Systematic Review.* J Cancer, 2011. **2**: p. 232-61.

128. Elsarraj, H.S., et al., *Expression profiling of in vivo ductal carcinoma in situ progression models identified B cell lymphoma-9 as a molecular driver of breast cancer invasion.* Breast Cancer Res, 2015. **17**: p. 128.

129. Einbond, L.S., et al., *Carnosic acid inhibits the growth of ER-negative human breast cancer cells and synergizes with curcumin.* Fitoterapia, 2012. **83**(7): p. 1160-8.

130. Wyckoff, J., et al., *A paracrine loop between tumor cells and macrophages is required for tumor cell migration in mammary tumors.* Cancer Res, 2004. **64**(19): p. 7022-9.

131. Oguma, K., et al., *Activated macrophages promote Wnt signalling through tumour necrosis factor-alpha in gastric tumour cells.* EMBO J, 2008. **27**(12): p. 1671-81.

132. Qian, B.Z. and J.W. Pollard, *Macrophage diversity enhances tumor progression and metastasis.* Cell, 2010. **141**(1): p. 39-51.